ROLE OF SMAD4 LOSS IN HEAD AND NECK SQUAMOUS CELL CARCINOMA

by

Sophia Bornstein

A DISSERTATION

Presented to the Department of Cell and Developmental Biology

and the Oregon Health & Science University

School of Medicine

in partial fulfillment of

the requirements for the degree of

Doctor of Philosophy

July 2008

School of Medicine
Oregon Health & Science University

CERTIFICATE OF APPROVAL

This is to certify that the Ph.D. dissertation of
Sophia Bornstein
has been approved

Dr. Xiao-Jing Wang, PhD Mentor

Dr. Susan Olson, Thesis Committee Chair

Dr. Charles Lopez

Dr. Mathew Thayer

Dr. Mihail Iordanov

TABLE OF CONTENTS

TABLE OF ABBREVIATIONS

General Terms	
ALK	Activin-like Kinase
AP-1	activating protein 1
BCC	Basal Cell Carcinoma
BMP	Bone Morphogenic Protein
Cal27-Smad4	Cal27 cells stably expressing Smad4
Co-Smad	Common Smad
Cre*PR1	Cre* fused to truncated progesterone receptor
CrePR1	Cre fused to Truncated Progesterone Receptor
CSC	Cancer Stem Cell
Ct	Cycle count
CTL	Cytotoxic T Cells
DAB	Diaminobenzidine
DC	Dendritic Cells
ΔPR	Truncated Progesterone Receptor
DSB	Double Strand Break
EGFR	Epidermal Growth Factor Receptor
EMT	Epithelial-Mesenchymal Transition
ER	Estrogen Receptor
FA	Fanconi Anemia
Fanc/Brca	Fanconi Anemia/Brca Pathway
FBS	Fetal bovine serum
GAPDH	Glyceraldehyde 3-phosphate dehydrogenase
GTPase	Guanosine Triphosphatase
h	hours
HEKn	neonatal human epidermal keratinocytes
HEKn + Smad4 siRNA	HEKn cells transfected with Smad4 siRNA
Het	heterozygous
HNSCC	Head and Neck Squamous Cell Carcinoma
HN-Smad4-/-	Smad4 null head-and-neck epithelia
HN-Smad4+/+	Control Smad4+/+ head-and-neck epithelia
HPV	Human Papilloma Virus
ICL	Interstrand Crosslink
IFN	Interferon
IL	Interleukin
IP	Immunoprecipitation
I-Smad	Inhibitory Smad
K1	Keratin 1
K13	Keratin 13
K14	Keratin 14
K5	Keratin 5
K6	Keratin 6
K8	Keratin 8
LOH	Loss of Heterozygosity
MCP	Monocyte-chemotactic protein

MIP	Macrophage inflammatory protein
MMP	Matrix metalloproteinase
NK cells	Natural killer cells
p	phosphorylated
PBS	Phosphate buffered saline
PI3K	Phosphoinositide-3 Kinase
Pol II	RNA Polymerase II
PTEN	Phosphatase and Tensin Homolog
R-Smad	Receptor Smad
SA	Sebaceous Adenoma
SBE	Smad Binding Element
SCC	Squamous Cell Carcinoma
SDF	Stromal-derived Factor
SEM	Standard Error of the Mean
siRNA	Small interfering RNA
SP	Side Population
Stat3	Signal Transducer and Activator of Transcription 3
TBS	Tris buffered saline
Tet	Tetracycline
TGFβ	Transforming Growth Factor Beta
TGFβRII	TGFβ Type II Receptor
Tregs	T regulatory cells
TSS	Transcriptional start site
TUNEL	Terminal deoxynucleotidyl Transferase Biotin-dUTP Nick End Labeling
WT	wildtype
ΔPR	Truncated Progesterone Receptor

Materials and Methods	
aCGH	Array Comparative Genomic Hybridization
ChIP	Chromatin Immunoprecipitation
ELISA	Enzyme-Linked ImmunoSorbent Assay
FBS	fetal bovine serum
H&E	hematoxylin and eosin
IF	Immunofluorescence
IHC	Immunohistochemistry
MMC	Mitomycin C
MMI	Molecular Microbiology and Immunology
MTT	3-(4,5-dimethylthiazol-2-yl)-2,5-diphenyl tetrasodium bromide
OCT	Optimal Cutting Temperature
PCR	Polymerase Chain Reaction
qChIP	Quantitative Chromatin immunoprecipitation
qRT-PCR	Quantitative Reverse Transcriptase Polymerase Chain Reaction
TUNEL	Tdt-mediated dUTP Nick-End Labeling

ACKNOWLEDGEMENTS

- My mentor, Dr. Xiao-Jing Wang, for excellent scientific mentorship and the wonderful opportunity to conduct interesting research
- My thesis committee members: Drs. Susan Olson, Mathew Thayer, Charles Lopez, Mihail Iordanov, and Xiao-Jing Wang for scientific and moral support during my thesis research
- Dr. Shi-Long Lu, for contributing to the establishment of the head and neck-specific Smad4 knockout animal model (Figures 13-16), and for help with troubleshooting throughout my training
- Ruth White, for contributing to cell transfection, nuclear foci, and tumor cell isolation experiments (Figure 24, Figure 25C, Figure 36)
- Kelli Salter, for contributing to LOH study (Figure 12B)
- Stephen Malkoski, for contributing to pStat3 Ser727, pAKT Thr308, and TUNEL staining (Figures 17 and 18)
- Yue-Xin Li, for contributing to mouse work
- Chuxia Deng, for providing Smad4 floxed mice, Tyler Jacks for providing $Kras^{G12D}$ mice, and Harold Moses, for providing TGFβRII floxed mice
- OHSU Cytogenetics Core, for contributing to breakage analysis (Figure 23B)
- Kazutoshi Murao (Dennis Roop Lab, UCD) for contributing to flow cytometry and skin graft studies (Figure 32)
- The Wang Lab, for support and ideas

- My friends and family, including the aforementioned individuals, whose advice and support was critical to my well-being and perseverance

ABSTRACT

Head and neck squamous cell carcinoma (HNSCC) is the sixth most common cancer in the United States. However, the prognosis of HNSCC has not improved in the past 20 years. While many molecular changes have been uncovered, few are known to play a causal role in HNSCC carcinogenesis. During my PhD thesis study, we found that Smad4 was frequently lost in preneoplastic and cancer lesions of HNSCC. When we deleted *Smad4* in mouse head and neck epithelia (*HN-Smad4-/-*), *HN-Smad4-/-* mice developed spontaneous HNSCC. Interestingly, *HN-Smad4-/-* head and neck tissue and HNSCCs exhibited increased genomic instability evidenced by increased centrosome numbers and chromosomal aberrations, which correlated with downregulated gene expression of genes in the Fanconi anemia/Brca (Fanc/Brca) pathway. Further analysis revealed a causal role for Smad4 loss in downregulation of the Fanc/Brca pathway in both human and mouse HNSCC cells. Additionally, *HN-Smad4-/-* head and neck tissue and HNSCCs exhibited severe inflammation, which was associated with increased TGFβ1 and activated Smad3. Additionally, inflammatory cytokines and chemokines, such as MCP-1, MCP-2, MMP2, and MIP-2, which have been shown to be upregulated by TGFβ1, were overexpressed in *HN-Smad4-/-* mucosa and HNSCCs in comparison with *HN-Smad4+/+* controls. Lastly, Smad4 loss in keratinocyte stem cells led to aberrant stem cell proliferation and retention of multipotency. Taken together, both the accumulation of genetic insults in epithelia and increased stromal inflammation appeared to contribute to Smad4 loss-initiated HNSCC carcinogenesis.

CHAPTER ONE

INTRODUCTION

1.1 Molecular Alterations in Head and Neck Squamous Cell Carcinoma

Head and neck cancer refers to malignant tumors derived from the nasal cavity, paranasal sinuses, nasopharynx, oral cavity, pharynx, and larynx; the majority of these tumors are squamous cell carcinomas (SCCs). Head and neck squamous cell carcinoma (HNSCC) is the sixth most common cancer worldwide (Hunter et al., 2005) with an incidence of 500,000 new cases of HNSCC worldwide and 50,000 cases in the United States, alone (Vokes et al., 1993). However, despite recent advances in cancer therapy, as well as in the medical and surgical management of the disease, the 5-year survival for patients with HNSCC has remained 50% for the past 20 years (Forastiere et al., 2001). Unlike other cancers in which lethality is associated with metastasis, primary HNSCCs can cause death as a result of internal bleeding, airway obstruction, and malnutrition related to difficulty with food intake. In early-stage disease, tumors can be surgically removed, but the risk of metastatic disease requires treatment with combined modalities. In cases where the tumor cannot be surgically removed, radiotherapy with or without chemotherapy is required. Despite progress in surgical, radiotherapy, and chemotherapy, there is a profound need for advances in the molecular understanding of HNSCC. Characterization of the underlying molecular alterations in human HNSCC would provide novel prognostic and therapeutic targets for HNSCC, and it is likely that targeted therapy may be the only means to improve the overall survival of HNSCC.

Historically, the two major risk factors for developing HNSCC are exposure to tobacco and alcohol (Neville and Day, 2002). The risk of developing HNSCC is elevated 3 - 9 fold in people who smoke or drink and up to 100-fold in people who both smoke and drink in comparison with those who abstain (Hecht, 2003). It is thought that both tobacco and alcohol cooperate with underlying genetic alterations to generate malignant disease. Chronic exposure to tobacco and alcohol results in "field cancerization," which refers to grossly normal oral mucosa that harbors carcinogenic genetic alterations (Hunter et al., 2005). This phenomenon results in increased risk of developing both multiple coexisting and subsequent primary tumors, severely impacting long-term survival. More recently, positive human papilloma virus (HPV) status has been linked to HNSCC susceptibility (D'Souza et al., 2007), and tailored prognosis and treatment strategies for HPV positive tumors has become a new focus of clinical HNSCC studies (pGillison et al., 2008).

Like many other epithelial cancers, HNSCC results from the accumulation of numerous genetic and epigenetic alterations that occur in a multistep process (Forastiere et al., 2001; Mao et al., 2004). These alterations affect several cancer-related pathways including genomic instability, cell proliferation, apoptosis, angiogenesis, inflammation, invasion, and metastasis. Several genetic alterations in HNSCC have been reported including changes at 17p13 (encoding *p53*) and 9p21 [encoding *p14 (DKN2/MTS1*) and *p16 (Arf)*] (Hunter et al., 2005). Several oncogenic signaling pathways are also upregulated in HNSCC, including Epidermal Growth Factor Receptor/Signal Transducer and Activator of Transcription 3 (EGFR/STAT3) (Pomerantz and Grandis, 2003; Song

and Grandis, 2000), Phosphoinositide-3 Kinase/Phosphatase and Tensin Homolog/Akt (PI3K/PTEN/Akt) (Pedrero et al., 2005), Ras (Lu et al., 2006), and Transforming Growth Factor β (TGFβ) pathways (Lu et al., 2004; Prime et al., 2004; Reiss, 1999).

Similar to many epithelial cancers, the mutation frequency of *p53* in HNSCC is approximately 50% (Hollstein et al., 1991; Somers et al., 1992). In addition to blocking cell division at the G1/S checkpoint, the p53 protein also induces apoptosis in the absence of efficient DNA repair, and thus is a potent tumor suppressor. Inactivation of p53 often occurs at a late stage during HNSCC tumor progression (Boyle et al., 1993). However, alterations of 9p21-22 occur at an early stage in 70% of HNSCCs (van der Riet et al., 1994), inactivating the two tumor suppressor genes p14 and p16 through homozygous deletion (Cairns et al., 1995; Reed et al., 1996), promoter hypermethylation (Herman et al., 1995), and less often, by point mutation (Reed et al., 1996). P16 inhibits cell cycle progression through inhibiting cyclin-dependent kinases CDK4 and CDK6, which can ultimately lead to cell cycle arrest in G1. P14 blocks the association of p53 with its inhibitor MDM2.

In addition to genetically inactivating tumor suppressors, HNSCCs often overactivate cancer-promoting signaling pathways. EGFR, a tyrosine kinase receptor that positively regulates cell growth, migration, and survival, is overexpressed in 80-90% of HNSCCs (Grandis and Tweardy, 1993). In human HNSCCs, EGFR is upregulated in mucosa adjacent to tumors and is further overexpressed in HNSCC. EGFR overexpression correlates with aggressive tumor behavior and poor clinical outcome (Shin et al., 1994;

van Oijen et al., 1998). Chronic activation of EGFR also activates STAT3 (Song and Grandis, 2000), a transcriptional factor involved in cell proliferation (Song and Grandis, 2000). Overexpression of Stat3 or activation of Stat3 by phosphorylation occurs in approximately 60% of HNSCCs (Nagpal et al., 2002). Lastly, Ras mutation, which is a common initiation event in many cancers (Yarbrough et al., 1994), is found in more than 50% of oral cancers associated with tobacco exposure in southern Asia (Saranath et al., 1991). Additionally although Ras mutation is not common in the western world, we have recently reported that Ras mRNA was overexpressed in the majority of human HNSCCs and mucosa adjacent to HNSCCs (Lu et al., 2006).

1.2 Review of Transforming Growth Factor Beta (TGFβ)/Smad Signaling

The TGFβ superfamily consists of three major subfamilies: TGFβ, Activins/Inhibins, and Bone Morphogenetic Proteins (BMPs) (Bornstein et al., 2007). These family members signal through two types of transmembrane serine/threonine kinase receptors, and Smad transcription factors were initially identified as their signaling mediators. Smads are divided into three groups: R-(receptor-activated) Smads, co-(common) Smad and I-(inhibitory) Smads (Massague and Gomis, 2006). R-Smads include Smad1, Smad5, and Smad8, which transduce BMP signaling, and Smad2 and Smad3, which transduce TGFβ/Activin signaling. When a TGFβ superfamily ligand binds its specific type II (RII) and type I (RI) receptor complex, the kinase domain of RI binds and phosphorylates R-Smads. Phosphorylated R-Smads then form heteromeric complexes with the co-Smad, Smad4 and translocate to the nucleus to regulate TGFβ responsive genes (Figure 1). Following nuclear translocation, heteromeric Smad complexes regulate

TGFβ–responsive genes via interaction with specific promoter sequences, termed Smad binding elements (SBEs). I-Smads, Smad6 and Smad7 block TGFβ signaling by competing with R-Smad binding to RI and by recruiting ubiquitin ligases to degrade RI and R-Smads (Massague et al., 2005). Moreover, several phosphatases that dephosphorylate R-Smads to regulate TGFβ signaling were recently identified (Figure 1) (Chen et al., 2006a; Lin et al., 2006).

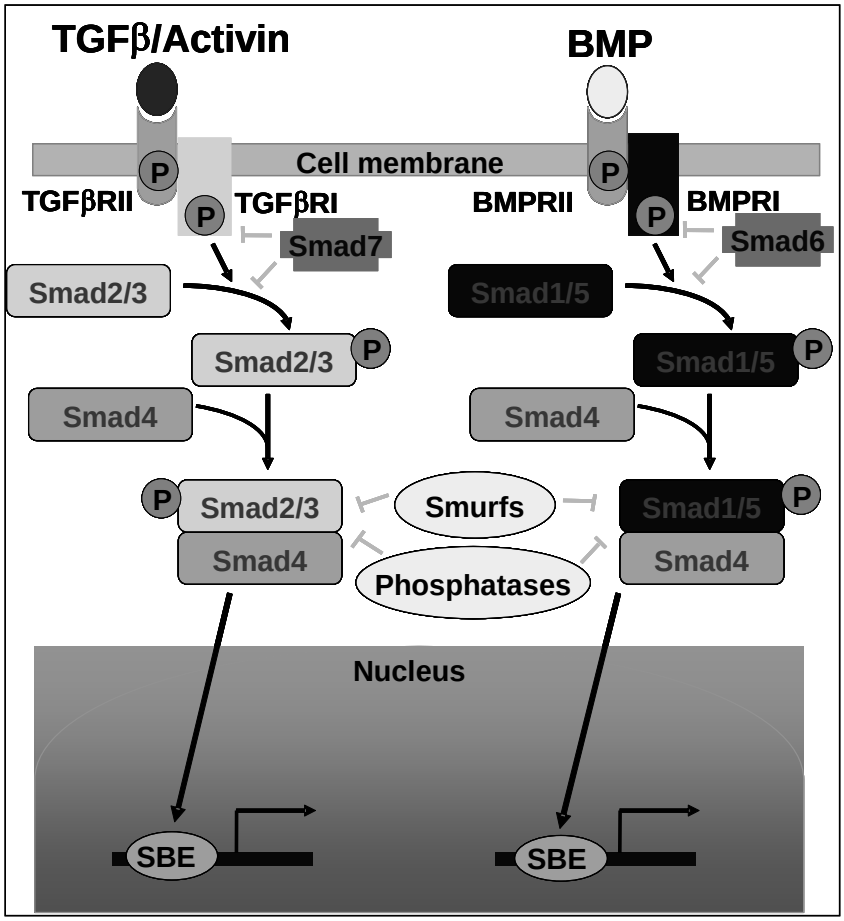

Figure 1. Schematic of TGFβ superfamily signaling mediated by Smads*. Smad4 binds with R-Smads 2 and 3 in response to TGFβ and Activin ligands and with R-Smads 1 and 5 in response to BMP ligands. Smad heterodimers then enter the nucleus and bind to Smad Binding Elements (SBEs) on target gene promoters to regulate transcription.*

1.3 TGFβ Signaling Alterations in HNSCC

The TGFβ signaling pathway plays an important role in tumor suppression, primarily via growth inhibition, apoptosis, and maintenance of differentiation. TGFβ signaling suppresses the growth of epithelial cells, and alterations of TGFβ signaling components, such as the type II receptor (TGFβRII) and the intracellular signaling mediators Smad2 and Smad4, block TGFβ-mediated growth inhibition. These alterations are commonly detected in many cancers including HNSCC (Prime et al., 2004; Reiss, 1999). In addition to the aforementioned genetic alterations in HNSCC, loss of 18q (encoding *Smad4*, and *Smad2*) (Kim et al., 1996; Papadimitrakopoulou et al., 1998; Takebayashi et al., 2000), and loss of the type II TGFβ receptor (*TGFβRII*) (Sparano et al., 2006) have been reported. Reduction or complete loss of TGFβRII expression has been frequently observed in human HNSCC at a rate of ~30% to 87% (Fukai et al., 2003; Wang et al., 1997), and loss of Smad4 and Smad2 expression was reported at 22% to 51% (Fukuchi et al., 2002; Xie et al., 2003) and 14% to 38% respectively (Muro-Cacho et al., 2001; Xie et al., 2003). We have recently reported that 69% of HNSCCs showed loss of TGFβRII (Lu 2006). However, only 6% of mucosa samples adjacent to HNSCCs exhibited TGFβRII loss, suggesting this change is involved in progression to malignancy rather than tumor initiation.

In contrast to its tumor suppressive effect, TGFβ signaling also promotes tumor progression and metastasis through increased angiogenesis, inflammation, and epithelial-mesenchymal transition (EMT) (Bierie and Moses, 2006a). TGFβ1 is often overexpressed in many human cancers (Reiss, 1999) including HNSCCs and the mucosa

adjacent to HNSCCs (Lu et al., 2004), suggesting that TGFβ1 overexpression may be involved in HNSCC development.

1.4 Mouse Models of HNSCC

Transgenic mouse models of HNSCC have only recently been developed. The first genetically engineered HNSCC mouse model targeted overexpression of the cyclin D1 transgene to the oral-esophageal epithelium using the Epstein-Barr virus promoter. These mice exhibited dysplasia in the tongue, esophagus, and forestomach but did not develop tumors (Nakagawa et al., 1997). Subsequently, the cyclin D1 transgenic mice were crossbred with germline heterozygous p53 knockout mice, and the bigenic mice developed invasive oral-esophageal cancer (Opitz et al., 2002). However, the simultaneous development of tumors in other organs due to germline p53 knockout confounded analysis of the phenotype. Because of the lack of tissue specificity of germline knockout/transgenic mice, and the inability to control transgene expression in constitutive transgenic models, inducible and tissue-specific models have been developed that provide control over the extent of transgene expression, and temporal and tissue-specific control of gene overexpression/deletion.

By utilizing a progesterone-based inducible system, in which the target transgene is activated upon progesterone exposure, and a keratinocyte-specific promoter, we have successfully developed transgenic mice in which the TGFβ1 transgene can be inducibly expressed specifically in head and neck epithelia, discussed in section 1.8 (Lu et al., 2004). We have also combined a progesterone-inducible, keratinocyte-specific system

with the Cre/LoxP system to generate inducible, head and neck specific knockout mice (Jonkers and Berns, 2002; Lewandoski, 2001). In this system, the progesterone antagonist, RU486, is used as an inducer to bind a truncated progesterone receptor (ΔPR) and activate a Cre recombinase fused with ΔPR (CrePR1). Without the RU486 inducer, the CrePR1 fusion protein is sequestered in the cytoplasm. After topical application of RU486, the CrePR1 fusion protein is translocated into the nucleus, where it excises a target gene that has been flanked by loxP sites (Kellendonk et al., 1996). When the CrePR1 transgene is targeted by the Keratin 5 (K5), Keratin 15 (K15) or Keratin 14 (K14) promoter, gene deletion will only occur in the epithelia of an RU486-treated oral cavity. Since the K5, K15, and K14 promoters target transgene expression to epithelial stem cells (Arin et al., 2001; Cao et al., 2001; Morris et al., 2004), the stratified epithelium is replaced and renewed by cells in which the targeted gene is deleted. We have utilized this system to inducibly delete TGFβRII specifically in head and neck epithelia (Lu et al., 2006), discussed in section 1.8.

The Cre/LoxP system can also be used to "knock-in" or turn on a mutant gene. In this system, a floxed "stop" cassette that disrupts gene transcription is placed before or after a mutant gene. When the CrePR1 fusion protein is activated, the floxed stop cassette is removed, resulting in expression of the mutant gene. Using this system, mutant K-ras was inducibly activated in mouse head and neck epithelia (Caulin et al., 2004). To investigate the role of the Ras activation in HNSCC development in vivo, the K5CrePR1 mice (Zhou et al., 2002) were crossbred with K-ras^{G12D} mice (Jackson et al., 2001), in which a floxed stop cassette was inserted upstream of a mutant Kras allele. Upon RU486

application to the oral cavity, the Cre recombinase was able to excise the stop cassette and lead to expression of mutant Kras specifically in head and neck epithelia. Activation of the K-ras^{G12D} allele induced benign oral squamous papilloma formation. This highlighted a causal role for mutant K-ras in the initiation of oral cancer; however by itself, mutant Kras was not sufficient for malignant progression to HNSCC. Lastly, the inducible head and neck specific mutant Kras mice were crossed with TGFβRII knockout mice (discussed in section 1.8), and the compound mice developed metastatic HNSCC with 100% penetrance, representing the first genetically engineered HNSCC model.

1.5 Role of the Fanconi/Brca (Fanc/Brca) Pathway in HNSCC

The karyotypes of human HNSCCs are complex and composed of multiple structural chromosomal abnormalities (Jin et al., 2005). It has been proposed that genomic instability is necessary for tumorigenesis, as several mutations are required for malignant cancer formation, and most tumors are ridden with numerous mutations that could only be explained by a mutator phenotype (Sieber et al., 2003). There is considerable controversy regarding the requirement for genomic instability in carcinogenesis, and the role of genomic instability in HNSCC remains unclear. However, germline mutations in genes involved in DNA repair almost invariably lead to cancer susceptibility syndromes including Hereditary Nonpolyposis Colorectal Cancer (*MLH1*, *MLH2*, *MSH6*, *PMS*, *PMS2* mutations), Hereditary Breast Ovarian Cancer Syndrome (*Brca1*, *Brca2* mutations), Cowden Syndrome *(PTEN* mutation), Ataxia telangiectasia (*ATM* mutation), Nijmegen Breakage Syndrome (*NBS* mutation), and Li-Fraumeni Syndrome (*p53* mutation), arguing that preexisting alterations in DNA repair pathways are tumorigenic

(Thompson and Schild, 2002). Germline mutations in the Fanc/Brca pathway lead to the cancer susceptibility syndrome Fanconi anemia (FA), in which cells from affected patients exhibit clastogen-induced chromosomal aberrations. The Fanc/Brca pathway is the only known pathway leading to HNSCC susceptibility in humans (Kutler et al., 2003). It has been shown that FA patients, who carry germline mutations in Fanc/Brca pathway genes have a high incidence of HNSCC at a young age, and 70% of FA patients diagnosed with HNSCC were in complementation group A, indicating that FancA mutations lead to increased susceptibility (Kutler et al., 2003). Moreover, studies have shown that Fanc/Brca pathway-associated genes are downregulated in sporadic HNSCCs (Marsit et al., 2004; Sparano et al., 2006; Weber et al., 2007; Wreesmann et al., 2007), building evidence that alterations in this pathway play an important role in sporadic HNSCC formation. Additionally, mice with epithelia-specific heterozygous knockout of *Brca1* developed oral SCCs, indicating that Brca1 loss plays an important role in HNSCC tumorigenesis (Berton et al., 2003).

Cells from patients with FA exhibit increased sensitivity to double strand breaks (DSB)s in DNA caused by DNA interstrand crosslinking (ICL) agents such as Mitomycin C (MMC), which is evidenced by increased chromosome breaks and radial structures on metaphase spreads; this phenotype is used to diagnose the disease. These chromosomal aberrations either lead to cellular apoptosis (evidenced by bone marrow failure) or genomic instability (evidenced by both blood and solid tumor formation); both are common disease phenotypes in FA patients (Figure 2) (D'Andrea and Grompe, 2003; Niedernhofer et al., 2005).

Figure 2. DNA Repair Defects Lead to Spontaneous Chromosomal Aberrations that Lead to Bone Marrow Failure and Cancer in FA Patients *[adopted from (Niedernhofer et al., 2005)].*

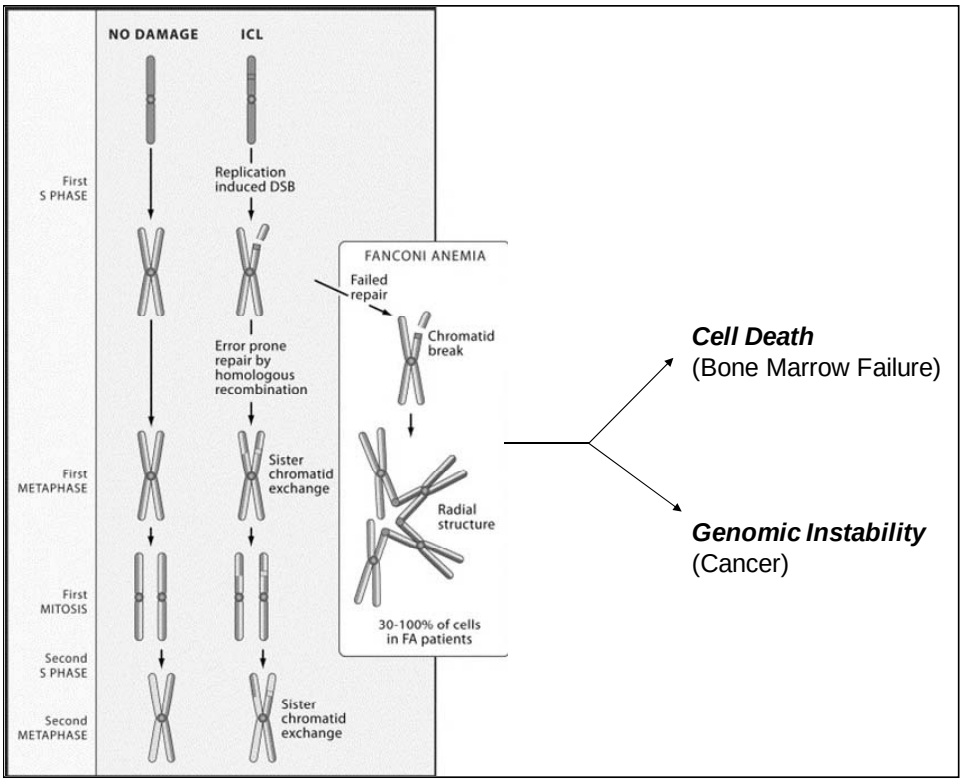

During DNA replication, homologous recombination complexes repair double strand breaks (DSBs). In patients with FA, this DNA repair process is defective, and chromosome breaks accumulate, as well as radial structures, which are thought to arise as a result of defective attempts to repair the chromosome breaks. The accumulation of DNA damage in the cells of these patients can lead to apoptosis and bone marrow failure, or genomic instability and cancer.

The Fanc/Brca pathway normally mediates resolution of ICL-induced DSB DNA damage through a complicated series of molecular events (Figure 3).

Figure 3. The Fanc/Brca pathway *[adopted from (Taniguchi and D'Andrea, 2006).] The FA core complex including FancA, monoubiquitinates FancD2, which then translocates to sites of DNA repair (DNA-repair foci) with several other proteins including Brca1, Brca2, and Rad51, to resolve DNA double strand breaks.*

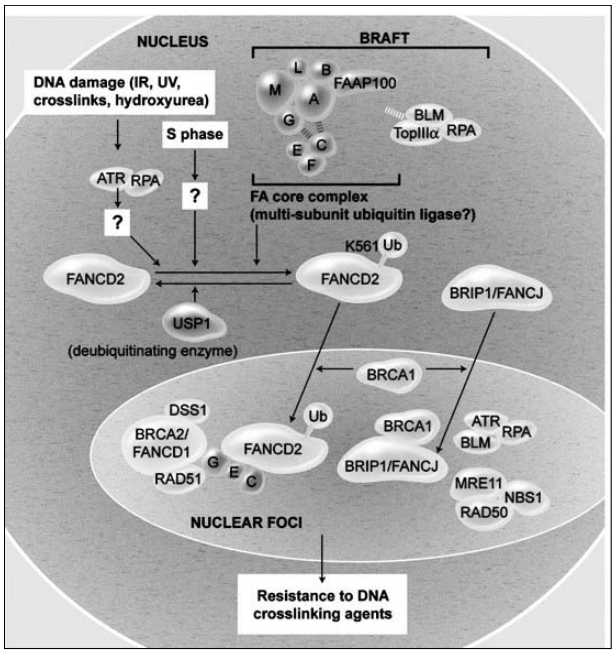

The FA core complex consists of several proteins including FancA, and is responsible for the mono-ubiquitination of FancD2. Mono-ubiquitinated FancD2 then translocates to sites of DNA damage, or nuclear foci, with several proteins including Brca1, Brca2 (FancD1), Rad51, and FancJ. It is still unclear why defects in the Fanc/Brca pathway lead to increased crosslinker sensitivity. However, as ICL-induced DSBs are thought to be resolved through homologous recombination during DNA replication, and radial strucutures are thought to arise from failed homologous recombination, the Fanc/Brca pathway is thought to be involved in homologous recombination repair of DSBs during DNA replication (See Figure 2). Additionally, the fact that cells from FA patients have fewer point mutations than unaffected cells, and the recent inclusion of error-prone translesion polymerases in the Fanc/Brca pathway, indicate that the Fanc/Brca pathway is

also involved in the toleration of DSBs through error prone bypass of DSBs during replication (Niedernhofer et al., 2005).

1.6 Interaction between TGFβ and Fanc/Brca Pathways

The TGFβ pathway has been implicated in maintenance of genomic integrity. Early studies indicated that alterations in the TGFβ signaling pathway lead to increased genomic aberrations. For example, TGFβ1 deficient keratinocytes demonstrated increased frequencies of gene amplification in response to N-phosphonoacetyl-L-aspartate (PALA), early aneuploidy, and increased chromosomal breaks compared to TGFβ1-expressing control keratinocytes, and these effects were suppressed upon exogenous TGFβ1 expression (Glick et al., 1999; Glick et al., 1996). Subsequently, connections between the TGFβ pathway and the Fanc/Brca pathway and genomic stability have been demonstrated. Administration of the TGFβ1 ligand led to decrease in Rad51 and correlated with decreased DNA repair efficiency in Mv1Lu lung epithelial cells (Kanamoto et al., 2002). Additionally, Brca2, a member of the Fanc/Brca pathway, which binds to Rad51 and localizes to sites of DNA damage, has been shown to form a complex with Smad3 and synergize in regulation of gene transcription (Preobrazhenska et al., 2002). Similarly, Smad3 was shown to colocalize with Brca1 in DNA repair complexes, and counteract BRCA1-dependent DNA repair in breast epithelial cells (Preobrazhenska et al., 2002).

1.7 Role of Inflammation in HNSCC

The association between immune and cancer cells has been observed for over a century (Balkwill and Mantovani, 2001). However, whether or not inflammatory cells are protective or carcinogenic is controversial, and likely immune cell specific. For example, antitumor cytotoxic T-cells and cytokine-mediated tumor lysis are important defenses against tumorigenesis. However, the elaboration by innate immune cells of mutagenic free radicals, growth factors, and tissue remodelling cytokines, chemokines, and matrix metalloproteinases (MMPs) promotes cancer formation, survival, invasion, and metastasis (Coussens and Werb, 2002). Epidemiological evidence has linked several chronic inflammatory conditions with susceptibility to cancer e.g., gastritis with gastric cancer, hepatitis with liver cancer, prostatitis with prostate cancer, and inflammatory bowel disease with colon cancer.

HNSCCs frequently develop from sites of chronic inflammation (*e.g.*, leukoplakia). Similarly, the infiltration of human HNSCCs with immune cells has been observed for several decades (Wolf et al., 1986), and this has been correlated with increased recurrence and metastasis (Young et al., 1997). In addition to exhibiting chronic inflammation, HNSCC cells secrete inflammatory cytokines and chemokines such as interleukin (IL)-1α, IL-6, IL-8, granulocyte-macrophage colony-stimulating factor, vascular endothelial growth factor, and basic fibroblast growth factor (Chen et al., 1999). Correspondingly, sera from patients with HNSCC exhibit increased acute phase proteins such as mean fibrinogen, C-reactive protein, and erythrocyte sedimentation rate, in comparison with normal control patient sera. Lastly, nuclear factor-κB (NFκB), a

transcription factor activated in response to inflammation, and involved in the elaboration of inflammatory cytokines and chemokines, is constitutively activated (phosphorylated) in HNSCC (Allen et al., 2007). Additionally, activated NFκB has been associated with tumorigenesis, metastasis, and poor clinical prognosis in HNSCC, further linking inflammation with tumorigenesis.

1.8 Role of TGFβ Signaling in Inflammation and HNSCC

TGFβ1 is ovexpressed in many epithelial cancers including HNSCC (Lu et al., 2006), and is a pleiotropic immunomodulator with both immunosuppressive and pro-inflammatory abilities (Teicher, 2007; Wrzesinski et al., 2007). TGFβ1 is able to suppress the activity of dendritic cells (DCs), natural killer (NK) cells, CD4+ T cells, and CD8+ cytotoxic T cells (CTLs), and recruit and activate T regulatory (Treg) cells (Figure 4).

Figure 4. TGFβ1 has Diverse Effects on a Wide Range of Immune Cells *(adopted from (Wrzesinski et al., 2007). Tumor cells from a wide variety of tissues secrete TGFβ1, as do stromal cells within solid tumors. TGFβ1 acts to inhibit tumor-killing cytotoxic T cells (CTLs) and natural killer*

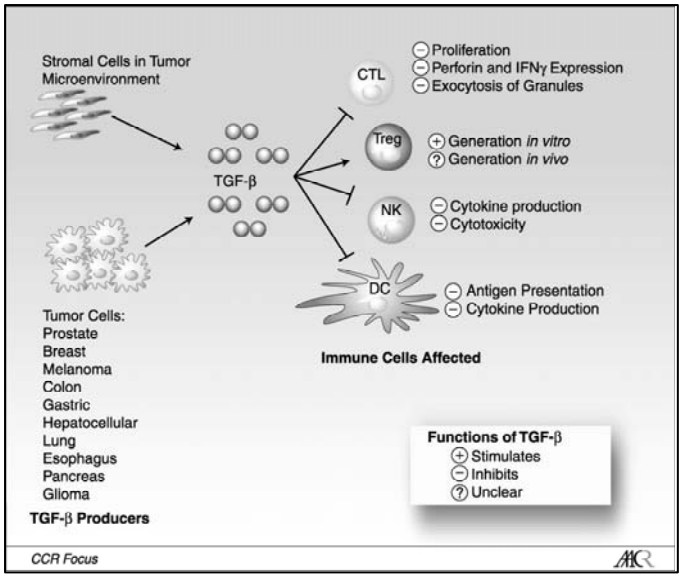

cells (NKs), and dendritic cells (DCs), but also stimulates immunosuppressive T regulatory cells (Tregs).

TGFβ1 is also important for B cell differentiation, including IgA isotype switching and antibody secretion (van Vlasselaer et al., 1992). Lastly, a new class of helper T cells, Th17 cells, which are characterized by the production of IL-17, have proven to be dependent on TGFβ1 for maturation and activation (Mangan 2006, Veldhoen 2006). Th17 cells promote granulopoiesis and neutrophil accumulation, and have been implicated in several inflammatory diseases.

CD4+ T cells, NK cells, DCs, and CTLs are key players in immune-mediated tumor suppression, but they are functionally inactivated in HNSCC (Moutsopoulos et al., 2008). Similarly, Treg cells, which serve to suppress DC maturation and anti-tumor immune responses, are found in HNSCC tissues and are elevated in sera from HNSCC patients. These data suggest that TGFβ is able to efficiently suppress the adaptive immune response to tumor antigens. TGFβ1 is also a potent chemoattractant of neutrophils and stimulates monocyte migration and differentiation, contributing to the chronic innate inflammation associated with carcinogenesis (Bierie and Moses, 2006b; Coussens and Werb, 2002).

We found that TGFβ1 transgene overexpression in the oral mucosa resulted in inflammation comprised of CD4+ T cells, granulocytes, and macrophages (Lu et al., 2004). TGFβ1-overexpressing mice also demonstrated increased angiogenesis and

epithelial hyperproliferation with overexpression of IL-1β, tumor necrosis factor α, and activation of NFκB compared to control mucosa. Similarly, we found that deletion of TGFβRII in head and neck epithelia resulted in elevated endogenous TGFβ1, which was associated with inflammation comprised of granulocytes and macrophages. TGFβRII knockout head and neck epithelia also exhibited increased angiogenesis and expression of IL-1β, macrophage inflammatory protein (MIP)-2 (the murine counterpart of IL-8), stromal-derived factor (SDF)-1, and the SDF-1 receptor, CXCR4 (Lu et al., 2006) in comparison with control mucosa. In combination with an activated Ras transgene, TGFβRII knockout epithelial cells developed invasive and metastatic HNSCCs, suggesting that the inflammation associated with blocking TGFβ signaling in head and neck epithelial cells was tumorigenic (Lu et al., 2006). In a similar study, TGFβRII was deleted in mammary epithelial cells, which led to the recruitment of Gr-1+CD11b+ myeloid cells to the invasive front of mammary carcinomas (Moses 2008). Additionally, in a 4T1 orthotopic tumor model of breast cancer metastasis, addition of Gr-1+CD11b+ immature myeloid cells significantly enhanced lung metastasis. Interestingly, CD11bhighGr-1+ cells were shown to be increased in a murine model of oral SCC, suggesting that this metastasis-promoting inflammation also applies to HNSCC (Oral Oncol 2007 Tanaka).

In addition to the above studies based on alterations of TGFβ signaling in epithelia, several studies have also highlighted the importance of TGFβ signaling components in the stromal compartment. Several genetic studies in T cells have shown that the immunosuppressive effect of TGFβ1 is important for tumorigenesis (Bierie and

Moses, 2006b; Wrzesinski et al., 2007). Expression of a dominant-negative TGFβRII in T cells led to excessive CD4+ T-cell differentiation and resistance to tumor engraftment, and the tumor resistance required the activity of both CD4+ and CD8+ T cells (Gorelik and Flavell, 2000; Gorelik and Flavell, 2001). Additionally, CTLs expressing a dominant negative TGFβRII were able to infiltrate tumors and block pulmonary metastasis in a mouse prostate cancer model, whereas normal CTLs were not (Zhang et al., 2005). Lastly, deletion of TGFβRII in fibroblasts led to prostatic intraepithelial neoplasia and invasive squamous cell carcinoma of the forestomach (Bhowmick et al., 2004), and also promoted mammary carcinoma growth and invasion through increased hepatocyte growth factor, macrophage stimulating factor 1, and transforming growth factor α (Cheng et al., 2005). Thus alteration of TGFβ signaling in both epithelial and stromal cells can lead to tumorigenesis through suppression of adaptive immune cells, recruitment of innate immune cells, and increased fibroblast paracrine signaling.

1.9 Role of Smad4 in Cancer

Smad4 was originally identified as a tumor suppressor in pancreatic cancer (Hahn et al., 1996), and subsequently characterized as a key mediator of TGFβ signaling (Zhang et al., 1996). Termed the "common Smad," Smad4 plays an instrumental role in TGFβ/BMP signaling by forming complexes with receptor activated Smads, i.e., Smads 2 and 3, or Smads 1 and 5. The Smad complexes then translocate to the nucleus to regulate gene expression of Smad targets involved in a wide variety of cancer-related processes including proliferation, apoptosis, and inflammation (Siegel and Massague, 2003). Somatic inactivation of *Smad4* is a frequent event in multiple tumor types including

pancreatic, colon, breast, and prostate cancer (Bierie and Moses, 2006a). *Smad4* deletion in murine tissues, in combination with other genetic alterations that provide tumor initiation events, resulted in cancer lesions of the colon (Kitamura et al., 2007; Takaku et al., 1998), pancreas (Bardeesy et al., 2006; Izeradjene et al., 2007), forestomach (Teng et al., 2006), and liver (Xu et al., 2006). Thus, Smad4 loss appears to play an important role in malignant progression. However, *Smad4* deletion in mice also resulted in spontaneous cancer formation of the stomach (Xu et al., 2000), skin (Li et al., 2003; Qiao et al., 2006; Yang et al., 2005) and mammary gland (Li et al., 2003), suggesting that Smad4 can both initiate and promote tumorigenesis in these tissues.

Our own studies and others have shown that Smad4 deletion blocks the growth inhibitory effect of TGFβ, resulting in hyperproliferation, with down-regulation of p21 and p27, and upregulation of c-Myc and cyclin D1 (Qiao et al., 2006; Yang et al., 2005). However, other than causing loss of expression of TGFβ target genes associated with growth inhibition, little is known about the molecular mechanisms of Smad4 loss-associated spontaneous tumorigenesis. The mechanisms associated with the tumor suppressive effect of Smad4 cannot simply be explained by its role as a TGFβ signaling mediator, as alterations of TGFβ ligands (e.g., TGFβ1) or receptors (e.g., TGFβRII) are generally insufficient for spontaneous cancer formation. SCCs generated from Smad4 deletion demonstrate inactivated Pten and activated Akt, (Qiao et al., 2006; Yang et al., 2005), and mice with deletion of both Smad4 and Pten resulted in accelerated tumor formation (Teng et al., 2006), suggesting there is crosstalk between TGFβ signaling and Akt/Pten signaling. Similarly, Kras can initiate tumorigenesis in tissues where Smad4

loss is insufficient for tumorigenesis (Izeradjene et al., 2007), indicating Ras activation may play a role in Smad4 loss-associated tumorigenesis.

Lastly, inflammation associated with loss of Smad4 has proven to be important for tumorigenesis. In a recent study, Smad4-deficient intestinal cells recruited immature myeloid cells expressing MMP2, MMP9, and the chemokine receptor CCR1 to the tumor invasion front (Kitamura et al., 2007). Further, deletion of CCR1 in this model prevented recruitment of immature myeloid cells and tumor invasion, indicating that recruitment of immune cells is a key mechanism in Smad4 loss-associated malignancy. Lastly, deletion of Smad4 specifically in T cells led to intestinal tumorigenesis, indicating that Smad4 signaling in T cells provides a tumor-suppressive effect (Kim et al., 2006). The mechanisms for spontaneous tumorigenesis through Smad4 loss, and the role of Smad4 loss in HNSCC tumorigenesis remain unclear.

1.10 Epidermal Stem Cells, Oral Stem Cells, and Keratinoctye Cancer Stem Cells

The cancer stem cell theory postulates that stem cells are the initiating cells for HNSCC cancer formation. With certain oncogenic alterations, normal stem cells are thought to convert into cancer stem cells (CSCs) that are not only able to self-renew, but also generate the entire tumor epithelia (Costea et al., 2006; Perez-Losada and Balmain, 2003). CSCs are largely quiescent but theoretically give rise to the much larger populations of proliferative cells (transiently amplifying cells) and post-mitotic differentiated cells. It remains unclear whether CSCs arise from tumorigenic changes in normal stem cells, or alterations in differentiated cells, yielding more undifferentiated

stem cell qualities. Putative CSCs are isolated on the bases of cell surface markers using flow cytometry, and are characterized by increased clonogenicity in vitro, and increased tumorigenicity in vivo (xenograft models).

While normal keratinocyte stem cells in the oral mucosa have not been well characterized, epidermal keratinocyte stem cells have been extensively investigated. Putative keratinocyte stem cells in the skin are located in the bulge region of the hair follicle, and are responsible for creating new hair follicles at the start of each hair follicle cycle. Label retaining studies have shown that bulge cells can also exit the bulge to participate in wound repair (Tumbar et al., 2004). Bulge stem cells can be identified with markers such as keratin 15 (K15), CD49f (alpha-6 Integrin), CD34, and more recently CD200 (Blanpain et al., 2004; Morris et al., 2004; Ohyama et al., 2006; Trempus et al., 2003). By transplanting either lacZ-labeled or GFP-labeled bulge cells onto immunodeficient mice, K15-expressing bulge stem cells were shown to be multipotent and capable of generating all skin lineages including the interfollicular epidermis, sebaceous glands, and hair follicles (Morris et al., 2004; Oshima et al., 2001). Microarray studies of FACS-sorted bulge cells compared to transiently-amplifying basal cells have shown that ~150 genes are preferentially expressed in the bulge, including genes in the Wnt and TGFβ signaling pathways (Tumbar et al., 2004). Additionally, BMP signaling is required for hair shaft differentiation (Kobielak et al., 2003), and deletion of BMP receptor 1a leads to bulge cell proliferation and inhibition of activated bulge cell differentiation (Kobielak et al., 2007).

It is generally thought that skin squamous cell carcinomas (SCCs) are derived from progenitor cells in the basal layer of the epidermis, sebaceous gland tumors are

derived from sebocyte progenitor cells, and basal cell carcinomas (BCCs) and other hair follicle tumors are derived from hair follicle progenitor cells (Owens and Watt, 2003). Therefore, since bulge stem cells are able to generate all lineages of the epidermis, oncogenic bulge stem cells can potentially give rise to all of the above tumor types. Supporting this idea, bulge stem cells from CD34 knockout mice were unable to proliferate and migrate out of their niche during hair follicle cycling and were also resistant to chemically-induced tumorigenesis, suggesting that bulge stem cells are the initiating cells for skin tumorigenesis (Trempus et al., 2007).

The oral cavity has a hierarchical structure of basal proliferating cells and suprabasal differentiated cells, similar to the skin epithelia. Cell lines derived from HNSCCs exhibit a hierarchical structure in vitro, with only a small percentage of cells exhibiting a clonogenic capacity (putative CSCs) (Mackenzie, 2004). However, few markers have been identified to isolate normal oral stem cells, and several of them are intracellular molecules that cannot be used for flow sorting (Costea et al., 2006; Tudor et al., 2004).

Similarly, until recently, there were few studies on HNSCC CSCs. However, CD44 has emerged as a CSC marker for HNSCC, as CD44+ cells isolated from HNSCC samples generated new tumors in a xenograft model, whereas CD44- cells did not (Prince et al., 2007). CD44+ cells also expressed K5/K14, whereas CD44- cells expressed more differentiated markers (i.e., Involucrin), confirming CD44+ cells were more primitive. Additionally, the ability of stem cells to exclude Hoechst dye (Goodell et al., 1996) has been used to isolate CSCs from HNSCC cell lines (Costea et al., 2006). The side population (SP) of Hoechst dye-excluding cells isolated by flow cytometry was shown to

be increased by EGF ligand exposure, indicating that dysregulated signaling pathways can lead to expansion of putative HNSCC CSCs (Chen et al., 2006b).

1.11. Role of Smad4 Loss in Keratinocyte Stem Cells

TGFβ1 has been shown to reduce the size of the SP in breast cancer cells and reduce their ability to form "mammospheres" in vitro (Tang et al., 2007). Similarly, breast cancer cells expressing a dominant negative TGFβRII exhibited a reduction in differentiated cells and an increase in progenitor cell proliferation rate. Lastly, in human breast cancer samples, TGFβ1 and TGFβRII expression correlated with more differentiated tumor cells. However, the role of Smad4 loss in epithelial stem cells is not known. Interestingly, deletion of Smad4 in the epidermis generates a range of skin tumor types including SCCs, sebaceous adenomas (SAs), BCCs, and trichoepitheliomas when driven by a K5 promoter, which targets a heterogeneous pool of progenitors including bulge stem cells (Perez-Losada and Balmain, 2003; Yang et al., 2005). Therefore, Smad4 loss in stem or progenitor cells in the bulge may lead to their tumorigenic expansion, and cause them to aberrantly retain multipotency. However, as K5 also targets differentiated cells in the basal layer of the epidermis, a role for differentiated cells in the generation of the aforementioned skin tumors can not be ruled out based on these studies (Figure 5).

Figure 5. Two Models for Tumor Heterogeneity – Genetic Changes in Bulge Stem Cells or Committed Progenitor Cells *[adopted from (Perez-Losada and Balmain, 2003)]. The skin consists of keratinocytes, sebaceous glands, and hair follicles. Tumors with differentiation along all three lineages are observed, however it is not know whether these arise from committed progenitors sensitive to different genetic insults (right panel) or if in accordance with cancer stem cell theory, they all arise from different genetic insults affecting only bulge stem cells (left panel).*

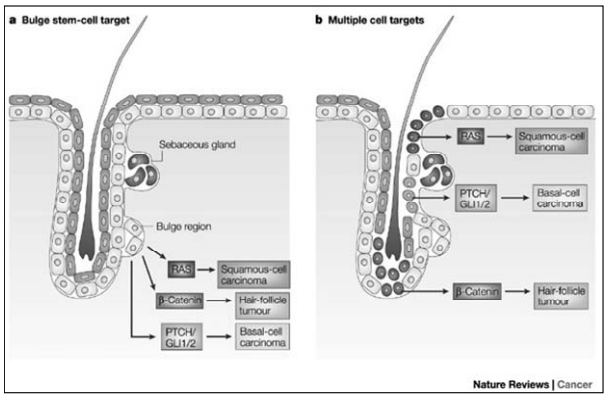

Recently, a K15 promoter fused to CrePR1 (K15CrePR1) has been generated, thus the effect of Smad4 loss on bulge stem cells can be adequately addressed. Understanding the effect of Smad4 loss on keratinocyte stem cells of the skin can inform future studies on the impact of Smad4 loss on head and neck stem cells, and the importance of this event in HNSCC tumorigenesis.

CHAPTER TWO

MATERIALS AND METHODS

2.1 Clinical Sample Collection

HNSCCs and case-matched adjacent tissue samples were surgically resected between the years 2000 and 2005 from consenting patients at the Department of Otolaryngology, Oregon Health & Science University, under an Institutional Review Board-approved protocol. Tissues examined in this study included 21 oral cavity SCCs, 9 larynx SCCs, 5 oropharynx SCCs, 1 nasal cavity SCC, and case-matched tissues adjacent to tumors. Seven normal oropharynx samples from sleep apnea patients were used as normal controls.

2.2 Mouse Strains

All animal experiments were performed using protocols approved by the IACUC at the Oregon Health & Science University. All animals used for the experiment are C57BL6 background.

Mouse Models for Head and Neck Cancer Study:

The inducible head and neck specific knockout system consists of two mouse lines (Figure 6), the *K14.CrePR1* or *K5.Cre*PR1* mice, in which Cre recombinase can be activated in head and neck epithelia by RU486 (Berton et al., 2000; Caulin et al., 2004), and the *Smad4f/f* mice, in which the *Smad4* gene is floxed (Yang et al., 2002). These

mouse lines were crossbred to generate compound mice, allowing for homozygous *Smad4* deletion.

Figure 6. Mating Strategy to Generate Smad4 Deletion in Head and neck Epithelia. *Mice expressing K14.CrePR1 or K5.Cre*PR1 were mated with mice expressing Smad4 with floxed Exon 8. Cre is only expressed in keratinocytes, through use of the keratin 14 and 5 promoters. RU486, a progesterone antagonist applied topically, binds to CrePR1 and translocates it into the nucleus to excise Smad4 Exon 8 in bigenic mice. Loss of Exon 8 renders the Smad4 transcript unstable, and it is rapidly degraded.*

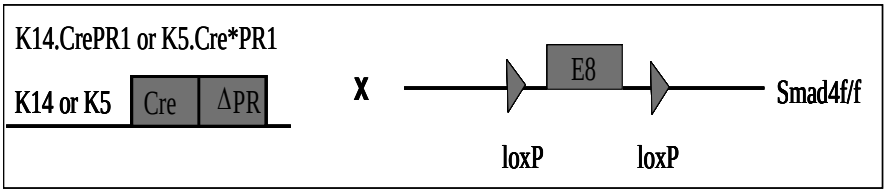

Littermates were genotyped at 3 weeks of age using primer pairs P9 and P10, which can differentiate between the floxed and wild-type allele (Figure 7, for genotyping primer sequences, see appendix B), and grouped based on genotypes for the experiments.

Figure 7. Smad4f/f Genotyping PCR*. Primers P9 and P10 were used to detect the floxed Smad4 allele; the larger PCR product contains the loxP sequence.*

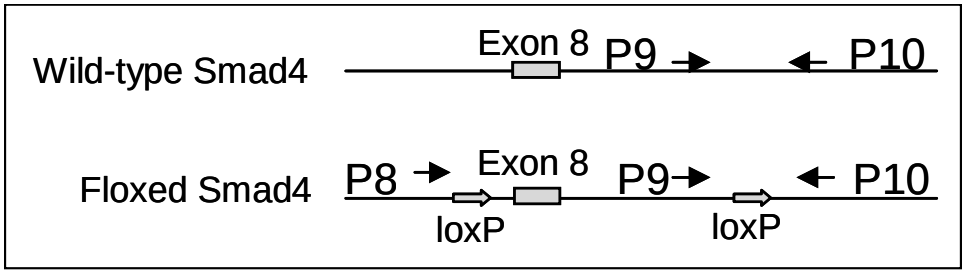

RU486 (100 μl of 0.2μg/μl in sesame oil) was applied in the oral cavity of 4-week-old bigenic mice daily for 5 consecutive days to induce homozygous deletion of the Smad4 gene. Monogenic littermates were treated with the same RU486 regimen as controls. To generate control tumors, we utilized an RU486-inducible *K15.CrePR1* line (Morris et al., 2004) in combination with a knock-in mutant *Kras* allele (Jackson et al., 2001) to generate *K15.CrePR1/Kras* mice (Figure 8).

Figure 8. Mating Strategy to Generate Kras Mutation in Head and neck Epithelia. *K15.CrePR1 mice were mated with K-rasG12D mice, which contain a floxed-stop allele in front of Exon 1. Upon Cre activation by RU486, the floxed stop cassette is removed, and mutant K-rasG12D is transcribed. K15 is expressed in keratinocyte stem cells of the skin and head and neck epithelia.*

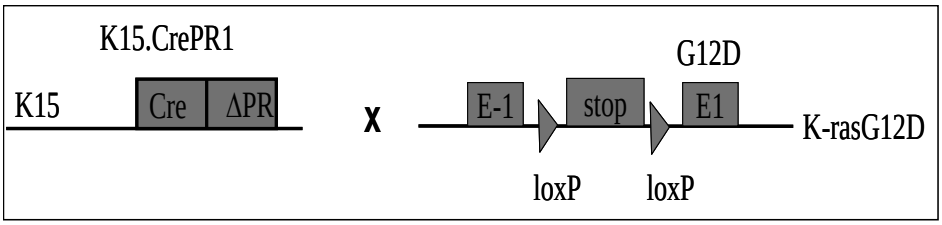

The *K15.CrePR1* promoter also targets *CrePR1* expression to head and neck epithelia. The general condition of the mice was checked at least once per week prior to the development of visible tumors. Mice with oral tumors were given soft food and monitored daily. Tumor-bearing mice were euthanized when oral tumors became ulcerated, or at the first sign of deteriorating health or pain resulting from tumors (e.g., huddled posture, vocalization, hypothermia, or ≥20% weight loss). Paired *Smad4f/f, Smad4f/w, K5.Cre*PR1*, or *K14.CrePR1* monogenic control littermates were euthanized

at the same time and the corresponding tissue samples were dissected as controls. Necropsy was performed on each euthanized mouse to identify primary tumors and distant metastases. To dissect early preneoplastic lesions, mice with each genotype were euthanized at 4 weeks after *Smad4* deletion, and head and neck tissue including the buccal tissue, tongue, esophagus, and forestomach were dissected.

Mouse Models for Skin Cancer Stem Cell Study:

Deletion of *Smad4* or *TGFβRII* and mutation of *Kras* in skin stem cells was accomplished using the *K15.CrePR1* promoter, which targets these genetic changes specifically to bulge stem cells in the skin. Bigenic *K15.CrePR1/Kras*^{G12D} mice were mated with either *Smad4f/f* mice or *TGFβRIIf/f* mice to generate tripligenic *K15.CrePR1/ Kras*^{G12D}*/Smad4f/f* (hereafter referred to as *K15.Kras/Smad4-/-* mice) and *K15.CrePR1/ Kras*^{G12D}*/TGFβRIIf/f* mice (hereafter referred to as *K15.Kras/RII-/-* mice, Figure 9).

Figure 9. Mating Strategy to Generate Deletion of Smad4 or TGFβRII and Mutation of Kras in Skin Stem Cells. *K15.CrePR1 mice were mated with K-rasG12D mice and either Smad4f/f mice or TGFβRIIf/f mice, in which Exon 2 of TGFβRII is floxed. Upon RU486 application, K-rasG12D is activated, and either Smad4 or TGFβRII are simultaneously deleted in keratinocyte stem cells.*

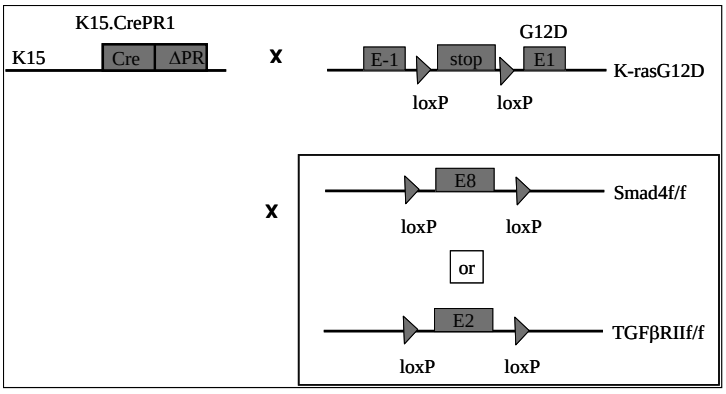

RU486 (100 μl of 0.2μg/μl in sesame oil) was applied to the backskin of 4-week-old triplegenic mice daily for 5 consecutive days to induce *Kras* mutation and homozygous deletion of the *Smad4* or *TGFβRII* genes. The general condition of the mice was checked at least once per week prior to the development of visible tumors. Mice with oral tumors were given soft food and monitored daily. Tumor-bearing mice were euthanized when oral tumors became ulcerated, or at the first sign of deteriorating health or pain resulting from tumors (e.g., huddled posture, vocalization, hypothermia, or ≥20% weight loss). Histological tumor types were determined by a dermatopathologist at the University of Colorado Health Sciences Center.

2.3 Characterization of Head and neck Epithelia-Specific Smad4 Knockout Mice

To verify Smad4 deletion in the head and neck epithelia, bigenic *K5.Cre*PR1/Smad4f/f or K14.CrePR1/Smad4f/f* mice and monogenic control mice were euthanized 10 days after the final RU486 treatment and extracted DNA from buccal mucosa, tongue, and esophagus. The recombinant Smad4 allele lacking exon 8 was readily detected in the above tissues by PCR in *K5.Cre*PR1/Smad4f/f* and *K14.CrePR1/Smad4f/f* bigenic mice, but not monogenic control littermates, using primer pairs P8 and P10 (Figure 10).

***Figure 10. Detection of Smad4 Deletion in Head and neck Tissue**. Primer pairs P8 and P10 were used to detect deletion of Exon 8, as the recombinant Smad4 allele can generate a*

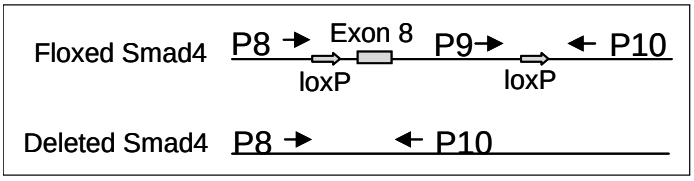

PCR product, while in the floxed Smad4 allele, primer pairs P8 and P10 are too far away to generate a PCR product.

2.4 Histology and Immunostaining

Parrafin Sections: Dissected epithelia and tumor samples were fixed in 10% neutral-buffered formalin at 4^{o}C overnight, embedded in paraffin, sectioned to 6 µm thickness and stained with H&E. HNSCCs were classified into well-, moderately- and poorly-differentiated groups based on disturbed cell polarity (mainly in basal cells), basal cell hyperplasia, disturbed maturational sequence, increased number of mitoses, mitoses in suprabasal layers, abnormal mitoses, nuclear hyperchromatism, prominent nucleoli, and increased nuclear/cytoplasmic ratio (Han et al., 2005).

Frozen Sections: Dissected epithelia and tumor samples were fixed in Optimal Cutting Temperature (OCT, Fisher Scientific) on dry ice and sectioned to 6 µm thickness using a cryotome.

For specific antibody dilutions and sources, see appendix A.

Parrafin Immunohistochemistry (IHC):

Sections were deparaffinized and rehydrated in Xylene for 30 minutes followed by 100% EtOH, 70% EtOH, and 50% EtOH for 5 minutes each. Slides were then boiled in 10mM Citric Acid for antigen retrieval. Sections were blocked in PBS with 5% serum from the host animal used for the secondary antibody for 1hr at room temperature. Primary antibodies were applied overnight in PBS at 4^{o}C. Secondary antibodies were applied for

20 minutes at room temperature. Avidin conjugated chromingen (M.O.M. kit, Vector Laboratories) was applied for 30 minutes at room temperature. DAB chromingen substrate (Dako Chemicals) was applied for 2 to 5 minutes. Sections were counterstained with Hematoxylin. Protein levels detected by immunohistochemistry were visually evaluated. Evaluation of Smad4, Brca1 and Rad51staining of human HNSCC samples was performed by two independent investigators.

Parrafin Immunofluorescence (IF):

After deparaffinization, antigen retrieval was performed by microwaving slides in 10 mM sodium citrate solution for 10 minutes. Sections were treated for 30 minutes at room temperature with Signal Enhancer (Invitrogen) to further enhance antigen retrieval, and incubated at room temperature for 15 minutes with a primary antibody diluted in phosphate-buffered saline (PBS) containing 12% bovine serum albumin (BSA). The sections were then washed with PBS and incubated for 10 minutes in the dark with fluorescence dye-conjugated secondary antibodies against the species of the primary antibody: Alexa Fluor 488-conjugated (green) or Alexa Fluor 594-conjugated (red) secondary antibody diluted in 12% BSA in PBS. Slides were mounted with Fluoromount G. Centrosome IF images were captured using confocal microscopy with a Leica SP2 confocal microscope (Leica Microsystems Inc.).

Tdt-mediated dUTP Nick-End Labeling (TUNEL) IF: Immunflurorescence of TUNEL assays was performed using the DeadEnd Fluoremetric TUNEL kit (Promega). Briefly, paraffin-embedded sections were deparrafinized, rehydrated, and washed in

0.85% NaCl. Sections were then sequentially prefixed in 4% formaldehyde in PBS, permeabilized in 20 μg/mL proteinase K, and postfixed in 4% formaldehyde in PBS. Slides were washed in PBS and incubated in a buffer containing fluorescein-dUTP and recombinant terminal deoxynucleotidyltransferase at 37^{o}C for 1 hour in the dark. The reaction was terminated in 2X SSC for 15 minutes at room temperature. The slides were then washed in PBS, and stained with 1 μg/mL propidium iodide for 15 minutes at room temperature to counterstain nuclei.

Frozen IHC and IF:

Slides were fixed in 4% paraformaldehyde for 40 minutes at room temperature. For IHC, sections were then blocked in PBS with 5% serum from the host animal used for the secondary antibody for 1hr at room temperature, and treated the same as paraffin sections for the remaining steps. For IF, sections were incubated in Signal Enhancer (Invitrogen) for 15 minutes and processed the same as paraffin sections after this step.

2.5 Cell Culture and Transfections

K5.CrePR1/Smad4f/w mice were mated with *Smad4f/f* mice, and pregnant mothers were exposed *in utero* to 100 μg/kg RU486 to accomplish *Smad4* deletion in bigenic *K5.CrePR1/Smad4f/f* embryos (Zhou et al., 2002). Pregnant mothers were then shipped to CellNTec (Millipore). Cell lines from neonatal bigenic mice (*Smad4-/-*) and monogenic *Smad4f/f* or *Smad4f/w* (*Smad4+/+*) control mice were generated by CellNTec (Millipore), and were cultured in keratinocyte-specific medium Cnt07 (Chemicon).

Human tongue SCC line Cal27 was purchased from ATCC and cultured in DMEM (ATCC) with 10% fetal bovine serum (FBS) and penicillin and streptomycin antibiotics. To create Cal27 lines stably expressing Smad4 (Cal27-Smad4), T25 flasks of subconfluent Cal27 cells were transfected with 8 μg pcDNA Flag-Smad4M purchased from Addgene, using Lipofectamine 2000 Transfection Reagent (Invitrogen) and selected in G418 (Sigma) for 4 weeks.

Human Epidermal Keratinocyte (neonatal) (HEKn) cells were purchased from Cascade Biologics and cultured in EpiLife medium with Human Keratinocyte Growth Supplement (HKGS, Cascade Biologics). To knockdown Smad4 in HEKn cells (HEKn + Smad4 siRNA), HEKn cells in 6-well plates at 50% confluency were treated with siRNA against Smad4 (Invitrogen) using XtremeGENE siRNA Transfection Reagent (Roche) at a final concentration of 50 pmol siRNA/uL in Optimem medium. Optimem medium with siRNA was changed to Epilife medium after 4 hours, and transfected cells were harvested after 48 hours. For siRNA sequence information, see appendix B.

HaCaT cells were cultured in high-glucose DMEM with 10% FBS and penicillin and streptomycin antibiotics. Twenty-four hours prior to siRNA transfection or TGFβ1/BMP-2 treatment, cells were switched to low-glucose DMEM with 0.2% FBS and penicillin and streptomycin antibiotics. Cells were transfected using XtremeGene siRNA Transfection Reagent (Roche) in 6-well plates at a final concentration of 50pmol siRNA/uL in Optimem medium. Optimem medium was switched to high-glucose DMEM after 4 hours, and cells were harvested after 72 hours. For siRNA sequence

information, see appendix B. For TGFβ1/BMP-2 treatment, cells were treated with 10 ng/mL ligand two hours before harvesting.

2.6 RNA Extraction and qRT-PCR

Total RNA was isolated from human and mouse skin and tumors using RNAzol B (Tel-Test), and a standard trizol-chloroform extraction, DNAnase treated, and further purified using a QIAGEN® RNeasy Mini kit (Qiagen). The qRT-PCR was performed using 100 ng of RNA per well using the One-Step Brilliant II QRT-PCR system (Stratagene). Transcripts were examined using Taqman® Assays-on-Demand™ probes (Applied Biosystems). An 18S, K14 or GAPDH RNA probe was used as an internal control. For TaqMan® probe details, see appendix C. Each sample was examined in triplicate. The relative RNA expression levels were determined by normalizing with internal controls, the values of which were calculated using the comparative C_T method.

2.7 Protein Extraction and Western Blotting

Protein was extracted as previously described (Li et al., 2004b). Briefly, cells were harvested in Complete Lysis Buffer M (Roche). Total protein was determined using detergent compatible to Bradford Assay reagents (BioRad). For Western blot, equal amounts of protein were separated on a 10% SDS-PAGE resolving gel with a 4% SDS-PAGE stacking gel. Protein was transferred to a nitrocellulose membrane and blocked using 5% non-fat milk in 0.1% Tween in TBS for 1 h at room temperature. Blots were double stained with 700nm and 800nm donkey IRDye-labeled secondary antibodies against target and loading control primary antibodies. For antibody details, see appendix

A. The blot was then incubated with an Alexa Fluor 700 or 800 secondary antibody (Molecular Probes), and scanned with the Odyssey Infrared Imaging System (LI-COR Biosciences).

2.8 DNA Extraction, PCR, and Sequencing

Genomic DNA was extracted from samples as previously described (Lu et al., 2006). Briefly, samples were lysed in DNA Extraction Buffer containing 50 mM Tris pH 8.0, 100 mM EDTA, 100 mM NaCl, 1% SDS, and 20 mg/ml Proteinase K overnight at 56 ^{o}C. Samples were vortexed and centrifuged to remove cellular debris, and cold 100% ethanol was added to precipitate DNA. Samples were centrifuged at 4^{o}C, and the DNA precipitate was washed in 70% ethanol through centrifugation at 4^{o}C. The DNA precipitate was air-dried at room temperature, and water was added to resuspend the DNA. A standard PCR reaction was performe (for PCR primers, see appendix B), and PCR products were sequenced by the OHSU Molecular Microbiology and Immunology (MMI) sequencing core. Sequences were uploaded and mutations were detected using Chromas Lite software.

2.9 Loss of heterozygosity (LOH) Analysis

DNA was extracted and PCR amplified using FAM-labeled forward primers for microsatellite markers adjacent to the Smad4 gene (for primer sequences, see appendix B). PCR products were column purified (Promega) and analyzed using fragment length polymorphism analysis (ABI) at the OHSU MMI sequencing core to determine the size of Smad4 alleles. Two PCR products (peaks) indicated a heterozygous sample, while one

product indicated a homozygous sample. LOH was positive if the following calculation: (peak height of allele 1 of tumor/peak height of allele 2 of tumor) compared to (peak height of allele 1 of adjacent skin/peak height of allele 2 of adjacent skin) was greater than or equal to 1.5.

2.10 SBE Identification and ChIP

SBE consensus sequences have been cataloged in the Transfac database and can be used to identify SBEs in gene promoters using Match software (Kel et al., 2003; Kloos et al., 2002). 4 kb promoter regions upstream of each gene's transcription start site were analyzed using Match and putative SBEs were given statistical likelihood for transcription factor binding. Criteria for SBEs were set at 100% core sequence match and 98% matrix match for Smad binding. For ChIP, 4 mouse backskins from wildtype neonatal micewere homogenized on ice in 5 mL 1% formalin to crosslink protein bound to DNA. An additional 5 ml of 1% formalin was added to each tube, and samples were incubated at room temperature for 30 minutes. ChIP was performed following the manufacturer's instructions (Active Motif ChIP-IT Express). Briefly, 1 ml of 10X Glycine Stop Solution was added, and samples were incubated at room temperature for 5 minutes. Samples were centrifuged and pelleted material was resuspended with 1 ml lysis buffer with protease inhibitors for 30 minutes on ice. Nuclei were released using a dounce homogenizer, pelleted, and chromatin shearing enzymes were added. After 10 minutes, sheared chromatin was pelleted. Sheared chromatin, Protein-G coated magnetic beads, and antibodies (1 μg) were incubated at 4 ^{o}C overnight to immunoprecipitate transcription factors bound to DNA. Immunoprecipitated chromatin was eluted, protein-

DNA crosslinks were reversed, and protein was degraded with proteinase K. The DNA products from each immunoprecipitation were used for PCR in triplicate using 5 μM ChIP primers (see appendix B).

2.11 aCGH

Mouse Whole-Genome CGH arrays (NimbleGen Systems, Inc.) comprised of 50-75mer oligo probes based on UCSC build MM8, with a median probe spacing of 5782 bp, were utilized to examine tumors for genetic imbalance. Genomic DNA from 5 *HN-Smad4-/-* HNSCCs were isolated and shipped to NimbleGen Systems, Inc., where they were fluorescently labeled, and hybridized to arrays. Tumor gene copy numbers were determined by comparison with reference DNA isolated from normal C57BL/6 mice after competitive hybridization. Data were analyzed with SignalMap software (Nimblegen Systems, Inc.) to identify deleted and amplified regions.

2.12 MMC Sensitivity Assay

Smad4-/- and *Smad4+/+* keratinocytes were seeded at a density of 10,000 to 20,000 cells/ml into 24-well plates, and treated the next day in triplicate with 0, 5, 10, 20, 40, and 80 ng/mL MMC in triplicate for 4 days. An MTT (3-(4,5-dimethylthiazol-2-yl)-2,5-diphenyl tetrasodium bromide) assay (Chemicon) was performed to assess for cell viability using the manufacturer's instructions. Briefly, medium containing MMC was gently removed, and fresh Cnt07 medium with 500 μg/ml MTT, which is cleaved by cells with active mitochondria to form formazan crystals, was added for 4 hours at 37^{o}C. Solution C (100 μl/ml) containing HCl (to alter the background color of phenol red from

tissue culture media) and isopropanol (to dissolve the MTT formazan crystals to a blue solution) was added for 30 minutes with vigourous pipetting, and the optical density of each sample at 570 nm was measured.

2.13 Chromosome Breakage Analysis

Chromosome breakage analysis was performed by the OHSU Cytogenetics Core. Cell cultures were treated with indicated concentrations of MMC (Sigma) in triplicate for 48 hours in the dark. Cells were then harvested after a 3 hour exposure to colcemid (0.05 μg/ml, Gibco). Following a 10 minute treatment with hypotonic solution (0.075M KCl, 5% fetal calf serum), the cells were fixed with a 3:1 mixture of methanol:acetic acid. Cells were dropped onto microscope slides for metaphase spreads and stained with Wright's stain (Fisher Scientific) for 3 minutes. 50 metaphase figures from each culture were scored for chromosome breaks and radial formations.

2.14 Nuclear Foci Immunofluorescence

Cells were cultured on chamber slides and treated with 20 ng/ml MMC (Sigma) for 24 hours. Cells were then fixed with 4% paraformaldehyde, permeabilized with 0.3% Triton X-100, digested in Pepsin Solution (Lab Vision), blocked for 1 hour with 10% normal goat serum + 0.1% NP-40, and incubated with Brca1 (Santa Cruz) or Rad51 (Santa Cruz) primary antibodies overnight. Alexa 488- or 594-conjugated secondary antibodies (Molecular Probes) were used for immunofluorescent staining, and images were taken using confocal microscopy with a Leica SP2 confocal microscope (Leica Microsystems Inc.).

2.15 TGFβ1 ELISA

Protein samples were extracted, acidified with 1 N HCl, and neutralized with 1.2 N NaOH/0.5 M HEPES to assay for the total amount of TGFβ1 protein (both latent and active forms). A TGFβ1 ELISA kit (R&D Systems) was used to quantify levels of TGFβ1 ligand, according to the manufacturer's instructions. Briefly, the ELISA plate coated with TGFβRII, was loaded with dilutions of recombinant TGFβ1 to create a standard curve, a TGFβ1 positive control, and 50 μl of tumor or mucosa samples in duplicate. A polyclonal antibody to TGFβ1 conjugated to horseradish peroxidase was added for 1.5 hours at room temperature, and a substrate solution (tetramethylbenzidine) was added for 20 minutes at room temperature. A stop solution containing 2 N sulfuric acid was added and the optical density of each plate at 450 nm and 540 nm was taken. 540 nm optical density values were subtracted from 450 nm values, and sample TGFβ1 concentrations were calculated using the standard curve. TGFβ1 concentrations were divided by the total protein concentrations (assessed by a Bradford assay) to determine the pg TGFβ1 per mg protein for each sample.

2.16 Superarray

RNA was amplified and labeled using Affymetrix protocols (http://www.affymetrix.com/support/technical/manual/expression_manual.affx) with the help of the OHSU Affymetrix Microarray Core and hybridized against the Oligo GEArray® Mouse Chemokines & Receptors Microarray (Superarray), following the manufacturer's instructions. Briefly, membranes were incubated with 10 μg biotinylated

RNA in triplicate, in a Multi-Chamber HybPlate (Superarray) at 60^{o}C overnight. Membranes were washed, blocked with GEAblocking Solution Q (Superarray) for 40 minutes, and incubated with a Streptavidin Alexa Fluor 680-conjugated antibody (Molecular Probes) at 1:7500 for 10 minutes. Membranes were washed and scanned with the Odyssey Infrared Imaging System (LI-COR Biosciences).

2.17 Tumor Cell Isolation and Flow Cytometry

After euthanasia, mice were placed in 70% ethanol to sterilize tumor tissue, and tumors were dissected to remove stromal tissues and finely minced. Minced tumor tissue was incubated in 0.35 g/mL collagenase (Invitrogen) in DMEM without serum for 45 minutes at 37^{o}C. The supernatant containing extracellular debris was discarded, and 0.25% trypsin (Invitrogen) was added for 30 minutes at 37^{o}C. The supernatant containing tumor cells was transferred into a 50 mL Falcon flask using a 70μm filter. The remaining cell pellet was incubated in 0.25% trypsin for 30 minutes at 37^{o}C and supernatants were combined, centrifuged at 2,000 rpm for 5 minutes, and cells were brought to 10^{6} cells/mL.in PBS with 3% FBS. For SP flow cytometry, 5 μl/ml Hoechst 33342 dye (Sigma), which is effluxed by stem cells, was added for 90 minutes at 37ºC. As a control, 100 μM verapamil (Sigma), which blocks stem cell efflux pumps, was added to an aliquot of Hoechst stained tumor cells. Cells were centrifuged and resuspended in 10^{6} cells/mL in PBS with 3% FBS. For CD34/CD49f flow cytometry, primary FITC-CD31, FITC-CD45, CD34-biotin, and PE-Cy5-CD49f antibodies (for antibody details, see appendix A) were incubated with tumor cells for 30 minutes. Single color controls were also added to aliquots of tumor samples. Streptavidin-PE was then added as a secondary for CD34-

biotin for 30 minutes, cells were centrifuged, and resuspended to 5 x 10^6 cells/ml in DMEM with 10% FBS. Before flow cytometry, Propidium Iodide (2 μg/ml, Sigma) was added to discriminate dead cells, and cells were filtered with a 40 μm filter.

2.18 Grafting

Nude mice were anesthetized and their backskins were disinfected with 70% ethanol. Using scissors, two small holes were made in the backskin and underlying connective tissue was dissected. Two plastic chambers containing a 1.5 mm hole exposed to the air were placed in each dissected hole between the muscle fascia and skin. A mixture of $1X10^6$ fibroblast cells isolated from neonatal mouse backskins, $1X10^6$ keratinocytes isolated from neonatal mouse backskins, and flow-sorted tumor cells (either test or negative controls) were injected into the chamber hole. The test and negative control flow-sorted cells were injected into chambers on the same mouse. The protruding portion of the chamber was cut after 1 week, the entire chamber was removed after 2 weeks and the mice were observed for tumor formation.

2.19 Statistical Analysis

Statistical differences between two groups of data were analyzed using a Student's *t*-test with the exceptions of centrosome quantification in Figure 23, foci quantification in Figure 29, and the correlation in Table 2, which were calculated using a two-tailed Fisher's Exact Test; and chromosome breakage data in Figure 25B, which was calculated using a chi-square test. The data are presented as mean ± SE (standard error).

CHAPTER THREE

RESULTS

3.1 Pretranslational Loss of Smad4 Occurred at an Early Stage in Human HNSCC

To determine which stage Smad4 was downregulated in human HNSCC, 36 pairs of human HNSCCs and mucosa samples adjacent to each HNSCC were analyzed for loss of Smad4 mRNA by quantitative RT-PCR (qRT-PCR), using normal mucosa samples from sleep apnea patients as a control. Compared to normal sleep apnea control samples normalized to 100 ± 25%, the average mRNA expression level in HNSCCs was 28 ± 4%, and the average mRNA expression level in adjacent mucosa samples was 43 ± 5%. Among these samples, 86% (31/36) of HNSCC samples exhibited downregulation of Smad4 mRNA to less than 50% of Smad4 levels in control mucosa samples. In addition, 67% (24/36) of adjacent mucosa samples exhibited more than 50% downregulation of Smad4, indicating that Smad4 loss occurred early in cancer development (Figure 11).

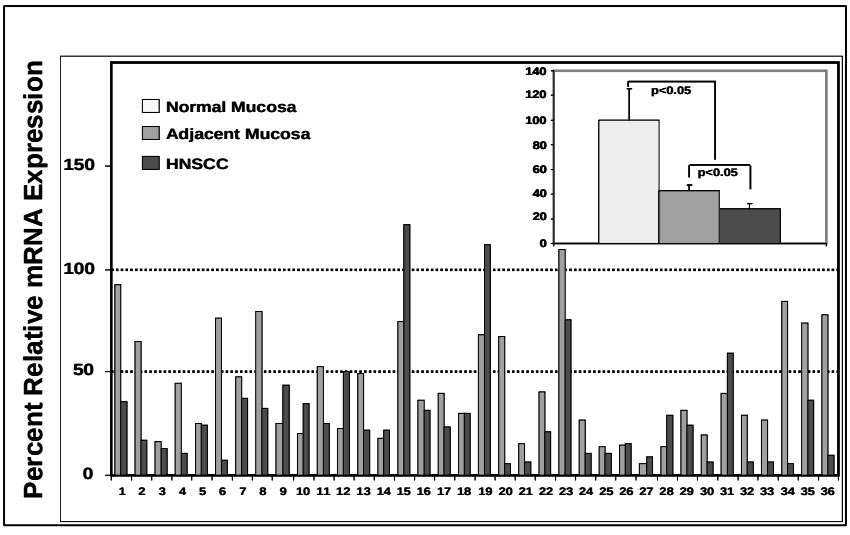

Figure 11. Smad4 is Lost at the mRNA Level in Human Adjacent Mucosa and HNSCC *Relative Smad4 mRNA expression examined by qRT-PCR of 7 normal*

sleep apnea controls, 36 HNSCC samples, and 36 matched adjacent mucosa samples. The relative expression of Smad4 in sleep apnea controls was arbitrarily set as 100%. Loss of expression was defined as less than 50% of normal sleep apnea controls. The average Smad4 expression from each group is presented in the inset. Error bars indicate the standard error of the mean (SE), and significance was determined using a Student's t-test.

We then performed Smad4 immunohistochemistry (IHC) on this sample set and found that while Smad4 stained strongly in the normal control group, Smad4 staining was significantly reduced or lost in adjacent mucosa samples and HNSCCs (Figure 12).

Figure 12. Loss of Smad4 in human HNSCC revealed by Immunohistochemistry (IHC). *IHC staining of Smad4 (brown) in an HNSCC (right panel), matched adjacent mucosa (middle panel), and a normal sleep apnea control (left panel). The scale bar in the left panel represents 40 μm for all panels.*

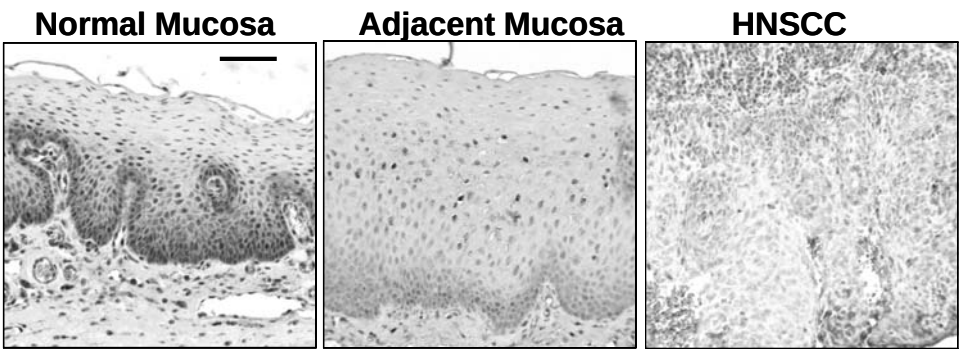

To determine the mechanism of Smad4 mRNA expression loss, a LOH analysis using microsatellite markers proximal to Smad4 (D18S46, D18S474, D18S1110) was performed. Previous studies have reported loss at this locus to be approximately 50% in

HNSCC (Kim et al., 1996; Papadimitrakopoulou et al., 1998; Takebayashi et al., 2000), although mutation of Smad4 was infrequent (Kim et al., 1996). We determined that 70% (7/10) of the samples exhibited loss of at least one of the microsatellite markers proximal to Smad4 (Figure 13).

Figure 13. Loss of heterozygosity analysis at the Smad4 locus occurred in the majority of adjacent mucosa and HNSCC pairs analyzed. *(A) The human Smad4 locus on the UCSC genome browser with microsatellite markers used for LOH analysis (top). Example of LOH, where the HNSCC sample had a reduction in the second allele peak compared to the adjacent mucosa sample (bottom). (B) Results of LOH analysis. Sample pairs are listed at the top, and microsatellite markers used for PCR are listed on the left side. Markers showing LOH, retention of heterozygosity, or that were homozygous in the adjacent mucosa sample (not informative) are displayed. * = LOH*

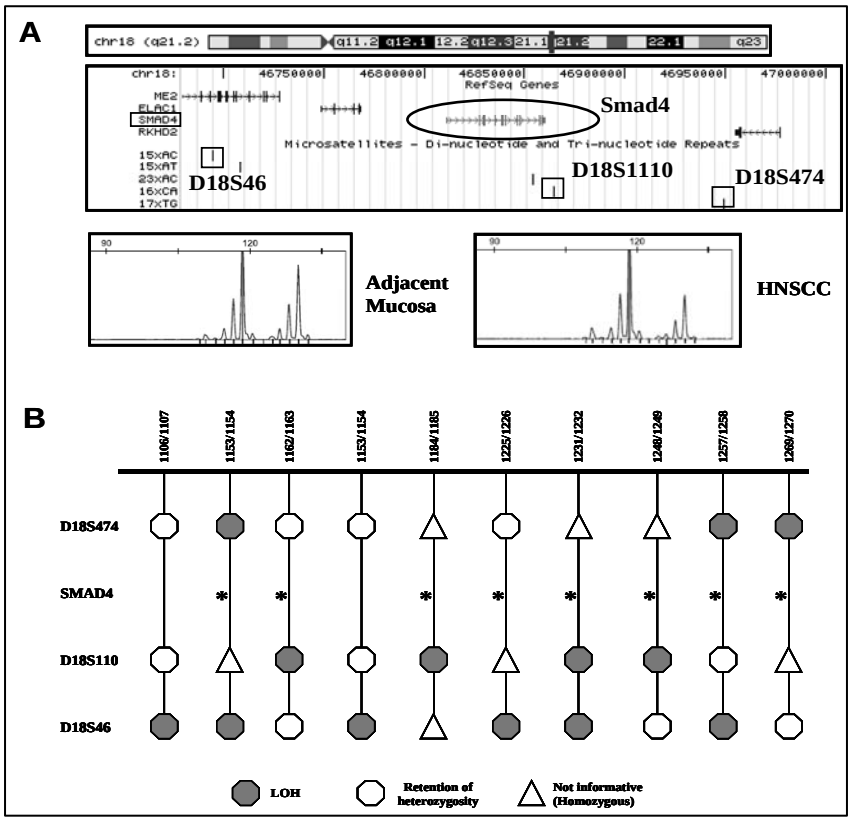

Notably, several adjacent mucosa samples that exhibited mRNA loss were heterozygous for the above microsatellite markers (informative cases), indicating that genetic loss was not responsible for the observed Smad4 downregulation in adjacent mucosa. These data indicate that at least one copy of Smad4 is lost during HNSCC tumorigenesis, but that other unknown mechanisms act to downregulate Smad4 expression in normal adjacent mucosa and HNSCC.

3.2 Characterization of Head and neck Epithelia-Specific Smad4 Knockout Mice

The floxed *Smad4* allele was detected in Cre-positive *Smad4f/f* or *Smad4f/w* mice using primers 9 and 10 (Figure 14, "WT" indicates the wild-type *Smad4* allele), and bigenic mice were treated with RU486 along with littermate controls (see section 2.2 for more details). To verify *Smad4* deletion in the head and neck epithelia of bigenic mice, *K5.Cre*PR1/Smad4f/f* or *K14.CrePR1/Smad4f/f* bigenic and control *K5.Cre*PR1*, *K14.CrePR1*, or *Smad4f/f* mice were euthanized 10 days after the final RU486 treatment and extracted DNA from buccal mucosa, tongue, and esophagus. The recombinant *Smad4* allele lacking exon 8 was readily detected in the above tissues by PCR in *K5.Cre*PR1/Smad4f/f* and *K14.CrePR1/Smad4f/f* bigenic mice (hereafter referred to as *HN-Smad4-/-* mice), but not monogenic control littermates (hereafter referred to as *HN-Smad4+/+* mice), using primer pairs P8 and P10 (Figure 14).

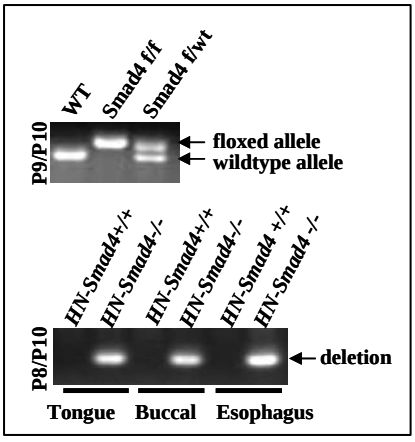

Figure 14. Detection of Smad4f/f allele*. An example of Smad4 genotyping PCR using primers 9 and 10 ("WT" indicates the wild-type Smad4 allele), and detection of the recombinant allele with deleted exon 8 in bigenic mice, using deletion-specific PCR with primers 8 and 10.*

To confirm that Smad4 was lost at the mRNA level in *HN-Smad4-/-* mucosa and HNSCCs, relative expression of Smad4 transcripts was examined by qRT-PCR. While Smad4 transcripts were detected in the buccal epithelia of a *HN-Smad4+/+* mouse orally treated with RU486, Smad4 was specifically ablated in the buccal mucosa of a *HN-Smad4-/-* mouse treated orally with RU486, and an HNSCC arising from a *HN-Smad4-/-* mouse (Figure 15A). Residual expression in these tissues is due to contaminating stromal cells that retain expression of Smad4. To confirm Smad4 was lost at the protein level in *HN-Smad4-/-* mucosa and HNSCC, IHC using an antibody to Smad4 was performed. While the Smad4 protein was detected in the buccal epithelia of a *HN-Smad4+/+* mouse orally treated with RU486, Smad4 was specifically ablated in the buccal mucosa of a *HN-Smad4-/-* mouse treated orally with RU486, and an HNSCC arising from a *HN-Smad4-/-* mouse (Figure 15B).

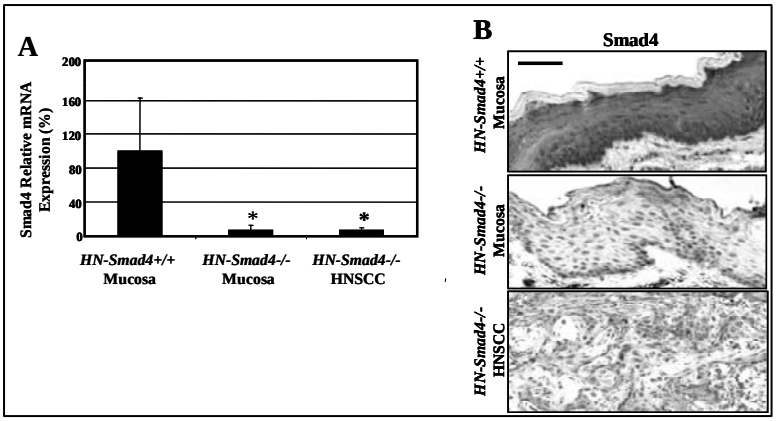

Figure 15. Detection of Smad4 loss at the mRNA and protein level. *(A) Relative expression of Smad4 transcripts examined by*

*quantitative RT-PCR (qRT-PCR). Smad4 expression was lost in HN-Smad4-/- mucosa and HNSCCs. Residual expression in these tissues is likely due to contaminating dermis that retains expression of Smad4. The average expression from 5-10 samples in each group are presented. The average expression of Smad4 in the HN-Smad4+/+ samples was arbitrarily set to 100%. Error bars indicate SE. Significance was calculated using a student's t-test: * = p<0.05 in comparison with HN-Smad4+/+ mucosa. (B) IHC of Smad4 in mouse buccal tissue and HNSCC. Note that the Smad4 protein was detected in the buccal epithelia of a HN-Smad4+/+ mouse orally treated with RU486. Smad4 was specifically ablated in the buccal mucosa of a HN-Smad4-/- mouse treated orally with RU486, and an HNSCC arising from a HN-Smad4-/- mouse. 5-10 samples from each group were examined and a representative picture is presented. The scale bar in the top panel represents 40 μm for all panels.*

3.3 Deletion of Smad4 in Murine Head and Neck Epithelia Resulted in Spontaneous HNSCC

The high frequency of Smad4 loss in human HNSCC, particularly at the stage prior to tumor formation, prompted us to investigate whether Smad4 loss played a causal role in HNSCC tumorigenesis. We used our inducible and head and neck specific knockout system (Caulin et al., 2004; Lu et al., 2006), which allows *Smad4* deletion (*HN-Smad4-/-*) in head and neck epithelial cell upon RU486 application to the oral cavity. We induced *Smad4* deletion in the head and neck epithelia at 4 weeks of age. In total, 35 *HN-Smad4-/-*, 9 *HN-Smad4+/-*, and 23 *HN-Smad4+/+* mice (all in the C57/BL6 background) were monitored for tumor formation for up to 80 weeks. Beginning at 29 weeks of age, *HN-*

Smad4-/- mice began to develop oral tumors. By 80 weeks, 74% (26/35) developed spontaneous oral tumors, and 12% (3/26) of tumor-bearing mice harbored regional lymph node metastases prior to being euthanized. Most tumor-bearing mice required euthanasia prior to potential metastasis, due to difficulties with food intake or excessive bleeding, which are problems often encountered in human HNSCC patients. No tumors were observed in either *HN-Smad4+/-* or *HN-Smad4+/+* mice (Figure 16).

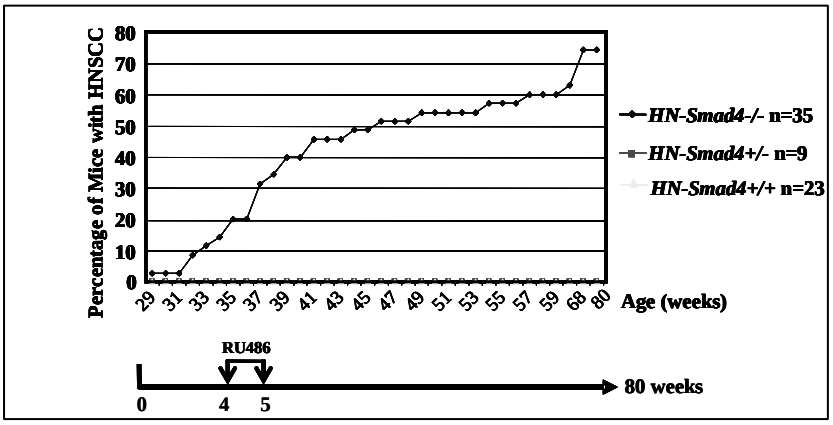

Figure 16. Kinetics of tumor formation in HN-Smad4-/- mice. *Tumor formation was assessed by bi-weekly examination of the oral cavity in live mice, and necropsy at the time of euthanasia. Data points represent the percentage of tumor-bearing mice compared to the total number of mice in each group. * Original tumorigenesis study for this figure performed by Dr. Shi-Long Lu.*

3.4 Smad4 Knockout HNSCC Mimicked Human HNSCC at Histological and Molecular Levels

Tumors generated from *HN-Smad4-/-* mice were derived from the buccal mucosa (Figure 17A) and palate (data not shown). Histologically, *HN-Smad4-/-* HNSCCs exhibited regions ranging from moderately to poorly differentiated squamous cell carcinoma

(SCC). The precursor lesions were developed from hyperplasia to dysplasia (Figure 17B), which were similar to head and neck cancer development in human patients. HNSCC cells displayed enlarged nuclei and increased mitoses (Figure 17C). Keratin staining revealed that the adjacent mucosa of *HN-Smad4-/-* HNSCCs expressed Keratin 13 (K13), which is a marker of oral epithelia (Bloor et al., 1998), but not hyperplastic epidermis, verifying the tumors were derived from the oral cavity rather than the skin (Figure 17D). However, *HN-Smad4-/-* HNSCCs exhibited patchy loss of this differentiation marker, which indicates malignant conversion (Figure 17D) (Lu et al., 2006). Histological sections of enlarged regional lymph nodes demonstrated HNSCC metastases. As shown in Figure 17E, keratin pearls, which are pathoneumonic for SCCs, are adjacent to lymphatic tissue. Keratin staining of these lymph nodes (Figure 17F) further verified that metastases arose from HNSCCs, as K13, as well as the general keratinocyte marker Keratin 14 (K14), both stained the lymph node section.

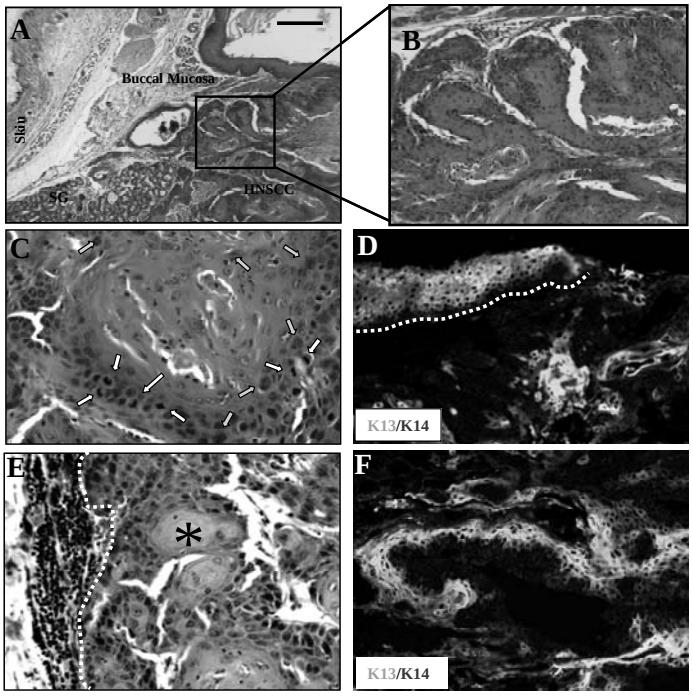

Figure 17. Characterization of HN-Smad4-/- HNSCC. *(A) A hematoxylin and eosin (H&E) stained tumor section of a buccal SCC in a HN-Smad4-/- mouse demonstrates that HNSCCs were derived from the buccal mucosa and not the skin of HN-Smad4-/- mice. SG: salivary gland*

*adjacent to the HNSCC. (B) A dysplastic region in the HNSCC from panel B. (C) High magnification shows SCC cells with enlarged nuclei (green arrows) and increased mitosis (white arrows), indicative of malignant pathology. (D) Staining of keratin 13 (green), which stains stratified epithelia, counterstained with general keratinocyte marker, keratin 14 (red), in a buccal SCC from a HN-Smad4-/- mouse indicates tumors are derived from buccal mucosa. The white dotted line highlights the adjacent mucosa. (E) H&E tumor section of a lymph node metastasis in a HN-Smad4-/- mouse. The white dotted line delineates the boundary between metastatic tumor cells and lymph node tissue. The asterisk indicates a keratin pearl. (F) Staining of keratin 13 (green), counterstained with keratin 14 (red) in a lymph node metastasis from a HN-Smad4-/- mouse indicates the tumor is derived from an HNSCC. The scale bar in panel B represents 100 mm for B; 40 mm for C, E, and G; and 20 mm for D and F. * Original characterization for this figure performed by Dr. Shi-Long Lu.*

In addition to the above histological changes, we found several molecular changes in the *HN-Smad4-/-* HNSCCs that are common in human HNSCC, including increased nuclear NFkB p50 and p65 subunits, increased pAKT, and increased pStat3 (Figure 18). Interestingly, increased nuclear NFkB subunits and pStat3 were also found in *HN-Smad4-/-* mucosa samples, indicating these might cooperate with Smad4 during HNSCC tumorigenesis (Figure 18).

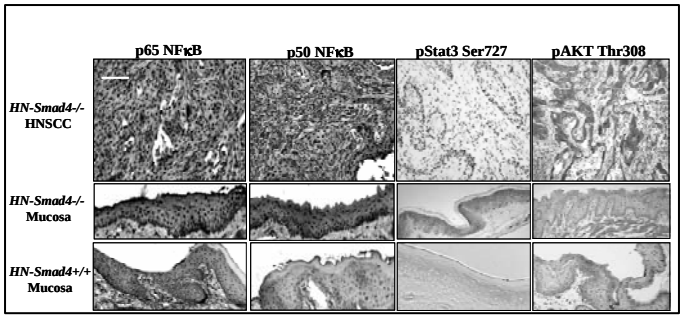

Figure 18. HN-Smad4-/- Mucosa and HNSCCs displayed molecular

alterations common in human HNSCCs*. IHC staining of HN-Smad4+/+ mucosa, HN-Smad4-/- mucosa, and HN-Smad4-/- HNSCCs. HN-Smad4-/- mucosa and HNSCC samples exhibited increased NFkB p50 and p65 subunits, as well as increased phosphorylated (activated) Stat3. HN-Smad4-/- HNSCCs also demonstrated increased activated AKT. The scale bar in the upper left panel represents 40 μm for all panels.*

3.5 Smad4 Knockout Mucosa and HNSCCs Exhibited Increased Proliferation and Reduced Apoptosis

As a central mediator of TGFβ signaling, Smad4 is able to mediate the tumor suppressor roles of TGFβ, such as growth inhibition and apoptosis, which are well-documented functions of Smad4 and are reflected in *HN-Smad4-/-* mucosa and HNSCCs. PCNA staining for proliferative cells and TUNEL staining for apoptotic cells revealed increased cell proliferation and reduced apoptosis in *HN-Smad4-/-* mucosa and HNSCCs compared to *HN-Smad4+/+* mucosa (Figure 19). The number of TUNEL positive cells was 3.7 ± 1.7 per section in *HN-Smad4+/+* mucosa, but was reduced to 2.6 ± 0.9 in *HN-Smad4-/-* mucosa and 1.0 ± 0.2 ($p<0.05$) in *HN-Smad4-/-* HNSCCs.

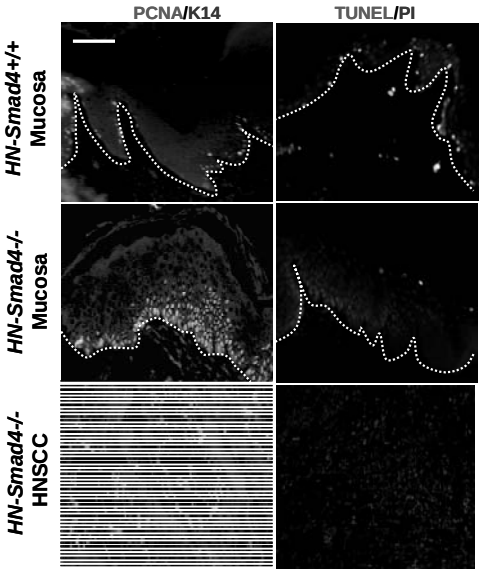

Figure 19. HN-Smad4-/- HNSCCs Exhibited Increased Proliferation and Reduced Apoptosis*. PCNA staining of HN-Smad4+/+ mucosa, HN-Smad4-/- mucosa, and HN-Smad4-/- HNSCCs (left panels). HN-Smad4-/- mucosa had increased proliferation compared to HN-*

*Smad4+/+ mucosa, and proliferation was further increased in HN-Smad4-/- HNSCCs. 5-10 samples were analyzed and a representative picture is presented. TUNEL staining of HN-Smad4+/+ mucosa, HN-Smad4-/- mucosa, and HN-Smad4-/- HNSCCs (right panel). Apoptosis was reduced in HN-Smad4-/- mucosa compared to HN-Smad4+/+ mucosa, and further reduced in HN-Smad4-/- HNSCCs. 5-10 samples were analyzed and a representative picture is presented. The scale bar in the upper left panel represents 20 μm for all panels. * TUNEL staining for this figure performed by Dr. Stephen Malkoski.*

3.6 Smad4 Cooperates with Ras Activation during HNSCC Tumorigenesis

While increased proliferation and reduced apoptosis play an important role in tumorigenesis, these changes did not explain why *Smad4* gene deletion alone was sufficient for HNSCC formation, as similar alterations were also observed in *TGFβRII-/-* head and neck keratinocytes, which required additional Ras activation for HNSCC tumorigenesis (Lu et al., 2006). Thus, we sequenced *K-ras* and *H-ras* genes in *HN-Smad4-/-* HNSCCs. From a total of 18 tumors examined, 4 exhibited *H-ras* mutations at codon 61. Among the tumors with *H-ra*s mutations, 2 changed CAA to CTA, 1 changed CAA to CAC, and 1 changed CAA to CGA (Figure 20A). All of these mutations are associated with *H-ras* activation (Rodriguez-Viciana et al., 2005). No *K-ras* mutation was detected in *HN-Smad4-/-* HNSCCs. However, similar to our previous observation in human HNSCCS, tumors without a *Ras* mutation exhibited increased Ras protein levels (Figure 20B). These data suggest that spontaneous Ras activation via mutation or overexpression could provide an initiation event for HNSCC formation in at least a subset of *HN-Smad4-/-* tumors. To test this, we generated mice with heterozygous

deletion of *Smad4* together with heterozygous *HN-K-ras*^{G12D} mutation in the head and neck epithelia (*HN-K-ras*^{G12D}*/Smad4+/-*) using a breeding strategy similar to our previous report (Lu et al., 2006). *HN-K-ras*^{G12D}*/Smad4+/-* mice developed HNSCCs within only 3 months of gene mutation/deletion (Figure 20C). This result not only further confirmed that spontaneous Ras activation could provide an initiation event, but also suggests a haploid insufficiency of Smad4 in the setting of other initiating alterations in head and neck epithelia.

Figure 20. Ras Activation Cooperates with Smad4 in HNSCC Tumorigenesis*. (A) H-ras sequencing traces in HN-Smad4-/- HNSCCs revealed mutations in codon 61. Examples of each type of mutation (CAA to CAC, CTA, or CGA) are presented. (B) IHC for Ras revealed that Ras proteins were overexpressed in HN-Smad4-/- mucosa and HNSCCs compared to HN-Smad4+/+ mucosa. (C) H&E staining of HN-K-ras*^{G12D}*/Smad4+/- dyspastic mucosa and HNSCC sections. Whereas HN-Smad4+/- mice did not develop tumors, HN-K-rasG12D/Smad4+/- mice*

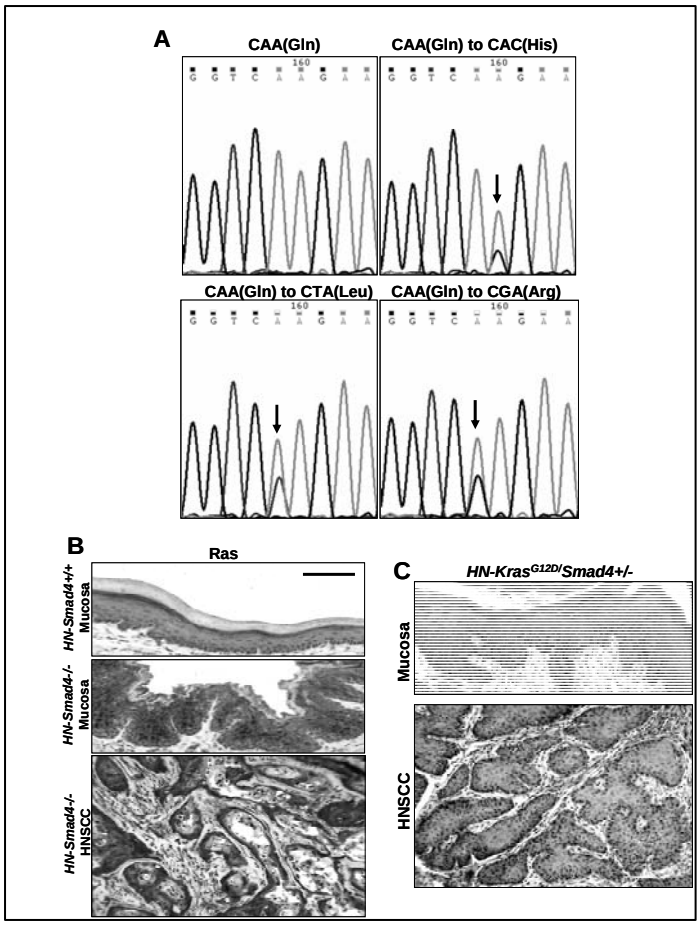

developed tumors with reduced latency compared to HN-Smad4-/- mice.The scale bar in the top panel of B represents 40 μm for all panels in B and C.

3.7 Smad4 HNSCCs Exhibited Downregulation of Fanc/Brca Pathway Genes

Invasive and metastatic HNSCC formation, as well as spontaneous Ras mutations, resulting from *Smad4* single-gene deletion prompted us to assess if DNA repair mechanisms resulting in genomic instability were perturbed after Smad4 loss. We examined expression levels of genes in the Fanc/Brca pathway, which is not only related to DNA repair and genomic instability but also the only known pathway leading to HNSCC susceptibility in humans (Kutler et al., 2003). Interestingly, compared to *HN-Smad4+/+* mucosa, *HN-Smad4-/-* HNSCCs exhibited decreased mRNA expression of Brca1 by 74 ± 13%, FancA by 95 ± 2%, FancD2 by 96 ± 2%, and Rad51 by 93 ± 2%. In addition, *HN-Smad4-/-* mucosa exhibited reduced expression of Brca1 by 84 ± 12%, FancA by 94 ± 1%, FancD2 by 91 ± 2%, and Rad51 by 61 ± 17%, suggesting that these alterations occurred prior to tumor formation (Figure 21A). The transcriptional downregulation of Brca1 and Rad51 in *HN-Smad4-/-* mucosa and HNSCCs also correlated with their protein loss detected by IHC (Figure 21B).

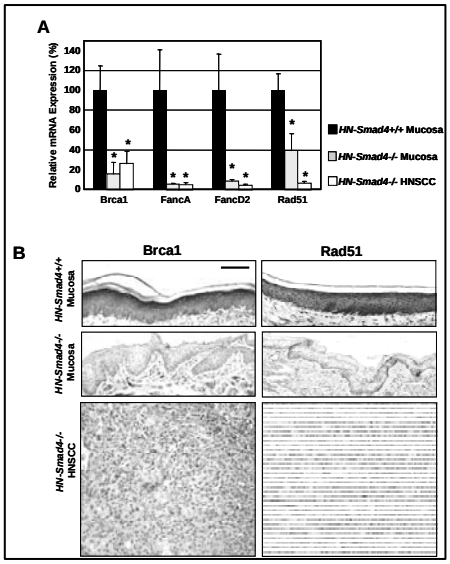

Figure 21. Downregulation of Fanc/Brca Transcripts in HN-Smad4-/- mucosa and HNSCCs*. (A) Decreased relative mRNA expression of Brca1,*

*FancA, FancD2, and Rad51 in HN-Smad4-/- mucosa and HNSCCs, compared to HN-Smad4+/+ mucosa by qRT-PCR. Averages of 5-10 samples from each group are presented and error bars indicate SE. The average expression of Smad4 in the HN-Smad4+/+ samples was arbitrarily set at 100%. Significance was determined using a student's t-test: * = p <0.05 compared to HN-Smad4+/+ mucosa. (B) Decreased Brca1 and Rad51 protein by IHC in HN-Smad4-/- mucosa and HNSCCs compared to HN-Smad4+/+ mucosa. 5-10 samples per group were analyzed, and a representative picture is presented. The scale bar in the upper left panel represents 40 μm for all panels.*

To determine whether Smad4 might directly bind to the promoters of Brca1, FancA, FancD2, or Rad51, we assessed 4 kb upstream of the transcription start site for potential SBEs and performed ChIP to determine if Smad4 bound with other R-Smads to directly regulate gene expression. While there were no putative SBEs in the promoter of FancD2, we found several SBEs in the promoters of Brca1, FancA, and Rad51, and found positive binding of Smads 2-4 on the promoters of FancA (136 bp upstream from the transcription start site or TSS) and Brca1 (3031 bp upstream from the TSS), and of Smads 3 and 4 on the promoter of Rad51 (797 bp upstream from the TSS). A negative IgG control did not bind, nor did a control primer amplify non-specifically. For ChIP PCR sequences, see appendix B. Additionally, RNA Polymerase II (Pol II) bound to the promoters of Brca1 and Rad51, indicating these genes are actively transcribed by Smads (Figure 22A).

To determine whether Smad4 regulated transcription of Fanc/Brca genes in response to TGFβ1 or BMP signals, we treated HaCaT keratinocytes with TGFβ1 or BMP2 ligand

2 hours prior to harvesting. Interestingly, while TGFβ1 treatment significantly upregulated Brca1 from 1.0 ± 0.2 fold in untreated cells to 8.4 ± 0.9 fold, FancA from 1.0 ± 0.1 to 1.7 ± 0.2 fold, and Rad51 from 1.0 to 0.1 fold to 2.7 ± 0.7 fold, BMP2 treatment significantly downregulated Brca1 by 0.2 ± 0.1 fold, FancA by 0.3 ± 0.1 fold, and Rad51 by 0.2 ± 0.1 fold, indicating that Smad4 may be involved in balancing these two signaling pathways to regulate transcription of Fanc/Brca pathway genes (Figure 22B). To determine which R-Smads might be involved Fanc/Brca transcription, we singly knocked down each R-Smad in Hacat cells using siRNA. While TGFβ1 R-Smads 2 and 3 did not have a significant effect on Fanc/Brca levels, Smad1 knockdown increased Brca1 expression from 1 ± 0.1 fold to 4.0 ± 0.3 fold, FancA expression from 1.0 ± 0.1 fold to 7.2 ± 0.7 fold, and Rad51 expression from 1.0 ± 0.1 fold to 2.8 ± 0.4 fold. Similarly, Smad5 knockdown increased Brca1 expression by 3.0 ± 0.3 fold, FancA expression by 4.3 ± 0.6 fold, and Rad51 expression by 3.5 ± 0.4 fold (Figure 22C).

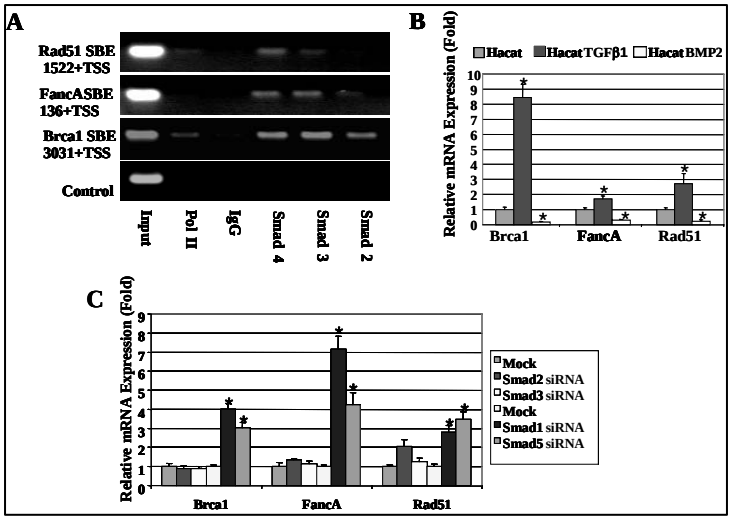

Figure 22. Transcriptional Regulation of Fanc/Brca Genes. *(A) Smads 2-4 bound the promoters of FancA (136 bp upstream from the transcription start site or TSS) and Brca1 (3031 bp upstream from the TSS), and of Smads 3 and 4 bound the promoter of Rad51 (797 bp upstream from the TSS). A negative control IgG antibody did not show nonspecific binding to these*

*promoter regions, and a negative control primer did not amplify the IP DNA. RNA Polymerase II (Pol II) bound to the promoters of Brca1 and Rad51, indicating these genes are actively transcribed by Smads. (B) Fanc/Brca genes are upregulated by TGFβ1 and downregulated by BMP2. Relative mRNA expression of Brca1, FancA, and Rad51 in TGFβ1 and BMP2 treated HaCaT cells, compared to untreated cells by qRT-PCR. Samples were run in triplicate for each experiment, and the average relative expression levels from 2-3 independent experiments are presented. The average expression of each gene in untreated cells was arbitrarily set to 1 for every experiment. Error bars indicate SE. Significance was determined using a student's t-test: * = p ≤0.05 compared to untreated cells. (C) Knockdown of BMP signaling Smads increases Fanc/Brca transcription, while knockdown of TGFβ1 signaling Smads had no effect. Relative mRNA expression of Brca1, FancA, and Rad51 in siRNA treated HaCaT cells, compared to mock transfected cells by qRT-PCR. Samples were run in triplicate for each experiment, and the average relative expression levels from 2 experiments are presented. The average expression of each gene in untreated cells was arbitrarily set to 1 for every experiment. Error bars indicate SE. Significance was determined using a student's t-test: * = p <0.05 compared to mock transfected cells.*

3.8 Smad4 HNSCCs Exhibited Increased Centrosome Numbers and Chromosomal Aberrations

As loss of Fanc/Brca proteins lead to abnormal centrosome amplification (Bertrand et al., 2003; Xu et al., 1999), which is associated with genomic instability (Fukasawa, 2007), we examined whether *HN-Smad4-/-* mucosa and HNSCCs exhibited increased abnormal centrosome numbers. Since genomic instability is common in all tumors, we used papillomas induced by head and neck-specific *K-ras*^{G12D} mutation (Caulin et al., 2004; Lu et al., 2006) (hereafter referred to as *HN-K-ras*^{G12D} papillomas) for comparison with *HN-Smad4-/-* HNSCCs. In wildtype mucosa, all cells exhibited 1 or 2 centrosomes (Figure 23). *HN-K-ras*^{G12D} papillomas exhibited an increase in cells with 2 centrosomes (38 ±7% compared to 23 ±5% in wildtype mucosa), which corresponds with increased G2/M phase cells, and 2.5 ± 2% of cells with abnormal centrosome numbers (Figure 23). By comparison, there were significantly more cells with abnormal centrosome numbers (31 ± 13%) in *HN-Smad4-/-* HNSCCs. Additionally, *HN-Smad4-/-* mucosa also exhibited a higher number of cells with abnormal centrosome numbers (5 ± 3%) than *HN-Smad4+/+* mucosa or *HN-K-ras*^{G12D} papillomas (Figure 23), suggesting that centrosome amplification was present in early stages of tumorigenesis in *HN-Smad4-/-* head and neck epithelia.

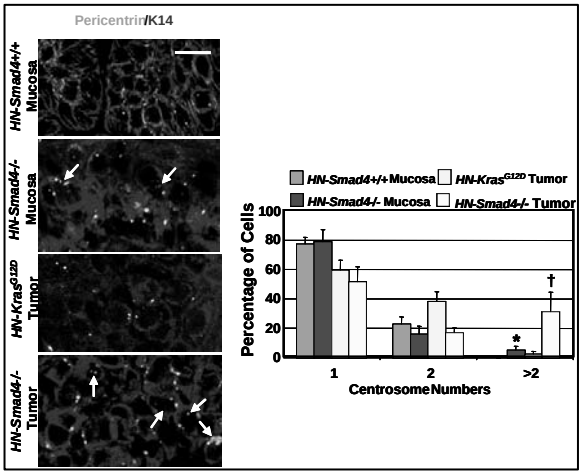

Figure 23. Abnormal Centrosomes and Increased Genomic Aberrations in HN-Smad4-/- mucosa and HNSCCs. *(A) Immunofluorescence for pericentrin (green or yellow). HN-Smad4-/- mucosa and HNSCCs have increased centrosome numbers compared to HN-Smad4+/+ mucosa and*

*control HN-K-rasG12D papillomas, respectively. K14 (red) was used to counterstain epithelial cells. 3-5 samples per group were analyzed and a representative picture is presented. Arrows highlight cells with ≥3 centrosomes. The histogram summarizes quantification of centrosome numbers. 100-200 cells per group were analyzed. Error bars indicate SE. Significance was determined using a Fisher's Exact Test: † = p<0.05 in comparison with HN-K-ras^{G12D} papillomas; * = p<0.05 in comparison with HN-Smad4+/+ mucosa. The scale bar in the top panel represents 10 mm for all panels.*

We then performed array Comparative Genomic Hybridization (aCGH) to assess genome-wide alterations in *HN-Smad4-/-* HNSCCs. *HN-Smad4-/-* HNSCCs exhibited several consistent genomic aberrations, including regions commonly lost in human HNSCC. We observed loss of genetic material at 4qA5 (Figure 24), which is syntenic to human 9p13 (Wreesmann et al., 2004a) and is associated with HNSCC metastases in humans (Wreesmann et al., 2004b). Additional regions included chromosomes 2qH4 and 3qF2 (Table 1), which are syntenic to human 19p13 and 17q21, respectively, and are often lost in human HNSCCs (Weber et al., 2007).

Figure 24*. Chromosome 4 aCGH of 3 HN-Smad4-/- HNSCCs indicates that HN-Smad4-/- HNSCCs have several consistent genomic aberrations.*

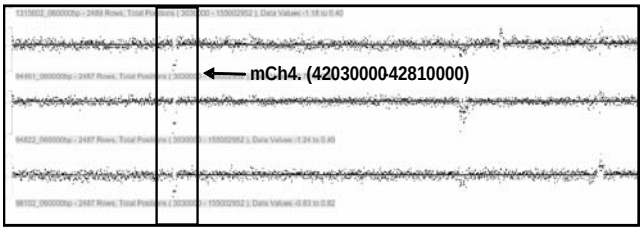

3.9 Smad4 Loss Led to Increased MMC Sensitivity

To further assess if the above changes represented functional defects in the Fanc/Brca pathway as a result of *Smad4* deletion, we examined *Smad4-/-* keratinocytes for sensitivity to mitomycin C (MMC) killing, an assay commonly used for FA diagnosis. Fanc/Brca-deficient cells are hypersensitive to MMC killing due to failed replication resulting from unrepaired MMC-induced DNA crosslinks (Kennedy and D'Andrea, 2005). While over 92 ± 0.4% of *Smad4+/+* cells were able to tolerate 40 ng/ml of MMC, only 52 ± 0.9% of *Smad4-/-* keratinocytes survived after treatment with 5 ng/ml of MMC (Figure 25A). Further, *Smad4-/-* keratinocytes that were able to survive after MMC treatment had a significant increase in chromosome breaks in comparison with *Smad4+/+* keratinocytes (Figure 25B, $p<0.001$). These data suggest that *Smad4-/-* keratinoyctes are deficient in Fanc/Brca-mediated repair of crosslinker-induced DNA damage.

Figure 25. HN-Smad4-/- cells exhibited increased MMC sensitivity. *(A) MMC sensitivity assay. Percent cell viability at increasing MMC concentrations indicates that Smad4-/- cells were significantly more sensitive to MMC than Smad4+/+ cells. The experiment was run in triplicate, and error bars indicate SE. Significance was determined using a Student's t-test: p<0.05 for all data points other than 0 ng/ml in comparison with Smad4+/+ cells. (B) Chromosome breakage assay. Plot of average chromosome breaks*

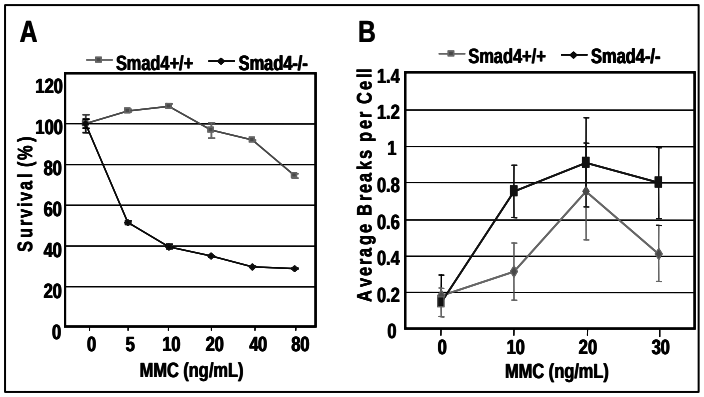

per cell for Smad4+/+ and Smad4-/- cells at increasing MMC concentrations indicates that Smad4-/- cells have increased chromosome breaks compared to Smad4+/+ cells. The experiments were run in triplicate, and error bars indicate SE. Significance was determined using a chi-square test: p<0.001 for all data points other than 0 ng/ml in comparison with Smad4+/+ cells.

3.10 Smad4 Loss Led to Downregulation of the Fanc/Brca Pathway In Vitro

To further assess whether Smad4 loss directly lead to downregulation of Brca1, FancA, FancD2, and Rad51, we manipulated Smad4 levels in human cell lines, and subsequently assayed for Fanc/Brca gene expression. First, we used siRNA to knock down Smad4 in normal primary human epidermal keratinocytes (HEKn). In response to 75 ± 1% knockdown of Smad4 mRNA and corresponding decrease in protein (HEKn + Smad4 siRNA, Figure 26),

Figure 26. Smad4 Knockdown in Normal Keratinocytes and Restoration in Smad4-deficient HNSCC cells *qRT-PCR and Western analysis of Smad4 levels in HEKn, HEKn + Smad4 siRNA, Cal27, and Cal27-Smad4 cells. The qRT-PCR values were calculated relative to HEKn cells arbitrarily set at 100% for every experiment, and the average relative expression levels from 3-4 pooled experiments are presented. Error bars indicate SE. Significance was determined using a student's t-test: * = p<0.05 for HEKn + Smad4 siRNA compared*

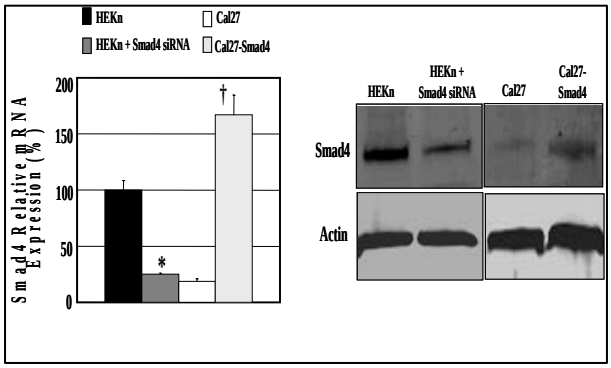

to HEKn cells, and † = p<0.05 for Cal27-Smad4 cells compared to Cal27 cells. Western blotting for Smad4 revealed that Smad4 was lost at the protein level by over 70% in HEKn + Smad4 siRNA compared to HEKn cells, and restored in Cal27-Smad4 compared to Cal27 cells.

Expression levels of Brca1 levels were reduced to 50 ± 4%, FancA to 47 ± 8%, FancD2 to 50 ± 2%, and Rad51 to 55 ± 8% in HEKn cells (Figure 27). Conversely, we stably transfected a wildtype Smad4 expression construct into a Smad4-deficient HNSCC cell line (Cal27) that harbors a nonsense mutation in the Smad4 gene (Qiu et al., 2007). In response to Smad4 restoration in Cal27 cells (Cal27-Smad4 cells, Figure 26), expression of Brca1 was increased 2 ± 0.1 fold and Rad51 was increased 1.8 ± 0.4 fold compared to parental Cal27 cells (Figure 27). The expression of FancA and FancD2 was not significantly increased by Smad4 expression in Cal27 cells, which suggests that either their reduction is not a primary effect of Smad4 loss, or other mechanisms regulate these molecules in HNSCC cancer cells.

Figure 27. Fanc/Brca Pathway Gene Expression and Function Are Dependent on Smad4*. Relative expression levels of Fanc/Brca transcripts examined by qRT-PCR.*

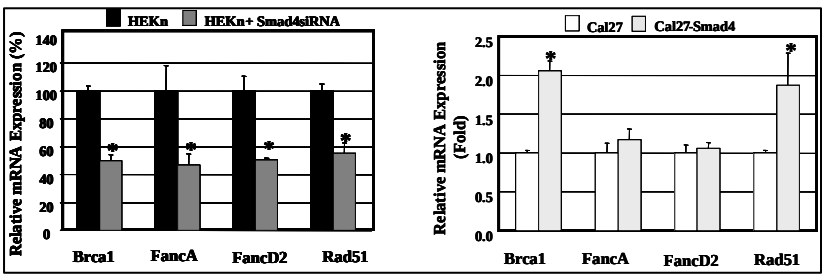

Brca1, FancA, FancD2, and Rad51 expression was decreased by Smad4 siRNA treatment of HEKn cells, and Brca1 and Rad51 expression was increased by Smad4 restoration in

*Cal27 cells. The expression level of each gene in normal HEKn and Cal27 cells was arbitrarily set at 100% for every experiment. Samples were run in triplicate for each experiment, and the average relative expression levels from 3-4 independent experiments are presented. Error bars indicate SE. Significance was determined using a student's t-test: * = p<0.05 compared to parental HEKn or Cal27 cells.*

3.11 Smad4 Loss Correlated with Fanc/Brca Pathway Downregulation in Human HNSCCs

To determine if Smad4 loss led to downregulation of Brca1 and Rad51 in primary human head and neck tissues, we assessed whether there was a correlation between Smad4 loss and Brca1 or Rad51 loss using IHC. Interestingly, 100% of Smad4-positive HNSCC and adjacent mucosa cases retained staining for Brca1 and Rad51 (Figure 27, Table 2). Additionally, in Smad4-negative HNSCC cases, 88% exhibited loss of Brca1 and 83% exhibited Rad51 loss. Similarly, among Smad4-negative adjacent mucosa cases, 92% showed loss of Brca1 and Rad51 (Figure 28, Table 2). These results represent a significant correlation between Smad4 loss and Brca1/Rad51 loss in both HNSCCs and adjacent mucosa.

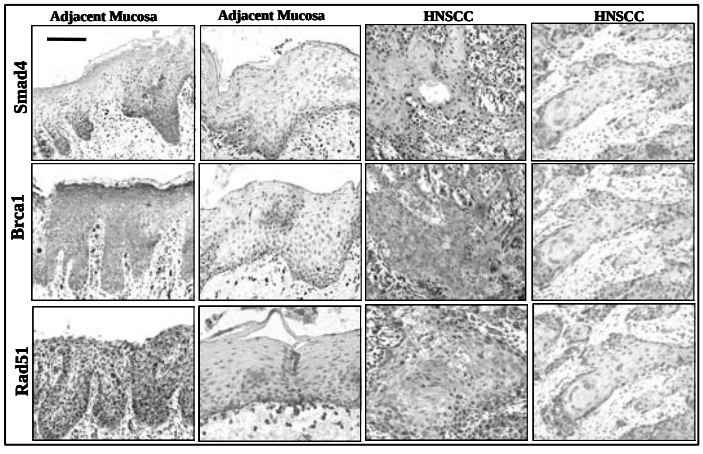

Figure 28. IHC staining of Smad4, Brca1, and Rad51 *(brown) in HNSCCs and adjacent mucosa samples. Mucosa adjacent to HNSCC and*

HNSCC samples from serial sections demonstrated a correlation between Smad4 loss and Brca1/Rad51 loss. The scale bar in the left panel represents 40 μm for all panels.

3.12 Smad4 Loss Led to Functional Defects in the Fanc/Brca Pathway In Vitro

To further determine whether Smad4 loss resulted in functional defects in the Fanc/Brca pathway, we examined Brca1 and Rad51 DNA repair nuclear foci formation by immunofluorescence staining using the Cal27 and Cal27-Smad4 cells. Under normal conditions, Brca1 and Rad51 localize to sites of MMC-induced DNA damage with other members of the Fanc/Brca pathway to form DNA repair nuclear foci (D'Andrea and Grompe, 2003). After MMC treatment, only 7 ± 2% of Cal27 cell were able to form Brca1 foci, and 17 ± 3% were able to form Rad51 foci. However, 27 ± 5% of Cal27-Smad4 cells able to form Brca1 foci and 58% ± 6% were able to form Rad51 foci (Figure 29). These data suggest that Smad4 loss not only leads to downregulation of Fanc/Brca molecules, but may also in inhibit their DNA repair efficiency.

Figure 29. *Brca1 and Rad51 nuclear foci detected by immunofluorescence in Cal27 and Cal27-Smad4 cells after MMC treatment. A representative picture is presented. The histogram indicates the percentage of cells with Brca1 or Rad51 foci in Cal27 and Cal27-Smad4 cells. 100-200 cells per*

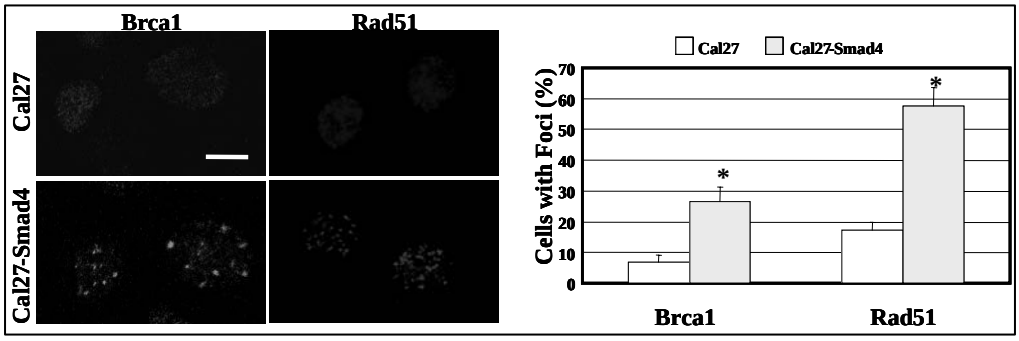

*group were analyzed. Error bars indicate SE. Significance was determined using a Fisher's Exact Test: * = p<0.05 in comparison with Cal27. The scale bar in the upper left panel represents 5 mm for all panels.*

3.13 Smad4 Loss Led to Increased Inflammation

In addition to the above changes in *HN-Smad4-/-* epithelia, we observed numerous infiltrated leukocytes in the stroma of *HN-Smad4-/-* mucosa and HNSCCs on histological sections, and by CD45 (total leukocyte) IHC staining (Figure 30). We further examined the subtypes of infiltrated leukocytes using IHC. While inflammatory cells were rarely detected in the stroma of *HN-Smad4+/+* buccal tissues, both the stroma adjacent to *HN-Smad4-/-* buccal mucosa and the tumor stroma of *HN-Smad4-/-* HNSCCs exhibited leukocyte infiltration comprised of macrophages (F4/80), granulocytes (Ly6G), T lymphocytes (CD3), B lymphocytes (B220) (Figure 30). Interestingly, IL-17 positive cells, which represent a subset of proinflammatory T lymphocytes that are activated by TGFβ1 in mice (Mangan et al., 2006; Veldhoen et al., 2006), were also detected in *HN-Smad4-/-* mucosa and HNSCCs (Figure 30).

Figure 30. Increased Inflammation in HN-Smad4-/- Lesions*. Immunostaining of HN-Smad4+/+ mucosa, HN-Smad4-/- mucosa, and HN-Smad4-/- HNSCCs with leukocyte markers CD45 (total leukocytes), F4/80 (Macrophages), Ly6G (granulocytes), CD3 (T-cells), IL-17 (Th17 cells), and B220 (B-cells). The black dotted lines indicate the boundary between mucosa and stroma. HN-Smad4-/- mucosa has increased inflammatory markers in the underlying stroma compared to HN-Smad4+/+ mucosa, and HN-Smad4-/- HNSCCs have marked inflammation in the tumor stroma. 4-7 samples from each group were analyzed and a representative picture is presented. The scale bar in the upper left panel represents 40 μm for all panels.*

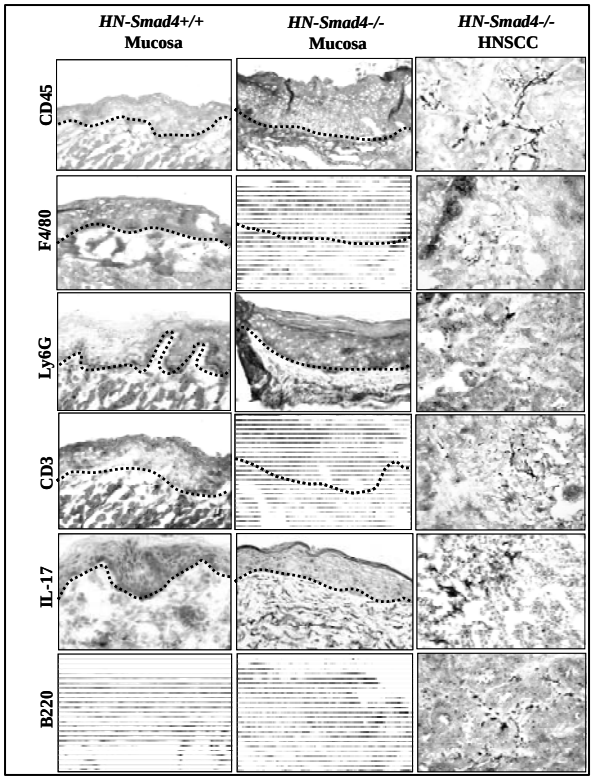

We then assessed which inflammatory cytokines were activated in *HN-Smad4-/-* buccal mucosa and HNSCCs, using an "Inflammatory Chemokines and Receptors" Superarray™. No inflammatory cytokines were detected in *HN-Smad4+/+* mucosa, but several cytokines were readily detected in *HN-Smad4-/-* mucosa and HNSCCs (Figure 31). Among them, MCP-1, MCP-2, MIP-2 and MMP-2 have been shown to be elevated by TGFβ1 overexpression in keratinocytes (Li et al., 2004b). Additionally, MMP 3, 9, and 13 and Il-1β were increased in *HN-Smad4-/-* mucosa compared to *HN-Smad4+/+*

mucosa using a custom Superarray membrane enriched for TGFβ1 target genes (Figure 31).

Figure 31. Increased Inflammatory Chemokines in HN-Smad4-/- Lesions*, (A) Pathway-specific SuperarrayTM for Mouse Chemokines & Receptors revealed increased inflammatory molecules in HN-Smad4-/- mucosa and HNSCCs compared to HN-Smad4+/+ mucosa. The experiment was run in triplicate, and a representative blot from each group is presented.*

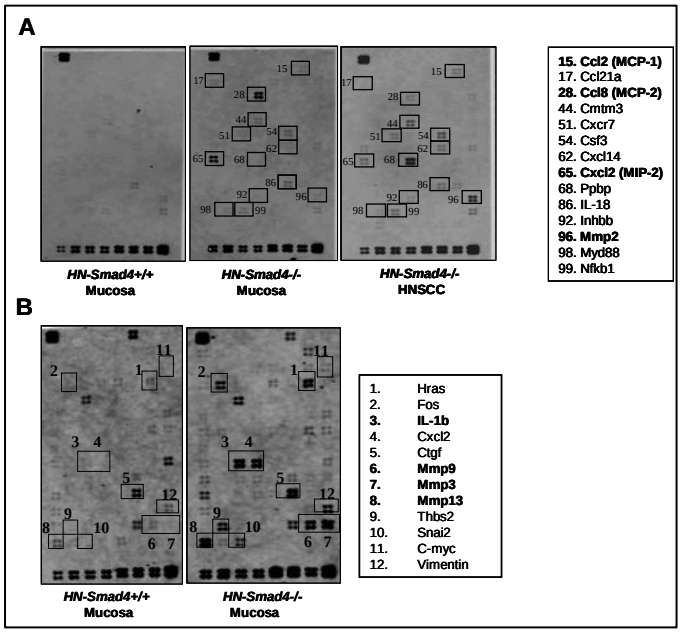

(B) Custom SuperarrayTM for TGFβ1 target genes indicated that Il-1β and Mmp 9, 3, and 13 were upregulated in Smad4-/- mucosa compared to Smad4+/+ mucosa. The experiment was run in triplicate, and a representative blot from each group is presented.

3.14 Inflammation in Smad4 Knockout Mucosa and HNSCCs was Associated with Increased TGFβ1 and Receptor-Associated Smads

To determine whether *HN-Smad4-/-* tissues had increased TGFβ1 ligand, we performed an ELISA for total TGFβ1. *HN-Smad4-/-* HNSCCs expressed significantly more TGFβ1 (514 ± 88 pg/mg total protein) than *HN-Smad4+/+* buccal mucosa (84 ± 32 pg/mg total protein) (Figure 32A). Interestingly, *HN-Smad4-/-* buccal mucosa also exhibited

significantly more TGFβ1 (156 ± 35 pg/mg total protein) than *HN-Smad4+/+* mucosa (Figure 32A), indicating that the Smad4 loss-associated increase in TGFβ1 occurred during early stages of tumorigenesis. To determine whether increased TGFβ1 conferred downstream signaling activation, we performed immunostaining of signaling Smads in *HN-Smad4-/-* mucosa and HNSCCs. Interestingly, while loss of nuclear phospho-Smad2 (pSmad2) was evident in *HN-Smad4-/-* mucosa and HNSCCs, increased nuclear staining for Smad3 and pSmad1/5/8 was observed in *HN-Smad4-/-* buccal mucosa and HNSCCs compared to *HN-Smad4+/+* mucosa (Figure 32B). These results suggest that Smad4 loss does not abrogate all the functions of signaling Smads, and that increased activation of Smad3 and Smad1/5/8 could mediate the inflammatory arm of TGFβ signaling in the absence of Smad4.

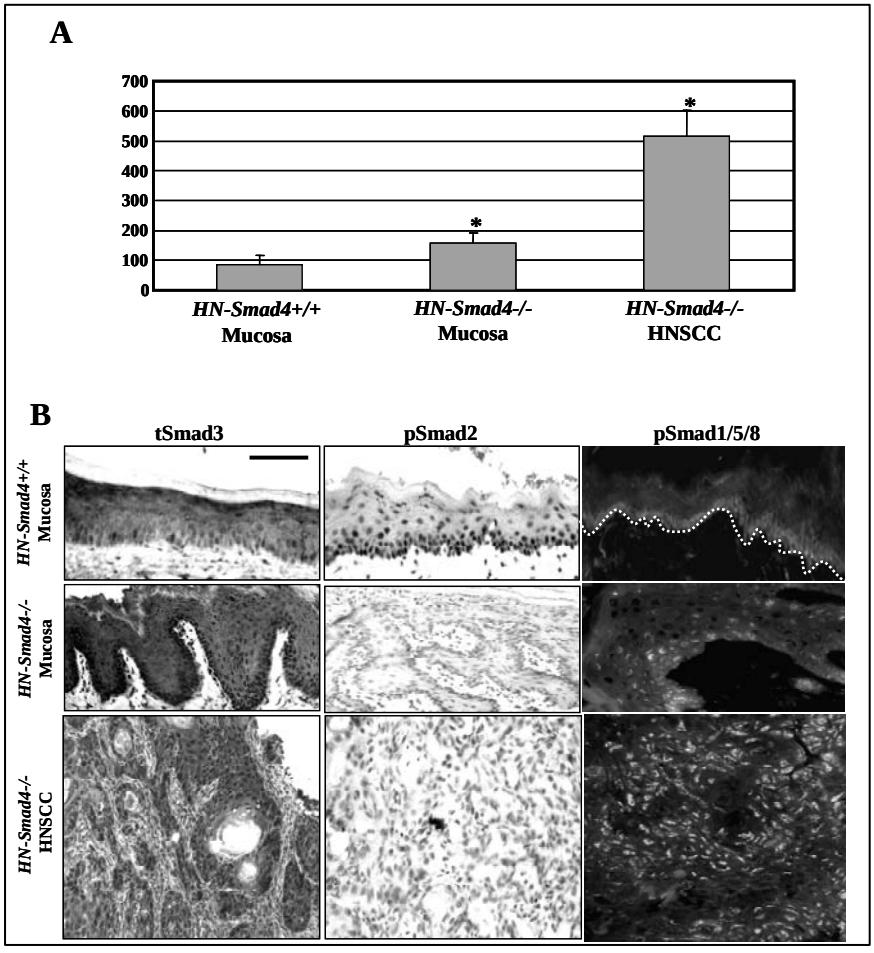

Figure 32. Increased TGFβ1, Smad3, and pSmad1/5/8 in HN-Smad4-/- Lesions. *(A) ELISA for total TGFβ1 protein. TGFβ1 levels were increased in HN-Smad4-/- mucosa and HNSCCs compared to HN-Smad4+/+*

*buccal mucosa. Each group contains 5-7 samples. Error bars indicate SE. Significance determined using a student's t-test: * = p<0.05 compared with HN-Smad4+/+ mucosa. (B) Immunostaining of HN-Smad4+/+ buccal mucosa, HN-Smad4-/- buccal mucosa, and HN-Smad4-/- HNSCCs for pSmad2, total (t)Smad3, and pSmad1/5/8. 5-7 samples from each group were examined and a representative picture is presented. The scale bar in the upper left panel represents 40 μm for all panels.*

3.15 Smad4 Deletion in Keratinocyte Stem Cells Led to Multiple Cancer Phenotypes

The K5 and K14 promoters used to generate *HN-Smad4-/-* mice target both stem cells and a variety of progenitor cells. Cancer stem cell theory hypothesizes that tumors arise from genetic changes in stem cells. To study the role of Smad4 loss in keratinocyte stem cells, we deleted Smad4 in K15-expressing skin stem cells harboring an activating Kras mutation (*K15.Kras/Smad4-/-* mice). We compared these tumors to tumors with deletion of TGFβRII in the same background (*K15.Kras/RII-/-* mice). We hypothesized that the above gene alterations in K15-expressing cells would expand the stem cell compartment and lead to tumor formation, but that *Smad4* deletion and *TGFβRII* deletion would have different effects on the tumor phenotype. We observed massive skin tumor formation in both *K15.Kras/Smad4-/-* and *K15.Kras/RII-/-* mice within 1-3 months with 100% penetrance. K15 IHC revealed that nests of K15-expressing cells harboring the gene alterations were scattered throughout the tumors (Figure 33).

Figure 33. K15-expressing cells were scattered in nests throughout the tumor epithelia. *K15 IHC on a K15.Kras/Smad4-/- skin tumor with a no primary control demonstrated positive K15 (brown) staining amidst hematoxylin counterstained (blue) tumor epithelia. 5 tumors were stained, and a representative picture is displayed.*

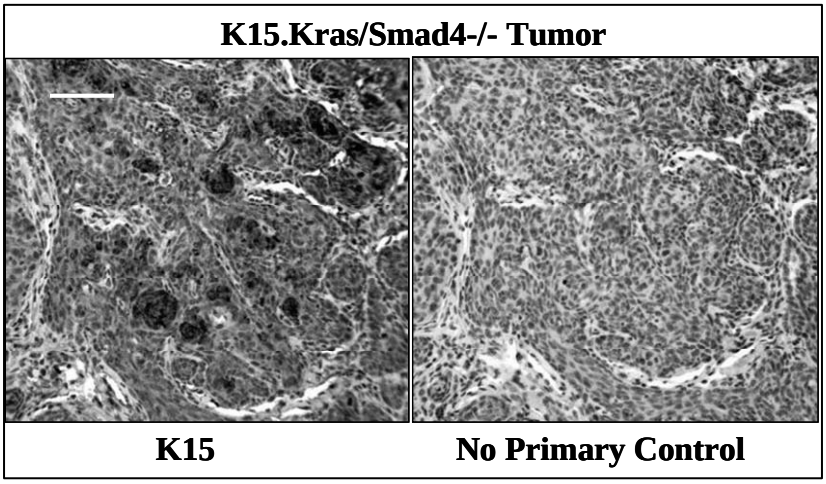

The scale bar in the left panel represents 40 μm for both panels.

Interestingly, histological sections of the *K15.Kras/Smad4-/-* and *K15.Kras/RII-/-* mice revealed that while *K15.Kras/RII-/-* mice developed exclusively SCCs, *K15.Kras/Smad4-/-* mice developed tumors containing SCC, "BCC-like" SCC, and SA differentiation, indicating that indeed the two genes had different effects on the differentiation of K15-expressing CSCs (Figure 34).

Figure 34. Tumor differentiation in K15.Kras/Smad4-/- and K15.Kras/RII-/- tumors. *H&E staining of K15.Kras/Smad4-/- and K15/Kras/RII-/- tumors revealed that K15.Kras/RII-/- tumors were exclusively SCCs, while K15.Kras/Smad4-/- tumors exhibited SCC, "BCC-like" SCC, and SA differentiation. At least 10 mice from each genotype were analyzed. The scale bar in the upper left panel represents 40 μm for all panels.*

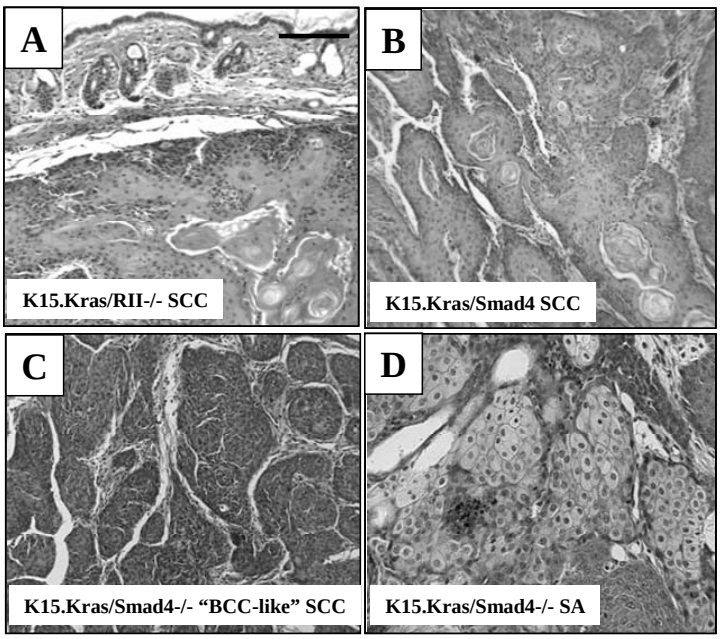

3.16 Tumors Derived from Stem-Cell Promotor-Driven Smad4 Deletion Exhibited a Hierarchical Structure

We were interested in determining whether tumors derived from *K15.Kras/Smad4-/-* and *K15.Kras/RII-/-* mice exhibited a stem cell hierarchy of quiescent, undifferentiated K15-expressing CSCs giving rise to proliferative transiently-amplifying cells and differentiated cells. Double immunofluorescence of K15 and the proliferative marker PCNA revealed that indeed, K15-expressing CSCs in both *K15.Kras/Smad4-/-* and *K15.Kras/RII-/-* mice did not express PNCA, while the tumor mass surrounding these cells did express PCNA (Figure 35). Additionally, double immunofluorescence of K15 and the differentiation marker K1 revealed that K15-expressing cells were mostly

mutually exclusive with K1-expressing cells in *K15.Kras/Smad4-/-* mice, but less so in *K15.Kras/RII-/-* mice, indicating that *K15.Kras/RII-/-* cells differentiate earlier than *K15.Kras/Smad4-/-* cells, as evidenced by the histological tumor differentiation. (Figure 35).

Figure 35. Putative CSCs K15.Kras/Smad4-/- and K15.Kras/RII-/- were quiescent and undifferentiated *Double immunofluorescence indicated that K15-expressing putative CSCs (green) in K15.Kras/Smad4-/- (left) and K15.Kras/RII-/- (right) tumors were mostly mutually exclusive with proliferative marker PCNA (red), indicating they were quiescent. K15.Kras/Smad4-/- putative CSCs (green) did not express K1 (red), indicating they were undifferentiated. K15.Kras/RII-/- putative CSCs showed a similar pattern, but exhibited more overlap with K1, indicating they differentiated earlier than K15.Kras/Smad4-/-. The scale bar in the upper left panel represents 20 μm for the top and bottom left panel, and 10 μm for the bottom right panel.*

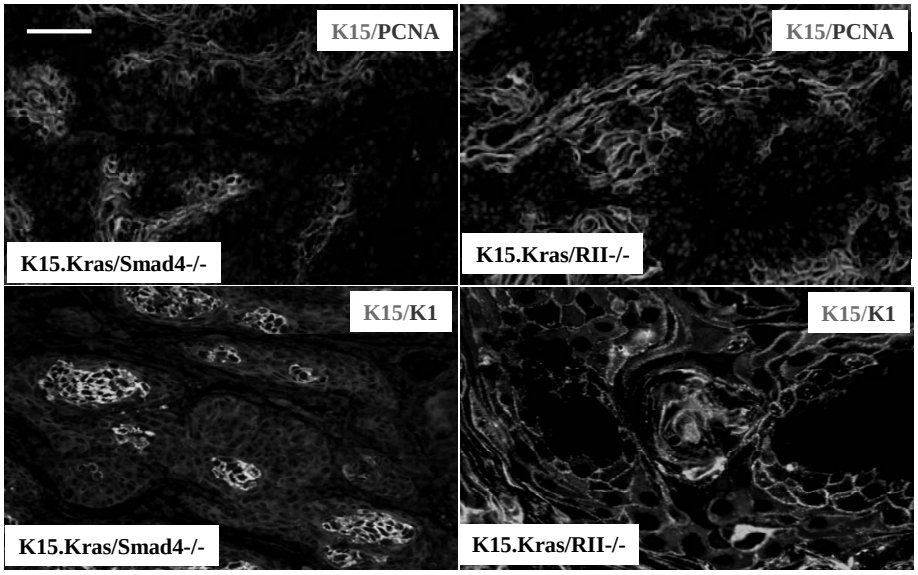

3.17 Cancer Stem Cells Isolated from Stem-Cell Promotor-Driven Smad4 Deletion Exhibited Increased Tumorigenicity Compared to Non-Cancer Stem Cells

In order to determine whether CSCs isolated from *K15.Kras/RII-/-* and *K15.Kras/Smad4-/-* exhibited increased tumorigenicity in vivo, we first isolated putative CSCs by either flow sorting out CD45+ cells (leukocytes) and CD31+ cells (endothelial) and collecting CD34+ and CD49f+ cells, or collecting Hoescht-dye retaining SP+ cells (Figure 36). We collected CD45-CD31-CD34-CD49f- and SP- cells as controls. Interestingly, only SP+ cells from *K15.Kras/Smad4* mice were able to form skin tumors in nude mice, while CD34+/CD49f+ cells were not. However, only CD34+/CD49f+ cells were able to form tumors in *K15.Kras/RII-/-* mice, while SP+ cells were not. These results are in accordance with previous findings that SP+ putative CSCs define a more primitive keratinocyte CSC population than CD34+ putative CSCs (unpublished data, Dennis Roop Lab, University of Colorado Health Sciences Center). Although the data is preliminary, these results indicate that *K15.Kras/Smad4-/-* CSCs are more primitive than *K15.Kras/RII-/-* CSCs, which fits with our previous histological and molecular findings.

Figure 36. Increased tumorigenicity of putative CSCs in K15.Kras/Smad4-/- and K15.Kras/RII-/- tumors. *Hoescht dye exclusion flow cytometry for dye-effluxing stem cells or the side population, indicated by gate R3 for a K15.Kras/Smad 4-/- tumor (top left panel). Skin graft experiment using 10,000 SP+ putative CSCs or 10,000 SP- cells FACS sorted from the above experiment (bottom left panel). SP+ cells were more tumorigenic than SP- cells. Flow cytometry for CD34+CD49f+ cells indicated by gate R37 for a K15.Kras/RII-/- tumor (top right panel). Skin graft experiment using 5,000 CD34+CD49f+ putative CSCs and 4,000 CD34-CD49f- cells (gate R38, upper right panel) for a K15.Kras/RII-/- tumor (bottom right panel). CD34+CD49f+ putative CSCs were more tumorigenic than CD34-CD49f- cells. The results are from 1-2 experiments.*

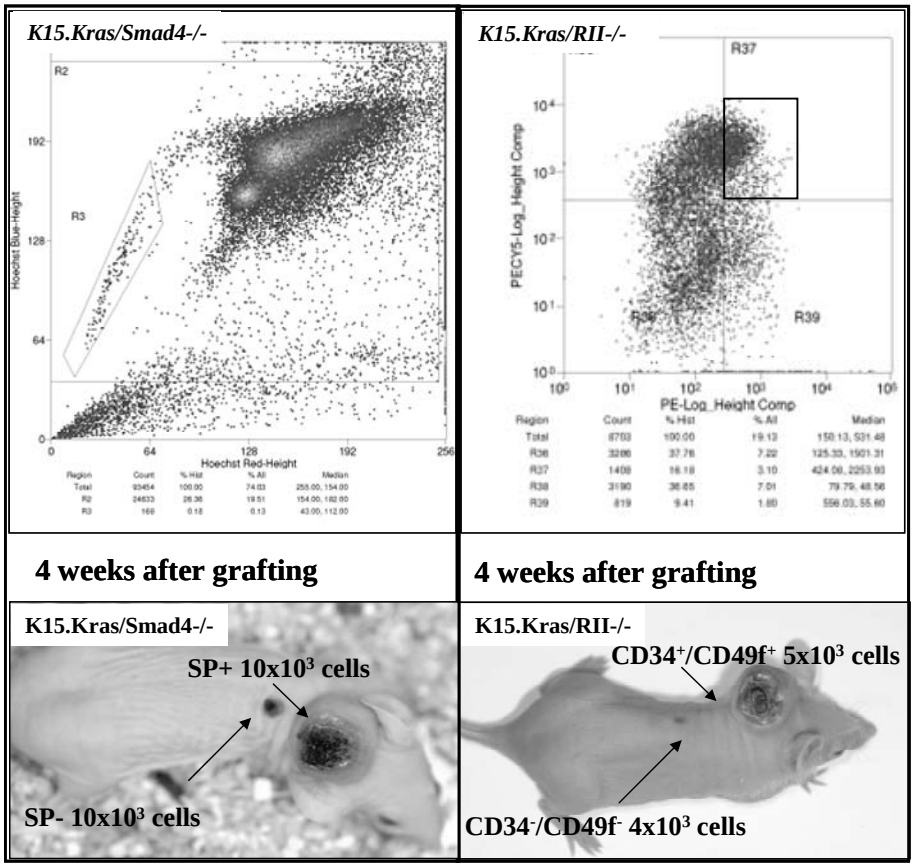

CHAPTER FOUR

DISCUSSION

4.1 Early Stage Smad4 Loss Plays a Causal Role in HNSCC Tumorigenesis

While Smad4 is lost at malignant stages in other cancer types, we detected frequent Smad4 loss in pre-neoplastic lesions of head and neck tissue. This result suggests that rather than only facilitating malignant conversion, Smad4 loss plays a causal role in HNSCC tumorigenesis. This notion is further supported by spontaneous HNSCC formation in mice with deletion of *Smad4* specifically in head and neck epithelia. Interestingly, pre-neoplastic *HN-Smad4-/-* mucosa exhibited increased abnormal centrosome numbers and reduced expression of Fanc/Brca genes, suggesting that homozygous Smad4 loss, through initiating genomic instability, may generate the necessary oncogenic changes required for tumorigenesis. For example, we found that a subset of *HN-Smad4-/-* HNSCCs exhibited *Ras* mutations, which have been associated with HNSCC initiation (Caulin et al., 2004; Lu et al., 2006). While heterozygous deletion of *Smad4* alone did not lead to HNSCC formation, when combined with a *K-ras* mutation, *K-ras*^{G12D}*/Smad4+/-* mice rapidly developed HNSCCs, indicating that Ras activation is able to cooperate with Smad4 loss in HNSCC tumorigenesis, which has been observed recently in pancreatic cancer (Izeradjene et al., 2007).

We were able to detect LOH at the Smad4 locus in the majority of HNSCCs examined, while several adjacent mucosa samples showing mRNA loss were heterozygous for the Smad4 locus. However, we were not able to determine the

mechanism of Smad4 downregulation in adjacent mucosa samples, nor the mechanism of loss of the remaining Smad4 expression in HNSCC. Previous studies in the lab did not detect methylation in the promoter of Smad4 in our HNSCC samples, which corresponds with prior studies of colorectal cancer (Roth et al., 2000). Similarly, mutation of Smad4 is infrequent in HNSCC (Kim et al., 1996). While it is unclear how Smad4 is downregulated in adjacent mucosa, it is possible that single-copy loss of *Smad4* in the setting of other oncogenic changes, such as the "field cancerization" observed in HNSCC patients (Hunter et al., 2005), is sufficient for HNSCC tumorigenesis. We have recently reported that Ras activation is common in adjacent mucosa and HNSCC (Lu et al., 2006), thus ~50% loss of Smad4 mRNA either at the genomic or transcriptional level in combination with Ras activation could be sufficient for tumorigenesis.

In addition to Ras activation, increased NFkB, Stat3, and Akt signaling could cooperate with Smad4 loss in HNCC formation or progression. All three molecules are involved in cell survival, which could protect genomically unstable *HN-Smad4-/-* cells from apoptosis. Additionally, NFkB and Stat3 are important intracellular mediators downstream of inflammatory stimuli, and could be involved in cytokine or chemokine release and the recruitment of tumorigenic inflammatory cells.

4.2 Smad4 Loss Contributes to Defects in the Fanc/Brca Pathway and Genomic Instability

It has been shown that FA patients, who carry germline mutations in Fanc/Brca pathway genes have a high incidence of HNSCC at a young age relative to sporadic HNSCC patients, and 70% of FA patients diagnosed with HNSCC have FancA mutations (Kutler

et al., 2003). Moreover, studies have shown that Fanc/Brca pathway-associated genes are downregulated in sporadic HNSCCs (Marsit et al., 2004; Sparano et al., 2006; Weber et al., 2007; Wreesmann et al., 2007), building evidence that alterations in this pathway play an important role in sporadic HNSCC formation. Additionally, mice with epithelia-specific heterozygous knockout of *Brca1* developed oral SCCs, indicating that Brca1 loss plays an important role in HNSCC tumorigenesis (Berton et al., 2003). In our current study, downregulation of Fanc/Brca pathway genes was detected in both pre-neoplastic and HNSCC lesions of *HN-Smad4-/-* mice, and restoration of normal Smad4 in a Smad4-deficient HNSCC cell line increased expression of Fanc/Brca pathway genes. Additionally, the majority of Smad4-deficient mucosa and HNSCC clinical samples demonstrated loss of both Brca1 and Rad51. Thus, our data suggest a causal role for Smad4 loss in downregulation of Fanc/Brca pathway genes, which appeared sufficient to cause functional defects in this pathway, as evidenced by increased sensitivity to MMC killing and chromosome breakage in Smad4-/- primary cells and defects in Rad51/Brca1 nuclear foci formation in Smad4-deficient HNSCC cells (Figure 37). Additionally, Smad4 bound with other R-Smads to the promoters of Rad51, FancA, and Brca1, suggesting Smad4 normally binds and transcribes these genes.

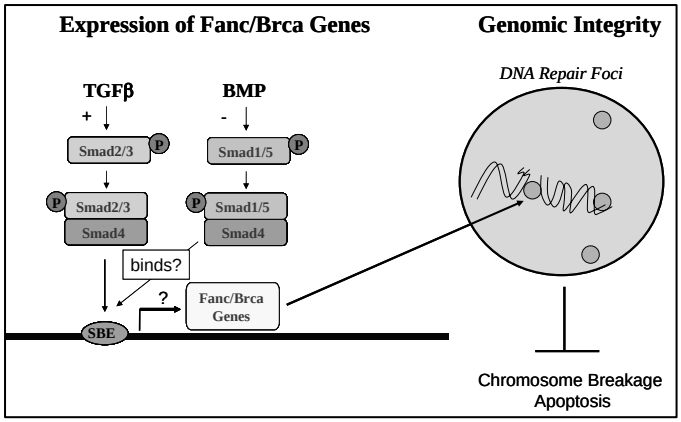

Figure 37. Schematic of Smad4-dependent regulation of Fanc/Brca genes and genomic integrity. *Smad4 with R-Smads,*

including Smads 2 and 3, binds to the SBE of Brca1, FancA, and Rad51. It is not known whether BMP R-Smads 1 and 5 also bind. TGFβ1 upregulates expression of these genes, while Smad4 knockdown downregulates their expression, suggesting that Smad4 is involved in active transcription at the promoter in response to TGFβ1. However, BMP2 treatment led to downregulation of these genes, and knockdown of Smads 1 and 5 led to increased levels, indicating that Smad4 might mediate opposing signals from both ligands. Loss of Smad4 led to loss of Fanc/Brca gene expression and DNA repair foci, which was evidenced by increased average breaks per cell and reduction in cell viability, presumably due to unrepaired DNA damage.

Defects in the Fanconi pathway lead to increased genomic instability in Fanconi patients (D'Andrea and Grompe, 2003), and could be responsible for the increased abnormal centrosome numbers and genomic aberrations observed in *HN-Smad4-/-* HNSCCs. Consistent with our observations, both Brca1-deficient cells (Xu et al., 1999) and cells expressing a dominant-negative form of Rad51 (Bertrand et al., 2003) exhibited increased centrosome numbers and chromosomal aberrations. Additionally, Smad3 has been shown to bind to the Brca1 protein and inhibit Brca1 nuclear foci formation and DNA repair efficiency (Dubrovska et al., 2005). Thus, increased TGFβ1 signaling through Smad3 in *HN-Smad4-/-* mucosa and HNSCCs may also play a role in reduced Fanc/Brca pathway DNA repair efficiency. These defects, coupled with Smad4 loss-induced hyperproliferation and reduced apoptosis, may allow *HN-Smad4-/-* cells to escape from DNA damaged-induced cell death during tumorigenesis.

Lastly, we have shown that Smad4 binds to the promoters and that Smad4 levels effect the expression of Fanc/Brca genes. We have also generated preliminary data that Fanc/Brca genes are upregulated by TGFβ1, but inhibited by BMP2. Since Smad4 is the only Smad able to mediate signals from both pathways, it is possible that Smad4 might balance opposing effects from both ligands. Knocking down individual Smads revealed that TGFβ1-signaling R-Smads had no effect on Fanc/Brca expression, while BMP-signaling Smads might be involved in Fanc/Brca repression. This preliminary data suggests that Smad4 might be solely responsible for the transcriptional activation of Fanc/Brca genes through binding their promoters with TGFβ1 Smads 2 and 3. While Smad4 is a well-characterized transcriptional activator of TGFβ1 targets, less is known about the ability of Smad4 to mediate BMP repression of transcriptional targets (Feng and Derynck, 2005). However, Smad 1 and 4 were able to recruit histone deacetylases in a BMP-dependent manner by binding with transcriptional repressor NKx3.2 (Kim and Lassar, 2003).

4.3 Smad4 Loss Results in Increased Inflammation

Human HNSCCs often exhibit chronic inflammation with increased levels of inflammatory cytokines and chemokines (Chen et al., 1999; Hunter et al., 2005). While the association with immune cells and cancer has been well documented, the role of each immune cell in tumorigenesis is unclear. Additionally, while TGFβ is a key cytokine involved in immune homeostasis, it is uncertain how TGFβ regulates different immune cells during tumorigenesis. It has been reported that Smad4 deletion in T cells, but not in gastrointestinal epithelia, resulted in gastrointestinal cancer associated with increased

inflammation and other tumor-promoting stromal changes (Kim et al., 2006). This study is consistent with the notion that TGFβ signaling in T cells has an anti-inflammatory and immunosuppressive effect. However, it has also been shown that Smad4 loss in intestinal epithelia led to increased inflammation that promoted tumor invasion (Kitamura et al., 2007). Consistent with the latter study, our findings show that loss of *Smad4* in head and neck epithelia resulted in marked inflammation, which was associated with increased TGFβ1. We have shown that TGFβ1 is overexpressed in human HNSCCs, and that overexpression of *TGFβ1* in head and neck epithelia resulted in marked inflammation (Lu et al., 2004). Interestingly, we also detected increased nuclear Smad1/5/8 and Smad3 in *HN-Smad4-/-* buccal mucosa and HNSCCs. Activation of Smad1 and Smad5 correlated with inflammation in allergic-airway epithelia (Rosendahl et al., 2002), and abrogation of TGFβ1 signaling has been shown to activate Smad1 and Smad5, which correlated with increased tumor invasion (Bharathy et al., 2008). Thus, increased nuclear Smad1/5/8 may play a role in the inflammatory and invasive phenotype observed in *HN-Smad4-/-* HNSCCs. Unlike Smad2 and Smad4, Smad3 is not thought to have a tumor suppressive role (Bornstein et al., 2007). We have shown that Smad3 is important for mediating TGFβ-induced inflammation, including expression of of MCP-1, IL-1β, and activating protein 1 (AP-1) family members (Li et al., 2004a), and nuclear localization of NFκB p50. It has also been reported that both Smad3 and AP-1 family members are important for *TGFβ1* promoter activity (Yue and Mulder, 2000). While historically, it was thought that Smad4 was required for TGFβ1 signal transduction, it has recently been shown that TIF1γ is able to bind R-Smads and mediate TGFβ1 responses (He et al.,

2006). Thus, it is possible that Smad4 loss-associated increased nuclear Smad3 led to TGFβ1 overexpression and increased tumor inflammation (Figure 38).

Figure 38. Schematic of Smad3-dependent Inflammation in HN-Smad4-/- tissue.

Smad4 loss in head and neck epithelia led to increased Smad3 and TGFβ1, and these proteins remained elevated in HN-Smad4-/- HNSCCs. Smad3 upregulates AP-1 family members, and Smad3 and AP-1 family members can lead to TGFβ1 promoter activation. Thus Smad3 may lead to increased TGFβ1 secretion by epithelial cells. Smad3 loss led to a reduction in several cytokines found to be upregulated in Smad4 HN-Smad4-/- mucosa and HNSCCs. Thus, increased Smad3 may lead to increased epithelial cytokine expression, possibly through direct promoter activation. Increased TGFβ1 and cytokine/chemokine expression could lead to the inflammatory cell infiltration observed in HN-Smad4-/- tissue.

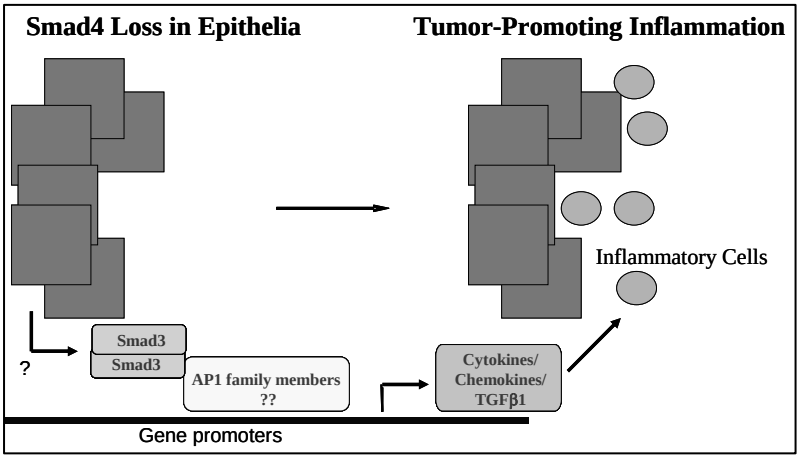

Previous reports have shown that changes in chemokine expression as a result of Smad4 loss can lead to recruitment of immature myeloid cells (Kitamura et al., 2007) that are also able to secrete TGFβ1 into the tumor stroma (Yang et al., 2008). As a result of increased TGFβ1 levels, *HN-Smad4-/-* buccal mucosa and HNSCCs exhibited increased

Th17 cells, and increased expression of MCP-1, MIP-1 and MMP-2, which are upregulated by TGFβ (Li et al., 2004b). These cytokines, secreted from either the tumor epithelia or stroma, are able to recruit innate immune cells, which have been closely linked to tumorigenesis (Coussens and Werb, 2002). Each of these cytokines is also upregulated in human HNSCC (Patel et al., 2007; Tang et al., 2001), further suggesting that TGFβ1-induced inflammation contributes to tumorigenesis in *HN-Smad4-/-* tissue.

4.4 Role of Smad4 Loss in Keratinocyte Cancer Stem Cells

We have shown that markers that identify normal keratinocyte stem cells, such as K15, CD34, and CD49f can be used to characterize and isolate putative cancer stem cells in *K15.Kras/Smad4-/-* mice as well as *K15.Kras/RII-/-* mice. Additionally, we have used Hoescht-dye exclusion, a general property of stem cells, to isolate putative cancer stem cells in *K15.Kras/Smad4-/-* mice. Interestingly, *K15.Kras/Smad4-/-* tumors displayed multiple neoplastic lineages including SCC, "BCC-like" SCC, and SA regions, indicating that genetic changes in keratinocyte stem cells can give rise to the variety of tumor types seen in the skin. K15-expressing putative CSCs in *K15.Kras/Smad4-/-* tumors were largely quiescent and undifferentiation, indicated by K1 and PCNA staining, respectively. However, *K15.Kras/RII-/-* exhibited only SCC differentiation, and while K15-expressing putative CSCs in *K15.Kras/RII-/-* were largely quiescent, they differentiated earlier, as indicated by increased overlap with K1-expressing cells. In agreement with these findings, only Hoescht-dye exclusion could isolate tumorigenic putative CSCs from *K15.Kras/Smad4-/-* tumors, while only CD34 and CD49f could isolate tumorigenic putative CSCs in *K15.Kras/RII-/-* tumors, which also indicates that *K15.Kras/Smad4-/-*

putative CSCs are more primitive. Thus, Smad4 may lead to spontaneous tumorigenesis through forcing stem cells to expand while aberrantly retaining stem cell plasticity.

CHAPTER FIVE

FUTURE DIRECTIONS

Mechanism of Smad4 mRNA Loss in Adjacent Epithlia and HNSCC

The mechanism of Smad4 downregulation in adjacent mucosa samples and the mechanism of loss of the remaining Smad4 expression in HNSCC are still unknown. Several of the normal adjacent mucosa samples demonstrating Smad4 loss at the mRNA were heterozygous at the Smad4 allele, indicating gene deletion or conversion did not occur. Although Smad4 mutation is infrequent, sequencing of the Smad4 gene could reveal inactivating mutations. Similarly, while we did not detect promoter methylation using previously published primers surrounding the most proximal Smad4 CpG island, other upstream CpG islands could be analyzed for methylation status. In addition to genetic mechanisms, the 3' UTR of the Smad4 gene could harbor AU-rich elements or micro-RNA binding sites for post-transcriptional degradation. Certain regulatory micro-RNAs or AU-rich element binding proteins could be dysregulated in adjacent mucosa and HNSCC and lead to increased Smad4 mRNA degradation. Analysis of the Smad4 promoter for AU-rich elements and microRNA binding sites, coupled with screening of HNSCC samples for dysregulated mRNA regulatory molecules could indicate a post-transcriptional mechanism of mRNA downregulation that could explain the loss of Smad4 expression in both adjacent mucosa and of the remaining expression in HNSCC samples showing mono-allelic loss by LOH.

Mechanism and Significance of Fanc/Brca Pathway Dysregulation in HN-Smad4-/- HNSCCs

We were able to show Smad4 bound to the promoters of Brca1, FancA, and Rad51 with Smads 2 and 3. However, it remains to be determined whether BMP R-Smads 1 and 5 can also bind the above promoters. Further studies are required to determine whether Smad4 can activate transcription directly, and how Smad4 balances activating input from TGFβ1 signaling and inhibitory input from BMP signaling. The promoter regions of the above genes containing ChIP-verified SBEs can be cloned into luciferase constructs to assess direct transcriptional regulation by Smad4 in combination with either TGFβ or BMP R-Smads. Similarly, Smad4-dependent luciferase activity after TGFβ or BMP treatment would indicate whether Smad4 mediates signals from both TGFβ and BMP ligands and what the effect is on Fanc/Brca genes. Additionally, if Smad4 directly regulates the transcription of these genes, the SBEs can be mutated to further confirm that Smad4 binds directly to the above gene promoters through the identified SBEs. Lastly, upregulation of BMPs in HNSCCs has been reported (Jin et al., 2001), but the role of BMP signaling in HNSCC warrants further investigation. While we have focused our studies on TGFβ signaling in HNSCC, Smad4 loss-associated dysregulation of the BMP pathway could have important implications for HNSCC tumorigenesis.

FA patients have increased susceptibility to HNSCC, however none of the FA gene knockout mice develop HNSCC (D'Andrea and Grompe, 2003), indicating other molecular alterations may cooperate with FA mutations in human HNSCC. To address this possibility and also the impact of Fanc/Brca dysregulation in *HN-Smad4-/-* mice,

HN-Smad4-/- mice could be crossed with various Fanc/Brca genes including FancA, Brca1, or Rad51 to determine if tumor latency is reduced, and if the cellular phenotype refects increased genomic instability. Additionally, Smad4-/- keratinocytes could be transfected with Fanc/Brca expression vectors to see if the MMC sensitivity phenotype can be alleviated, thus pinpointing which Fanc/Brca genes are most important for Smad4-/- tumorigenesis. Similarly, although we have shown that *HN-Smad4-/-* mucosa and HNSCCs exhibit genomic instability, it isn't clear whether this phenotype is a cause or consequence of the tumorigenesis program. To address this possibility, *HN-Smad4-/-* mucosa could be harvested at various timepoints after *Smad4* gene deletion to determine whether increased centrosome numbers, chromosomal aberrations, or MMC sensitivity could be detected before tumors have formed in the oral mucosa. Lastly, as the Fanc/Brca pathway has also been implicated in repairing damage caused by ionizing radiation (Taniguchi et al., 2002), it would be interesting to determine if Smad4-/- cells have increased radiosensitivity.

Lastly, the mechanism of downregulation of Brca1 and FancA proteins in human HNSCC has not been determined. Smad4 loss could lead to downregulation of Fanc/Brca gene expression, however it is also possible that heterozygous mutations or polymorphisms in Fanc/Brca genes could lead to their downregulation (Mathew, 2006). Methylation of the FancF promoter has been demonstrated in HNSCC (Marsit et al., 2004), and it is possible that other Fanc/Brca genes could undergo promoter methylation. Lastly, protein-protein interactions (modification or degradation) could play a role in Fanc/Brca protein loss.

Mechanism and Significance of TGFβ Signaling Alterations and Inflammation in HN-Smad4-/- HNSCCs

While we have shown increased TGFβ1 and Smad3 *HN-Smad4-/-* tissue, it is not clear whether increased Smad3 and TGFβ1 are responsible for chemokine/cytokine overexpression and recruitment of immune cells. One way to address this question would be to breed *HN-Smad4-/-* mice with our Smad3-/- or knockin soluble TGFβRII-Fc (antibody against TGFβ1) mice and assess chemokine expression and leukocyte recruitment in *HN-Smad4-/-/Smad3+/-* (as Smad3 is haploinsufficient in inducing inflammation (Li et al., 2004a)) and *HN-Smad4-/-/TGFβ1* mice. Similarly, assessment of inflammatory cytokine/chemokine promoters for Smad3 binding sites and subsequent transcriptional regulation analysis could indicate whether any of these inflammatory mediators are direct targets of Smad3 (Figure 38).

In addition to innate immune infiltration, adaptive immune cells have also been linked to tumorigenesis (DeNardo and Coussens, 2007). We showed increased infiltrated T cells, including Th17 cells, and increased B cells in *HN-Smad4-/-* tissue. Both Th17 and B cells have been linked to autoimmune inflammation, and chronic infiltration of B cells has been linked to tumorigenesis (DeNardo and Coussens, 2007). However, it is still not known whether the infiltrated immune cells in our model are present in an inactive or active state, and whether they are tumor suppressive or tumor promoting. Ex vivo isolation of each immune cell type from *HN-Smad4-/-* tissues and assays for leukocyte activation, such as detection of tumorigenic cytokine expression or cell surface

diifferentiation/activation markers could indicate whether these immune cells are involved in tumorigenesis, or merely just present and possibly inhibited by TGFβ1. To determine whether each immune cell type can increase the tumorigenicity of *HN-Smad4-/-* cells, ex vivo removal of total leukocytes (CD45+ cells) by flow cytometry, and subsequent isolation of each immune subtype by cell surface marker expression could be performed. Each isolated immune cell populations could then be mixed with CD45- *HN-Smad4-/-* cells and grafted onto nude mice. The results of these experiments could indicate whether any immune cell subsets are involved in *HN-Smad4-/-* tumorigenesis.

Mechanism of Smad4-loss Associated CSC Tumorigenesis

Further studies are needed to determine the mechanism by which Smad4 affects tumor differentiation in keratinocyte stem cells. As deletion of BMP receptor 1a leads to bulge cell proliferation and inhibition of activated bulge cell differentiation (Kobielak et al., 2007), it is possible that Smad4 normally maintains bulge stem cell differentiation through mediating BMP signals. Deletion of BMP receptor 1a in K15-expressing cells should thus recapitulate the phenotype observed in *K15.Kras/Smad4-/-* mice. Additionally, future optimization of SP and CD44 sorting techniques could lead to the identification and characterization of putative CSCs in *HN-Smad4-/-* HNSCCs. Lastly, gene expression analysis of CSCs from *K15.Kras/Smad4-/-* tumors compared to non-CSCs from *K15.Kras/Smad4-/-* tumors could reveal targets essential for CSC tumorigenicity. These could be tested through siRNA treatment of isolated CSCs before grafting. As it is possible that CSCs are responsible for primary tumor relapse and distant

site metastasis, and most tumor therapies target only proliferating cells, novel therapies that target the largely quiescent CSCs are warranted.

CHAPTER SIX

SUMMARY AND CONCLUSIONS

In summary, we found that Smad4 was lost at the pre-translational level early in human HNSCC tumorigenesis, which correlated with loss of Brca1 and Rad51. We present a model where Smad4 loss leads to spontaneous HNSCC formation. Our results indicate that Smad4 loss contributes to defects in the Fanc/Brca DNA repair pathway. This effect, coupled with abrogation of TGFβ-induced growth inhibition and apoptosis but enhanced inflammation, could allow expansion of genetically damaged cells during HNSCC tumorigenesis. Additionally, we provided evidence that Smad4 loss in keratinocyte stem cells leads to their proliferation and aberrant retention of multipotency. Thus, Smad4 loss could lead to increased susceptibility to HNSCC, and also serve as a poor prognostic indicator. Our study instigates future investigations of the cooperative effects of aberrant Smad signaling and defects in the Fanc/Brca pathway, chronic inflammation, and keratinocyte stem cell expansion in HNSCC tumorigenesis.

CHAPTER SEVEN

REFERENCES

Allen, C. T., Ricker, J. L., Chen, Z., and Van Waes, C. (2007). Role of activated nuclear factor-kappaB in the pathogenesis and therapy of squamous cell carcinoma of the head and neck. Head Neck *29*, 959-971.

Arin, M. J., Longley, M. A., Wang, X. J., and Roop, D. R. (2001). Focal activation of a mutant allele defines the role of stem cells in mosaic skin disorders. J Cell Biol *152*, 645-649.

Balkwill, F., and Mantovani, A. (2001). Inflammation and cancer: back to Virchow? Lancet *357*, 539-545.

Bardeesy, N., Cheng, K. H., Berger, J. H., Chu, G. C., Pahler, J., Olson, P., Hezel, A. F., Horner, J., Lauwers, G. Y., Hanahan, D., and DePinho, R. A. (2006). Smad4 is dispensable for normal pancreas development yet critical in progression and tumor biology of pancreas cancer. Genes Dev *20*, 3130-3146.

Berton, T. R., Matsumoto, T., Page, A., Conti, C. J., Deng, C. X., Jorcano, J. L., and Johnson, D. G. (2003). Tumor formation in mice with conditional inactivation of Brca1 in epithelial tissues. Oncogene *22*, 5415-5426.

Berton, T. R., Wang, X. J., Zhou, Z., Kellendonk, C., Schutz, G., Tsai, S., and Roop, D. R. (2000). Characterization of an inducible, epidermal-specific knockout system: differential expression of lacZ in different Cre reporter mouse strains. Genesis *26*, 160-161.

Bertrand, P., Lambert, S., Joubert, C., and Lopez, B. S. (2003). Overexpression of mammalian Rad51 does not stimulate tumorigenesis while a dominant-negative Rad51 affects centrosome fragmentation, ploidy and stimulates tumorigenesis, in p53-defective CHO cells. Oncogene *22*, 7587-7592.

Bharathy, S., Xie, W., Yingling, J. M., and Reiss, M. (2008). Cancer-associated transforming growth factor beta type II receptor gene mutant causes activation of bone morphogenic protein-Smads and invasive phenotype. Cancer Res *68*, 1656-1666.

Bhowmick, N. A., Chytil, A., Plieth, D., Gorska, A. E., Dumont, N., Shappell, S., Washington, M. K., Neilson, E. G., and Moses, H. L. (2004). TGF-beta signaling in fibroblasts modulates the oncogenic potential of adjacent epithelia. Science *303*, 848-851.

Bierie, B., and Moses, H. L. (2006a). TGF-beta and cancer. Cytokine Growth Factor Rev *17*, 29-40.

Bierie, B., and Moses, H. L. (2006b). Tumour microenvironment: TGFbeta: the molecular Jekyll and Hyde of cancer. Nat Rev Cancer *6*, 506-520.

Blanpain, C., Lowry, W. E., Geoghegan, A., Polak, L., and Fuchs, E. (2004). Self-renewal, multipotency, and the existence of two cell populations within an epithelial stem cell niche. Cell *118*, 635-648.

Bloor, B. K., Su, L., Shirlaw, P. J., and Morgan, P. R. (1998). Gene expression of differentiation-specific keratins (4/13 and 1/10) in normal human buccal mucosa. Lab Invest *78*, 787-795.

Bornstein, S., Hoot, K., Han, G. W., Lu, S. L., and Wang, X. J. (2007). Distinct roles of individual Smads in skin carcinogenesis. Mol Carcinog *46*, 660-664.

Boyle, J. O., Hakim, J., Koch, W., van der Riet, P., Hruban, R. H., Roa, R. A., Correo, R., Eby, Y. J., Ruppert, J. M., and Sidransky, D. (1993). The incidence of p53 mutations increases with progression of head and neck cancer. Cancer Res *53*, 4477-4480.

Cairns, P., Polascik, T. J., Eby, Y., Tokino, K., Califano, J., Merlo, A., Mao, L., Herath, J., Jenkins, R., Westra, W., and et al. (1995). Frequency of homozygous deletion at p16/CDKN2 in primary human tumours. Nat Genet *11*, 210-212.

Cao, T., Longley, M. A., Wang, X. J., and Roop, D. R. (2001). An inducible mouse model for epidermolysis bullosa simplex: implications for gene therapy. J Cell Biol *152*, 651-656.

Caulin, C., Nguyen, T., Longley, M. A., Zhou, Z., Wang, X. J., and Roop, D. R. (2004). Inducible activation of oncogenic K-ras results in tumor formation in the oral cavity. Cancer Res *64*, 5054-5058.

Chen, H. B., Shen, J., Ip, Y. T., and Xu, L. (2006a). Identification of phosphatases for Smad in the BMP/DPP pathway. Genes Dev *20*, 648-653.

Chen, J. S., Pardo, F. S., Wang-Rodriguez, J., Chu, T. S., Lopez, J. P., Aguilera, J., Altuna, X., Weisman, R. A., and Ongkeko, W. M. (2006b). EGFR regulates the side population in head and neck squamous cell carcinoma. Laryngoscope *116*, 401-406.

Chen, Z., Malhotra, P. S., Thomas, G. R., Ondrey, F. G., Duffey, D. C., Smith, C. W., Enamorado, I., Yeh, N. T., Kroog, G. S., Rudy, S., *et al.* (1999). Expression of proinflammatory and proangiogenic cytokines in patients with head and neck cancer. Clin Cancer Res *5*, 1369-1379.

Cheng, N., Bhowmick, N. A., Chytil, A., Gorksa, A. E., Brown, K. A., Muraoka, R., Arteaga, C. L., Neilson, E. G., Hayward, S. W., and Moses, H. L. (2005). Loss of TGF-beta type II receptor in fibroblasts promotes mammary carcinoma growth and invasion through upregulation of TGF-alpha-, MSP- and HGF-mediated signaling networks. Oncogene *24*, 5053-5068.

Costea, D. E., Tsinkalovsky, O., Vintermyr, O. K., Johannessen, A. C., and Mackenzie, I. C. (2006). Cancer stem cells - new and potentially important targets for the therapy of oral squamous cell carcinoma. Oral Dis *12*, 443-454.

Coussens, L. M., and Werb, Z. (2002). Inflammation and cancer. Nature *420*, 860-867.

D'Andrea, A. D., and Grompe, M. (2003). The Fanconi anaemia/BRCA pathway. Nat Rev Cancer *3*, 23-34.

DeNardo, D. G., and Coussens, L. M. (2007). Inflammation and breast cancer. Balancing immune response: crosstalk between adaptive and innate immune cells during breast cancer progression. Breast Cancer Res *9*, 212.

D'Souza, G., Kreimer, A. R., Viscidi, R., Pawlita, M., Fakhry, C., Koch, W. M., Westra, W. H., and Gillison, M. L. (2007). Case-control study of human papillomavirus and oropharyngeal cancer. N Engl J Med *356*, 1944-1956.

Dubrovska, A., Kanamoto, T., Lomnytska, M., Heldin, C. H., Volodko, N., and Souchelnytskyi, S. (2005). TGFbeta1/Smad3 counteracts BRCA1-dependent repair of DNA damage. Oncogene *24*, 2289-2297.

Feng, X. H., and Derynck, R. (2005). Specificity and versatility in tgf-beta signaling through Smads. Annu Rev Cell Dev Biol *21*, 659-693.

Forastiere, A., Koch, W., Trotti, A., and Sidransky, D. (2001). Head and neck cancer. N Engl J Med *345*, 1890-1900.

Fukai, Y., Fukuchi, M., Masuda, N., Osawa, H., Kato, H., Nakajima, T., and Kuwano, H. (2003). Reduced expression of transforming growth factor-beta receptors is an unfavorable prognostic factor in human esophageal squamous cell carcinoma. Int J Cancer *104*, 161-166.

Fukasawa, K. (2007). Oncogenes and tumour suppressors take on centrosomes. Nat Rev Cancer *7*, 911-924.

Fukuchi, M., Masuda, N., Miyazaki, T., Nakajima, M., Osawa, H., Kato, H., and Kuwano, H. (2002). Decreased Smad4 expression in the transforming growth factor-beta signaling pathway during progression of esophageal squamous cell carcinoma. Cancer *95*, 737-743.

Glick, A., Popescu, N., Alexander, V., Ueno, H., Bottinger, E., and Yuspa, S. H. (1999). Defects in transforming growth factor-beta signaling cooperate with a Ras oncogene to cause rapid aneuploidy and malignant transformation of mouse keratinocytes. Proc Natl Acad Sci U S A *96*, 14949-14954.

Glick, A. B., Weinberg, W. C., Wu, I. H., Quan, W., and Yuspa, S. H. (1996). Transforming growth factor beta 1 suppresses genomic instability independent of a G1 arrest, p53, and Rb. Cancer Res *56*, 3645-3650.

Goodell, M. A., Brose, K., Paradis, G., Conner, A. S., and Mulligan, R. C. (1996). Isolation and functional properties of murine hematopoietic stem cells that are replicating in vivo. J Exp Med *183*, 1797-1806.

Gorelik, L., and Flavell, R. A. (2000). Abrogation of TGFbeta signaling in T cells leads to spontaneous T cell differentiation and autoimmune disease. Immunity *12*, 171-181.

Gorelik, L., and Flavell, R. A. (2001). Immune-mediated eradication of tumors through the blockade of transforming growth factor-beta signaling in T cells. Nat Med *7*, 1118-1122.

Grandis, J. R., and Tweardy, D. J. (1993). Elevated levels of transforming growth factor alpha and epidermal growth factor receptor messenger RNA are early markers of carcinogenesis in head and neck cancer. Cancer Res *53*, 3579-3584.

Hahn, S. A., Schutte, M., Hoque, A. T., Moskaluk, C. A., da Costa, L. T., Rozenblum, E., Weinstein, C. L., Fischer, A., Yeo, C. J., Hruban, R. H., and Kern, S. E. (1996). DPC4, a candidate tumor suppressor gene at human chromosome 18q21.1. Science *271*, 350-353.

Han, G., Lu, S. L., Li, A. G., He, W., Corless, C. L., Kulesz-Martin, M., and Wang, X. J. (2005). Distinct mechanisms of TGF-beta1-mediated epithelial-to-mesenchymal transition and metastasis during skin carcinogenesis. J Clin Invest *115*, 1714-1723.

He, W., Dorn, D. C., Erdjument-Bromage, H., Tempst, P., Moore, M. A., and Massague, J. (2006). Hematopoiesis controlled by distinct TIF1gamma and Smad4 branches of the TGFbeta pathway. Cell *125*, 929-941.

Hecht, S. S. (2003). Tobacco carcinogens, their biomarkers and tobacco-induced cancer. Nat Rev Cancer *3*, 733-744.

Herman, J. G., Merlo, A., Mao, L., Lapidus, R. G., Issa, J. P., Davidson, N. E., Sidransky, D., and Baylin, S. B. (1995). Inactivation of the CDKN2/p16/MTS1 gene is frequently associated with aberrant DNA methylation in all common human cancers. Cancer Res *55*, 4525-4530.

Hollstein, M., Sidransky, D., Vogelstein, B., and Harris, C. C. (1991). p53 mutations in human cancers. Science *253*, 49-53.

Hunter, K. D., Parkinson, E. K., and Harrison, P. R. (2005). Profiling early head and neck cancer. Nat Rev Cancer *5*, 127-135.

Izeradjene, K., Combs, C., Best, M., Gopinathan, A., Wagner, A., Grady, W. M., Deng, C. X., Hruban, R. H., Adsay, N. V., Tuveson, D. A., and Hingorani, S. R. (2007). Kras(G12D) and Smad4/Dpc4 haploinsufficiency cooperate to induce mucinous cystic neoplasms and invasive adenocarcinoma of the pancreas. Cancer Cell *11*, 229-243.

Jackson, E. L., Willis, N., Mercer, K., Bronson, R. T., Crowley, D., Montoya, R., Jacks, T., and Tuveson, D. A. (2001). Analysis of lung tumor initiation and progression using conditional expression of oncogenic K-ras. Genes Dev *15*, 3243-3248.

Jin, Y., Jin, C., Lv, M., Tsao, S. W., Zhu, J., Wennerberg, J., Mertens, F., and Kwong, Y. L. (2005). Karyotypic evolution and tumor progression in head and neck squamous cell carcinomas. Cancer Genet Cytogenet *156*, 1-7.

Jin, Y., Tipoe, G. L., Liong, E. C., Lau, T. Y., Fung, P. C., and Leung, K. M. (2001). Overexpression of BMP-2/4, -5 and BMPR-IA associated with malignancy of oral epithelium. Oral Oncol *37*, 225-233.

Jonkers, J., and Berns, A. (2002). Conditional mouse models of sporadic cancer. Nat Rev Cancer *2*, 251-265.

Kanamoto, T., Hellman, U., Heldin, C. H., and Souchelnytskyi, S. (2002). Functional proteomics of transforming growth factor-beta1-stimulated Mv1Lu epithelial cells: Rad51 as a target of TGFbeta1-dependent regulation of DNA repair. Embo J *21*, 1219-1230.

Kel, A. E., Gossling, E., Reuter, I., Cheremushkin, E., Kel-Margoulis, O. V., and Wingender, E. (2003). MATCH: A tool for searching transcription factor binding sites in DNA sequences. Nucleic Acids Res *31*, 3576-3579.

Kellendonk, C., Tronche, F., Monaghan, A. P., Angrand, P. O., Stewart, F., and Schutz, G. (1996). Regulation of Cre recombinase activity by the synthetic steroid RU 486. Nucleic Acids Res *24*, 1404-1411.

Kennedy, R. D., and D'Andrea, A. D. (2005). The Fanconi Anemia/BRCA pathway: new faces in the crowd. Genes Dev *19*, 2925-2940.

Kim, B. G., Li, C., Qiao, W., Mamura, M., Kasprzak, B., Anver, M., Wolfraim, L., Hong, S., Mushinski, E., Potter, M., *et al.* (2006). Smad4 signalling in T cells is required for suppression of gastrointestinal cancer. Nature *441*, 1015-1019.

Kim, D. W., and Lassar, A. B. (2003). Smad-dependent recruitment of a histone deacetylase/Sin3A complex modulates the bone morphogenetic protein-dependent transcriptional repressor activity of Nkx3.2. Mol Cell Biol *23*, 8704-8717.

Kim, S. K., Fan, Y., Papadimitrakopoulou, V., Clayman, G., Hittelman, W. N., Hong, W. K., Lotan, R., and Mao, L. (1996). DPC4, a candidate tumor suppressor gene, is altered infrequently in head and neck squamous cell carcinoma. Cancer Res *56*, 2519-2521.

Kitamura, T., Kometani, K., Hashida, H., Matsunaga, A., Miyoshi, H., Hosogi, H., Aoki, M., Oshima, M., Hattori, M., Takabayashi, A., *et al.* (2007). SMAD4-deficient intestinal tumors recruit CCR1+ myeloid cells that promote invasion. Nat Genet *39*, 467-475.

Kloos, D. U., Choi, C., and Wingender, E. (2002). The TGF-beta--Smad network: introducing bioinformatic tools. Trends Genet *18*, 96-103.

Kobielak, K., Pasolli, H. A., Alonso, L., Polak, L., and Fuchs, E. (2003). Defining BMP functions in the hair follicle by conditional ablation of BMP receptor IA. J Cell Biol *163*, 609-623.

Kobielak, K., Stokes, N., de la Cruz, J., Polak, L., and Fuchs, E. (2007). Loss of a quiescent niche but not follicle stem cells in the absence of bone morphogenetic protein signaling. Proc Natl Acad Sci U S A *104*, 10063-10068.

Kutler, D. I., Auerbach, A. D., Satagopan, J., Giampietro, P. F., Batish, S. D., Huvos, A. G., Goberdhan, A., Shah, J. P., and Singh, B. (2003). High incidence of head and neck squamous cell carcinoma in patients with Fanconi anemia. Arch Otolaryngol Head Neck Surg *129*, 106-112.

Lewandoski, M. (2001). Conditional control of gene expression in the mouse. Nat Rev Genet *2*, 743-755.

Li, A. G., Lu, S. L., Zhang, M. X., Deng, C., and Wang, X. J. (2004a). Smad3 knockout mice exhibit a resistance to skin chemical carcinogenesis. Cancer Res *64*, 7836-7845.

Li, A. G., Wang, D., Feng, X. H., and Wang, X. J. (2004b). Latent TGFbeta1 overexpression in keratinocytes results in a severe psoriasis-like skin disorder. Embo J *23*, 1770-1781.

Li, W., Qiao, W., Chen, L., Xu, X., Yang, X., Li, D., Li, C., Brodie, S. G., Meguid, M. M., Hennighausen, L., and Deng, C. X. (2003). Squamous cell carcinoma and mammary abscess formation through squamous metaplasia in Smad4/Dpc4 conditional knockout mice. Development *130*, 6143-6153.

Lin, X., Duan, X., Liang, Y. Y., Su, Y., Wrighton, K. H., Long, J., Hu, M., Davis, C. M., Wang, J., Brunicardi, F. C., *et al.* (2006). PPM1A functions as a Smad phosphatase to terminate TGFbeta signaling. Cell *125*, 915-928.

Lu, S. L., Herrington, H., Reh, D., Weber, S., Bornstein, S., Wang, D., Li, A. G., Tang, C. F., Siddiqui, Y., Nord, J., *et al.* (2006). Loss of transforming growth factor-beta type II receptor promotes metastatic head-and-neck squamous cell carcinoma. Genes Dev *20*, 1331-1342.

Lu, S. L., Reh, D., Li, A. G., Woods, J., Corless, C. L., Kulesz-Martin, M., and Wang, X. J. (2004). Overexpression of transforming growth factor beta1 in head and neck epithelia results in inflammation, angiogenesis, and epithelial hyperproliferation. Cancer Res *64*, 4405-4410.

Mackenzie, I. C. (2004). Growth of malignant oral epithelial stem cells after seeding into organotypical cultures of normal mucosa. J Oral Pathol Med *33*, 71-78.

Mangan, P. R., Harrington, L. E., O'Quinn, D. B., Helms, W. S., Bullard, D. C., Elson, C. O., Hatton, R. D., Wahl, S. M., Schoeb, T. R., and Weaver, C. T. (2006).

Transforming growth factor-beta induces development of the T(H)17 lineage. Nature *441*, 231-234.

Mao, L., Hong, W. K., and Papadimitrakopoulou, V. A. (2004). Focus on head and neck cancer. Cancer Cell *5*, 311-316.

Marsit, C. J., Liu, M., Nelson, H. H., Posner, M., Suzuki, M., and Kelsey, K. T. (2004). Inactivation of the Fanconi anemia/BRCA pathway in lung and oral cancers: implications for treatment and survival. Oncogene *23*, 1000-1004.

Massague, J., and Gomis, R. R. (2006). The logic of TGFbeta signaling. FEBS Lett *580*, 2811-2820.

Massague, J., Seoane, J., and Wotton, D. (2005). Smad transcription factors. Genes Dev *19*, 2783-2810.

Mathew, C. G. (2006). Fanconi anaemia genes and susceptibility to cancer. Oncogene *25*, 5875-5884.

Morris, R. J., Liu, Y., Marles, L., Yang, Z., Trempus, C., Li, S., Lin, J. S., Sawicki, J. A., and Cotsarelis, G. (2004). Capturing and profiling adult hair follicle stem cells. Nat Biotechnol *22*, 411-417.

Moutsopoulos, N. M., Wen, J., and Wahl, S. M. (2008). TGF-beta and tumors-an ill-fated alliance. Curr Opin Immunol.

Muro-Cacho, C. A., Rosario-Ortiz, K., Livingston, S., and Munoz-Antonia, T. (2001). Defective transforming growth factor beta signaling pathway in head and neck squamous cell carcinoma as evidenced by the lack of expression of activated Smad2. Clin Cancer Res *7*, 1618-1626.

Nagpal, J. K., Mishra, R., and Das, B. R. (2002). Activation of Stat-3 as one of the early events in tobacco chewing-mediated oral carcinogenesis. Cancer *94*, 2393-2400.

Nakagawa, H., Wang, T. C., Zukerberg, L., Odze, R., Togawa, K., May, G. H., Wilson, J., and Rustgi, A. K. (1997). The targeting of the cyclin D1 oncogene by an Epstein-Barr virus promoter in transgenic mice causes dysplasia in the tongue, esophagus and forestomach. Oncogene *14*, 1185-1190.

Neville, B. W., and Day, T. A. (2002). Oral cancer and precancerous lesions. CA Cancer J Clin *52*, 195-215.

Niedernhofer, L. J., Lalai, A. S., and Hoeijmakers, J. H. (2005). Fanconi anemia (cross)linked to DNA repair. Cell *123*, 1191-1198.

Ohyama, M., Terunuma, A., Tock, C. L., Radonovich, M. F., Pise-Masison, C. A., Hopping, S. B., Brady, J. N., Udey, M. C., and Vogel, J. C. (2006). Characterization and isolation of stem cell-enriched human hair follicle bulge cells. J Clin Invest *116*, 249-260.

Opitz, O. G., Harada, H., Suliman, Y., Rhoades, B., Sharpless, N. E., Kent, R., Kopelovich, L., Nakagawa, H., and Rustgi, A. K. (2002). A mouse model of human oral-esophageal cancer. J Clin Invest *110*, 761-769.

Oshima, H., Rochat, A., Kedzia, C., Kobayashi, K., and Barrandon, Y. (2001). Morphogenesis and renewal of hair follicles from adult multipotent stem cells. Cell *104*, 233-245.

Owens, D. M., and Watt, F. M. (2003). Contribution of stem cells and differentiated cells to epidermal tumours. Nat Rev Cancer *3*, 444-451.

Papadimitrakopoulou, V. A., Oh, Y., El-Naggar, A., Izzo, J., Clayman, G., and Mao, L. (1998). Presence of multiple incontiguous deleted regions at the long arm of chromosome 18 in head and neck cancer. Clin Cancer Res *4*, 539-544.

Patel, B. P., Shah, S. V., Shukla, S. N., Shah, P. M., and Patel, P. S. (2007). Clinical significance of MMP-2 and MMP-9 in patients with oral cancer. Head Neck *29*, 564-572.

Pedrero, J. M., Carracedo, D. G., Pinto, C. M., Zapatero, A. H., Rodrigo, J. P., Nieto, C. S., and Gonzalez, M. V. (2005). Frequent genetic and biochemical alterations of the PI 3-K/AKT/PTEN pathway in head and neck squamous cell carcinoma. Int J Cancer *114*, 242-248.

Perez-Losada, J., and Balmain, A. (2003). Stem-cell hierarchy in skin cancer. Nat Rev Cancer *3*, 434-443.

pGillison, M. L., D'Souza, G., Westra, W., Sugar, E., Xiao, W., Begum, S., and Viscidi, R. (2008). Distinct risk factor profiles for human papillomavirus type 16-positive and human papillomavirus type 16-negative head and neck cancers. J Natl Cancer Inst *100*, 407-420.

Pomerantz, R. G., and Grandis, J. R. (2003). The role of epidermal growth factor receptor in head and neck squamous cell carcinoma. Curr Oncol Rep *5*, 140-146.

Preobrazhenska, O., Yakymovych, M., Kanamoto, T., Yakymovych, I., Stoika, R., Heldin, C. H., and Souchelnytskyi, S. (2002). BRCA2 and Smad3 synergize in regulation of gene transcription. Oncogene *21*, 5660-5664.

Prime, S. S., Davies, M., Pring, M., and Paterson, I. C. (2004). The role of TGF-beta in epithelial malignancy and its relevance to the pathogenesis of oral cancer (part II). Crit Rev Oral Biol Med *15*, 337-347.

Prince, M. E., Sivanandan, R., Kaczorowski, A., Wolf, G. T., Kaplan, M. J., Dalerba, P., Weissman, I. L., Clarke, M. F., and Ailles, L. E. (2007). Identification of a subpopulation of cells with cancer stem cell properties in head and neck squamous cell carcinoma. Proc Natl Acad Sci U S A *104*, 973-978.

Qiao, W., Li, A. G., Owens, P., Xu, X., Wang, X. J., and Deng, C. X. (2006). Hair follicle defects and squamous cell carcinoma formation in Smad4 conditional knockout mouse skin. Oncogene *25*, 207-217.

Qiu, W., Schonleben, F., Li, X., and Su, G. H. (2007). Disruption of transforming growth factor beta-Smad signaling pathway in head and neck squamous cell carcinoma as evidenced by mutations of SMAD2 and SMAD4. Cancer Lett *245*, 163-170.

Reed, A. L., Califano, J., Cairns, P., Westra, W. H., Jones, R. M., Koch, W., Ahrendt, S., Eby, Y., Sewell, D., Nawroz, H., *et al.* (1996). High frequency of p16 (CDKN2/MTS-1/INK4A) inactivation in head and neck squamous cell carcinoma. Cancer Res *56*, 3630-3633.

Reiss, M. (1999). TGF-beta and cancer. Microbes Infect *1*, 1327-1347.

Rodriguez-Viciana, P., Tetsu, O., Oda, K., Okada, J., Rauen, K., and McCormick, F. (2005). Cancer targets in the Ras pathway. Cold Spring Harb Symp Quant Biol *70*, 461-467.

Rosendahl, A., Pardali, E., Speletas, M., Ten Dijke, P., Heldin, C. H., and Sideras, P. (2002). Activation of bone morphogenetic protein/Smad signaling in bronchial epithelial cells during airway inflammation. Am J Respir Cell Mol Biol *27*, 160-169.

Roth, S., Laiho, P., Salovaara, R., Launonen, V., and Aaltonen, L. A. (2000). No SMAD4 hypermethylation in colorectal cancer. Br J Cancer *83*, 1015-1019.

Saranath, D., Chang, S. E., Bhoite, L. T., Panchal, R. G., Kerr, I. B., Mehta, A. R., Johnson, N. W., and Deo, M. G. (1991). High frequency mutation in codons 12 and 61 of H-ras oncogene in chewing tobacco-related human oral carcinoma in India. Br J Cancer *63*, 573-578.

Shin, D. M., Ro, J. Y., Hong, W. K., and Hittelman, W. N. (1994). Dysregulation of epidermal growth factor receptor expression in premalignant lesions during head and neck tumorigenesis. Cancer Res *54*, 3153-3159.

Sieber, O. M., Heinimann, K., and Tomlinson, I. P. (2003). Genomic instability--the engine of tumorigenesis? Nat Rev Cancer *3*, 701-708.

Siegel, P. M., and Massague, J. (2003). Cytostatic and apoptotic actions of TGF-beta in homeostasis and cancer. Nat Rev Cancer *3*, 807-821.

Somers, K. D., Merrick, M. A., Lopez, M. E., Incognito, L. S., Schechter, G. L., and Casey, G. (1992). Frequent p53 mutations in head and neck cancer. Cancer Res *52*, 5997-6000.

Song, J. I., and Grandis, J. R. (2000). STAT signaling in head and neck cancer. Oncogene *19*, 2489-2495.

Sparano, A., Quesnelle, K. M., Kumar, M. S., Wang, Y., Sylvester, A. J., Feldman, M., Sewell, D. A., Weinstein, G. S., and Brose, M. S. (2006). Genome-wide

profiling of oral squamous cell carcinoma by array-based comparative genomic hybridization. Laryngoscope *116*, 735-741.

Takaku, K., Oshima, M., Miyoshi, H., Matsui, M., Seldin, M. F., and Taketo, M. M. (1998). Intestinal tumorigenesis in compound mutant mice of both Dpc4 (Smad4) and Apc genes. Cell *92*, 645-656.

Takebayashi, S., Ogawa, T., Jung, K. Y., Muallem, A., Mineta, H., Fisher, S. G., Grenman, R., and Carey, T. E. (2000). Identification of new minimally lost regions on 18q in head and neck squamous cell carcinoma. Cancer Res *60*, 3397-3403.

Tang, B., Yoo, N., Vu, M., Mamura, M., Nam, J. S., Ooshima, A., Du, Z., Desprez, P. Y., Anver, M. R., Michalowska, A. M., *et al.* (2007). Transforming growth factor-beta can suppress tumorigenesis through effects on the putative cancer stem or early progenitor cell and committed progeny in a breast cancer xenograft model. Cancer Res *67*, 8643-8652.

Tang, K. F., Tan, S. Y., Chan, S. H., Chong, S. M., Loh, K. S., Tan, L. K., and Hu, H. (2001). A distinct expression of CC chemokines by macrophages in nasopharyngeal carcinoma: implication for the intense tumor infiltration by T lymphocytes and macrophages. Hum Pathol *32*, 42-49.

Taniguchi, T., and D'Andrea, A. D. (2006). Molecular pathogenesis of Fanconi anemia: recent progress. Blood *107*, 4223-4233.

Taniguchi, T., Garcia-Higuera, I., Xu, B., Andreassen, P. R., Gregory, R. C., Kim, S. T., Lane, W. S., Kastan, M. B., and D'Andrea, A. D. (2002). Convergence of the fanconi anemia and ataxia telangiectasia signaling pathways. Cell *109*, 459-472.

Teicher, B. A. (2007). Transforming growth factor-beta and the immune response to malignant disease. Clin Cancer Res *13*, 6247-6251.

Teng, Y., Sun, A. N., Pan, X. C., Yang, G., Yang, L. L., Wang, M. R., and Yang, X. (2006). Synergistic function of Smad4 and PTEN in suppressing forestomach squamous cell carcinoma in the mouse. Cancer Res *66*, 6972-6981.

Thompson, L. H., and Schild, D. (2002). Recombinational DNA repair and human disease. Mutat Res *509*, 49-78.

Trempus, C. S., Morris, R. J., Bortner, C. D., Cotsarelis, G., Faircloth, R. S., Reece, J. M., and Tennant, R. W. (2003). Enrichment for living murine keratinocytes from the hair follicle bulge with the cell surface marker CD34. J Invest Dermatol *120*, 501-511.

Trempus, C. S., Morris, R. J., Ehinger, M., Elmore, A., Bortner, C. D., Ito, M., Cotsarelis, G., Nijhof, J. G., Peckham, J., Flagler, N., *et al.* (2007). CD34 expression by hair follicle stem cells is required for skin tumor development in mice. Cancer Res *67*, 4173-4181.

Tudor, D., Locke, M., Owen-Jones, E., and Mackenzie, I. C. (2004). Intrinsic patterns of behavior of epithelial stem cells. J Investig Dermatol Symp Proc *9*, 208-214.

Tumbar, T., Guasch, G., Greco, V., Blanpain, C., Lowry, W. E., Rendl, M., and Fuchs, E. (2004). Defining the epithelial stem cell niche in skin. Science *303*, 359-363.

van der Riet, P., Nawroz, H., Hruban, R. H., Corio, R., Tokino, K., Koch, W., and Sidransky, D. (1994). Frequent loss of chromosome 9p21-22 early in head and neck cancer progression. Cancer Res *54*, 1156-1158.

van Oijen, M. G., Rijksen, G., ten Broek, F. W., and Slootweg, P. J. (1998). Increased expression of epidermal growth factor receptor in normal epithelium adjacent to head and neck carcinomas independent of tobacco and alcohol abuse. Oral Dis *4*, 4-8.

van Vlasselaer, P., Punnonen, J., and de Vries, J. E. (1992). Transforming growth factor-beta directs IgA switching in human B cells. J Immunol *148*, 2062-2067.

Veldhoen, M., Hocking, R. J., Atkins, C. J., Locksley, R. M., and Stockinger, B. (2006). TGFbeta in the context of an inflammatory cytokine milieu supports de novo differentiation of IL-17-producing T cells. Immunity *24*, 179-189.

Vokes, E. E., Weichselbaum, R. R., Lippman, S. M., and Hong, W. K. (1993). Head and neck cancer. N Engl J Med *328*, 184-194.

Wang, D., Song, H., Evans, J. A., Lang, J. C., Schuller, D. E., and Weghorst, C. M. (1997). Mutation and downregulation of the transforming growth factor beta type II receptor gene in primary squamous cell carcinomas of the head and neck. Carcinogenesis *18*, 2285-2290.

Weber, F., Xu, Y., Zhang, L., Patocs, A., Shen, L., Platzer, P., and Eng, C. (2007). Microenvironmental genomic alterations and clinicopathological behavior in head and neck squamous cell carcinoma. Jama *297*, 187-195.

Wolf, G. T., Hudson, J. L., Peterson, K. A., Miller, H. L., and McClatchey, K. D. (1986). Lymphocyte subpopulations infiltrating squamous carcinomas of the head and neck: correlations with extent of tumor and prognosis. Otolaryngol Head Neck Surg *95*, 142-152.

Wreesmann, V. B., Estilo, C., Eisele, D. W., Singh, B., and Wang, S. J. (2007). Downregulation of Fanconi anemia genes in sporadic head and neck squamous cell carcinoma. ORL J Otorhinolaryngol Relat Spec *69*, 218-225.

Wreesmann, V. B., Shi, W., Thaler, H. T., Poluri, A., Kraus, D. H., Pfister, D., Shaha, A. R., Shah, J. P., Rao, P. H., and Singh, B. (2004a). Identification of novel prognosticators of outcome in squamous cell carcinoma of the head and neck. J Clin Oncol *22*, 3965-3972.

Wreesmann, V. B., Wang, D., Goberdhan, A., Prasad, M., Ngai, I., Schnaser, E. A., Sacks, P. G., and Singh, B. (2004b). Genetic abnormalities associated with nodal metastasis in head and neck cancer. Head Neck *26*, 10-15.

Wrzesinski, S. H., Wan, Y. Y., and Flavell, R. A. (2007). Transforming growth factor-beta and the immune response: implications for anticancer therapy. Clin Cancer Res *13*, 5262-5270.

Xie, W., Bharathy, S., Kim, D., Haffty, B. G., Rimm, D. L., and Reiss, M. (2003). Frequent alterations of Smad signaling in human head and neck squamous cell carcinomas: a tissue microarray analysis. Oncol Res *14*, 61-73.

Xu, X., Brodie, S. G., Yang, X., Im, Y. H., Parks, W. T., Chen, L., Zhou, Y. X., Weinstein, M., Kim, S. J., and Deng, C. X. (2000). Haploid loss of the tumor suppressor Smad4/Dpc4 initiates gastric polyposis and cancer in mice. Oncogene *19*, 1868-1874.

Xu, X., Kobayashi, S., Qiao, W., Li, C., Xiao, C., Radaeva, S., Stiles, B., Wang, R. H., Ohara, N., Yoshino, T., *et al.* (2006). Induction of intrahepatic cholangiocellular carcinoma by liver-specific disruption of Smad4 and Pten in mice. J Clin Invest *116*, 1843-1852.

Xu, X., Weaver, Z., Linke, S. P., Li, C., Gotay, J., Wang, X. W., Harris, C. C., Ried, T., and Deng, C. X. (1999). Centrosome amplification and a defective G2-M cell cycle checkpoint induce genetic instability in BRCA1 exon 11 isoform-deficient cells. Mol Cell *3*, 389-395.

Yang, L., Huang, J., Ren, X., Gorska, A. E., Chytil, A., Aakre, M., Carbone, D. P., Matrisian, L. M., Richmond, A., Lin, P. C., and Moses, H. L. (2008). Abrogation of TGF beta signaling in mammary carcinomas recruits Gr-1+CD11b+ myeloid cells that promote metastasis. Cancer Cell *13*, 23-35.

Yang, L., Mao, C., Teng, Y., Li, W., Zhang, J., Cheng, X., Li, X., Han, X., Xia, Z., Deng, H., and Yang, X. (2005). Targeted disruption of Smad4 in mouse epidermis results in failure of hair follicle cycling and formation of skin tumors. Cancer Res *65*, 8671-8678.

Yang, X., Li, C., Herrera, P. L., and Deng, C. X. (2002). Generation of Smad4/Dpc4 conditional knockout mice. Genesis *32*, 80-81.

Yarbrough, W. G., Shores, C., Witsell, D. L., Weissler, M. C., Fidler, M. E., and Gilmer, T. M. (1994). ras mutations and expression in head and neck squamous cell carcinomas. Laryngoscope *104*, 1337-1347.

Young, M. R., Wright, M. A., Lozano, Y., Prechel, M. M., Benefield, J., Leonetti, J. P., Collins, S. L., and Petruzzelli, G. J. (1997). Increased recurrence and metastasis in patients whose primary head and neck squamous cell carcinomas secreted granulocyte-macrophage colony-stimulating factor and contained CD34+ natural suppressor cells. Int J Cancer *74*, 69-74.

Yue, J., and Mulder, K. M. (2000). Requirement of Ras/MAPK pathway activation by transforming growth factor beta for transforming growth factor beta 1 production in a smad-dependent pathway. J Biol Chem *275*, 35656.

Zhang, Q., Yang, X., Pins, M., Javonovic, B., Kuzel, T., Kim, S. J., Parijs, L. V., Greenberg, N. M., Liu, V., Guo, Y., and Lee, C. (2005). Adoptive transfer of tumor-reactive transforming growth factor-beta-insensitive CD8+ T cells: eradication of autologous mouse prostate cancer. Cancer Res *65*, 1761-1769.

Zhang, Y., Feng, X., We, R., and Derynck, R. (1996). Receptor-associated Mad homologues synergize as effectors of the TGF-beta response. Nature *383*, 168-172.

Zhou, Z., Wang, D., Wang, X. J., and Roop, D. R. (2002). In utero activation of K5.CrePR1 induces gene deletion. Genesis *32*, 191-192.

CHAPTER EIGHT

TABLES

Table 1. aCGH changes in *HN-Smad4-/-* HNSCCs.

Chr.	Region	Sample	Position	Score	gain/loss	Genes (MM8 Assembly, UCSC)	Human Synteny
1	1	94822	33750000-33990000	0.869	gain	Zfp451, Dst	6p12.1
		98102	33570000-33930000	0.288	gain	Prim2, Rab23, Bag2, Zfp451	6p11.2, 6p12.1
1	2	94461	84870000-87450000	0.417	gain	Sp110, Sp140	2q37.1
		94822	84870000-87330000	0.491	gain	-	-
1	3	94461	175650000-175830000	-0.273	loss	Mnda, Ifi203, Ifi202b	1q23.1
		98102	175350000-175950000	-0.334	loss	Pyhin1, Ifi204, Mnda, Ifi203, Ifi202b, Ifi205, Olfr cluster	1q23.1
2	1	98990	174690000-177990000	-0.785	loss	Etohi1	19p13.2
		94461	177030000-177990000	-0.445	loss	-	-
		94822	174690000-177990000	-0.707	loss	Etohi1	19p13.2
		98102	177030000-177990000	-0.447	loss	-	-
	2	98990	77730000-77790000	-3.318	loss	-	-
		94461	77730000-77790000	-0.793	loss	-	-
		94822	77730000-77790000	-0.78	loss	-	-
		98102	77670000-77790000	0.69	gain	-	-
3	1	94461	94110000-94350000	-0.439	loss	Tdpoz5	17q21.33
		94822	93690000-94290000	-0.282	loss	Tdpoz1-5	17q21.33
4	1	98990	41970000-42030000	1.021	gain	Ccl21a,c;	9p13.3
		94461	42030000-42810000	-0.569	loss	Ccl21a,b,c; Il11ra2, Ccl19, Ccl27	9p13.3
		94822	42030000-42810000	-0.845	loss	Ccl21a,b,c; Il11ra2, Ccl19, Ccl27	9p13.3
		98102	42030000-42810000	-0.625	loss	Ccl21a,b,c; Il11ra2, Ccl19, Ccl27	9p13.3
	2	94822	111570000-113130000	-0.413	loss	Skint6	-
		1315602	111390000-113790000	-0.324	loss	Slc5a9, Skint1,6,8	1p33
	3	98990	121470000-121650000	-1.064	loss	-	-
		94461	121230000-122070000	0.307	gain	-	-
		1315602	121470000-121650000	-0.662	loss	-	-
5	1	98990	11130000-11910000	0.414	gain	-	-
		94461	11010000-11910000	0.313	gain	-	-
		94822	11010000-11910000	0.437	gain	-	-
		98102	11010000-11910000	0.39	gain	-	-
	2	94461	14970000-15150000	0.246	gain	Speer4d	-
		94822	14970000-15150000	0.258	gain	Speer4d	-
		98102	14910000-15150000	0.306	gain	Speer4d	-
		1315602	14970000-15210000	0.6	gain	Speer4d	-
	3	98102	94470000-96030000	0.593	gain	-	-
		1315602	94470000-96030000	-0.531	loss	-	-
6	1	98990	70470000-70590000	-1.524	loss	-	-
		94461	68910000-70590000	-0.237	loss	-	-
		94822	68610000-70590000	-0.281	loss	-	-
		1315602	68610000-70650000	-0.424	loss	-	-
	2	98990	85650000-85710000	-0.63	loss	Alms1	2p13.2
		94461	85650000-85710000	-0.416	loss	Alms1	2p13.2
		94822	85650000-85710000	-0.329	loss	Alms1	2p13.2
	3	94461	129930000-130350000	-0.56	loss	Klra cluster	12p13.2
		94822	129930000-130350000	-0.563	loss	Klra cluster	12p13.2
		98102	130170000-130350000	-0.57	loss	Klra cluster	12p13.2
7	1	98990	7050000-8370000	-0.559	loss	Vmn2r cluster	-
		94461	7050000-8970000	-0.487	loss	Vmn2r cluster	-
		94822	6810000-8970000	-0.255	loss	Clcn4-2, Vmn2r cluster	Xp22.2
		1315602	6750000-8850000	-0.453	loss	Zfp418, Clcn4-2, Vmn2r cluster	19q13.43, Xp22.2
	2	94461	9030000-9690000	0.002	gain	Vmn2r52, V1re9,10,11, Zik1, V1rl1, Nlrp4b, V1re13	19q13.41,19q13.43, 16p11.2
		94822	9030000-9690000	0.131	gain	Vmn2r52, V1re9,10,11, Zik1, V1rl1, Nlrp4b, V1re13	19q13.41,19q13.43, 16p11.2
	3	94461	9750000-10530000	0.541	gain	Gm397, Zscan4d&f	19q13.43
		94822	9750000-10470000	0.637	gain	Gm397, Zscan4d&f	19q13.43
		98102	9750000-10530000	0.349	gain	Gm397, Zscan4d&f	19q13.43
	4	98990	13590000-14850000	-0.677	loss	Obox1&3	-
		94461	13590000-14610000	-0.297	loss	Obox1&3	-
		1315602	13830000-14550000	-0.395	loss	Obox1&3	-
	5	94822	20130000-20610000	0.801	gain	-	-
		1315602	20130000-20610000	-0.7	loss	-	-
	6	98990	38070000-39150000	0.75	gain	-	-
		94822	38070000-39150000	-0.314	loss	-	-
		1315602	38190000-39150000	-0.585	loss	-	-

Chr.	Region	Sample	Position	Score	gain/loss	Genes (MM8 Assembly, UCSC)	Human Synteny	
8	1	94822	19710000-20070000	0.275	gain	-	-	
		1315602	19710000-22590000	0.347	gain	Defcr21&23	-	
	2	94461	22650000-22890000	0.381	gain	Defcr cluster	-	
		1315602	22650000-23010000	-0.37	loss	Defcr cluster	-	
9	1	98990	46650000-46890000	0.453	gain	-	-	
		94461	46650000-46890000	0.32	gain	-	-	
		98102	46650000-46890000	0.328	gain	-	-	
		1315602	46650000-46890000	0.411	gain	-	-	
10	1	98990	21870000-22050000	0.452	gain	Raet1a-e	6q25.1	
		94461	21990000-22110000	0.229	gain	Raet1a-e	6q25.1	
		98102	21930000-22110000	0.319	gain	Raet1a-e	6q25.1	
		1315602	22170000-22230000	-0.341	loss	-	-	
11	1	98990	71010000-71070000	-0.623	loss	N1rp1b&c	-	
		94461	71010000-71070000	0.602	gain	N1rp1b&c	-	
12								
13	1	98990	68670000-69030000	-0.401	loss	Mtrr	5p15.31	
		1315602	68670000-69030000	-0.336	loss	Mtrr	5p15.31	
14	1	98990	3090000-6450000	0.367	gain	-	-	
		1.3E+07	3090000-5670000	0.478	gain	-	-	
	2	98990	51990000-52050000	-1.061	loss	-	-	
		1315602	51930000-52050000	-0.628	loss	-	-	
15								
16								
17	1	94461	6210000-6450000	0.263	gain	Syt13, Tmem181, Dynlt1	11p11.2, 6q25.3	
		98102	6210000-6390000	0.457	gain	Syt13, Tmem181	11p11.2, 6q25.3	
	2	94461	30210000-30570000	-0.215	loss	Btbd9, Glo1, Dnahc8	6p21.2	
		94822	30210000-30570000	-0.598	loss	Btbd9, Glo1, Dnahc8	6p21.2	
		98102	30210000-30630000	-0.646	loss	Btbd9, Glo1, Dnahc8, Glp1r	6p21.2	
18								
19								
X	1	98990	3030000-4290000	0.92	gain	-	-	
		94461	3030000-3210000	-0.447	loss	-	-	
		94822	3030000-4290000	-0.914	loss	-	-	
		98102	3030000-4290000	-0.426	loss	-	-	
		1315602	3030000-4290000	0.929	gain	-	-	
	2	94822	24450000-26790000	-0.564	loss	Xmr, Xmr-like	-	
		98102	25830000-30450000	-0.311	loss	Xmr-like	-	
		1315602	24570000-30450000	0.936	gain	Xmr, Xmr-like	-	
	3	98990	30270000-30450000	1.091	gain	-	-	
		94461	30270000-30450000	-0.466	loss	-	-	
		94822	30270000-30450000	-1.051	loss	-	-	
	4	98990	120210000-121650000	-0.23	loss	-	-	
		94822	120330000-121650000	0.503	gain	-	-	
		1315602	119130000-121650000	0.091	gain	Vmn2r121	-	
	5	94461	143070000-144930000	0.458	gain	Ott	-	
		98102	143070000-145290000	0.456	gain	Ott	-	
		1315602	143910000-144930000	0.909	gain	Ott	-	

The chromosome number, with sample numbers and genomic positions are listed. Losses or gains are expressed as the log2 ratio of *HN-Smad4-/-* DNA copy number compared to *Smad4+/+* DNA copy number. Genes in the region are listed, as well as genes in the syntenic human region.

Table 2. Correlation Between Smad4 and Brca1/Rad51 Expression in Adjacent Mucosa and HNSCCs

	Sample	**Smad4 +**	**Smad4 -**
Brca1 Loss	Mucosa adjacent to HNSCC	0/8 (0%)	12/13 (92%)*
	HNSCC	0/8 (0%)	21/24 (88%)*
Rad51 Loss	Mucosa adjacent to HNSCC	0/8 (0%)	12/13 (92%)*
	HNSCC	0/8 (0%)	20/24 (83%)*

Adjacent mucosa (21 cases) and HNSCCs (32 cases) were IHC stained with Brca1 and Rad51 antibodies. Of the cases staining positive for Smad4, none of the cases showed Brca1 and Rad51 loss. Of the cases with Smad4 loss, a high percentage of cases had both Brca1 and Rad51 loss. * $p < 0.05$ compared to Smad4+ cases.

APPENDIX A

ANTIBODIES

Antibody	Protocol	Host	Vendor	Catalog #	Tissue Species	Primary Conc.	Secondary Conc.
IgG	ChIP	Rabbit	Santa Cruz Biotechnologies	sc-2027	Mouse	3 mg	NA
Smad2	ChIP	Rabbit	Zymed	51-1300	Mouse	3 mg	NA
Smad3	ChIP	Rabbit	Upstate	06-920	Mouse	3 mg	NA
Smad4	ChIP	Rabbit	Upstate	06-693	Mouse	3 mg	NA
CD3	Frozen/IHC	Hamster	BD Pharmingen	550275	Mouse	1:20	1:200
B220	Frozen/IHC	Rat	eBioscience	14-0452	Mouse	1:160	1:200
CD45	Frozen/IHC	Rat	BD Pharmingen	550539	Mouse	1:160	1:200
F4/80	Frozen/IHC	Rat	Invitrogen (Caltag)	MF48000	Mouse	1:160	1:200
IL-17 (biotinylated)	Frozen/IHC	Rat	BD Pharmingen	555067	Mouse	1:200	NA
Ly6G	Frozen/IHC	Rat	BD Pharmingen	550291	Mouse	1:160	1:200
Brca1 (D-9)	Nuclear Foci	Mouse	Santa Cruz Biotechnologies	sc-6954	Human	1:100	1:200
Rad51 (H-92)	Nuclear Foci	Rabbit	Santa Cruz Biotechnologies	sc-8349	Human	1:100	1:200
pSmad2	Paraffin/IHC	Rabbit	Cell Signaling	3104S	Mouse	1:100	1:200
Smad4 (B-8)	Paraffin/IHC	Mouse	Santa Cruz Biotechnologies	sc-7966	Mouse, Human	1:200	1:400
total Smad3	Paraffin/IHC	Rabbit	Santa Cruz Biotechnologies	sc-8332	Mouse	1:100	1:200
Keratin 15	Paraffin/IHC	Chicken	Covance	PCK-153P	Mouse	1:200	1:400
NFkB p50 (H-119)	Paraffin/IHC	Rabbit	Santa Cruz Biotechnologies	sc-7178	Mouse	1:100	1:200
pAkt Thr308	Parrafin/IHC	Rabbit	Cell Signaling	9275	Mouse	1:100	1:400
NFkB p65 (C-20)	Paraffin/IHC	Rabbit	Santa Cruz Biotechnologies	sc-372	Mouse	1:100	1:200
pStat3	Paraffin/IHC	Rabbit	Cell Signaling	9134	Mouse	1:100	1:200
Brca1 (MS13)	Paraffin/IHC	Mouse	Abcam	ab16781-100	Mouse	1:50	1:400
Brca1 (D-9)	Paraffin/IHC	Mouse	Santa Cruz Biotechnologies	sc-6954	Human	1:50	1:100
Rad51 (H-92)	Paraffin/IHC	Rabbit	Santa Cruz Biotechnologies	sc-8349	Human	1:100	1:400
Rad51 (I-20)	Paraffin/IHC	Goat	Santa Cruz Biotechnologies	sc-7410	Mouse	1:100	1:400
Keratin 13	Parrafin/IF	Mouse	Chemicon	CBL176	Human	1:100	1:100
Keratin 14	Parrafin/IF	Giunea Pig	Fitzgerald	20R-CP002	Mouse, Human	1:200	1:100
Pericentrin	Parrafin/IF	Rabbit	Covance	PRB-432C	Mouse	1:150	1:200
pSmad1/5/8	Parrafin/IF	Rabbit	Cell Signaling	9511S	Mouse	1:100	1:100
PCNA (PC10)	Parrafin/IF	Mouse	Santa Cruz Biotechnologies	sc-56	Mouse	1:100	1:100
Keratin 1	Parrafin/IF	Rabbit	Covance	PRB-165P	Mouse	1:200	1:100
Keratin 15	Parrafin/IF	Chicken	Covance	PCK-153P	Mouse	1:200	1:100
Actin (I-19)	Western	Goat	Santa Cruz Biotechnologies	sc-1616	Human	1:1000	1:5000
Smad4 (B-8)	Western	Mouse	Santa Cruz Biotechnologies	sc-7966	Human	1:500	1:5000
FITC-CD31	Flow Cytometry	Rat	eBioscience		11-0311	2 µl /1*10^6 cells	
FITC-CD45	Flow Cytometry	Rat	eBioscience		11-0451	0.5 µl /1*106 cells	
CD34-biotin	Flow Cytometry	Rat	eBioscience		13-0341	5 µl /1*106 cells	
Streptavidine-PE	Flow Cytometry		eBioscience		12-4317		20 µl /1*106 cells
PE-Cy5-CD49f	Flow Cytometry	Rat	BD Biosciences		551129	10 µl /1*106 cells	

APPENDIX B

SEQUENCES

Assay	Gene	Primer Sequences
Genotyping	K14CrePR1	CGGTCGATGCAACGAGTGAT
		CCACCGTCAGTACGTGAGAT
	K5Cre*PR1	TACAGCTCCTGGGCAACGTG
		CACAGCATTGGAGTCAGAAG
	K15CrePR1	CGGTCGATGCAACGAGTGAT
		CCACCGTCAGTACGTGAGAT
	Smad4 floxed	GGGCAGCGTAGCATATAAGA (P9)
		GACCCAAACGTCACCTTCA (P10)
	Kras	CCTTTACAAGCGCACGCAGACTGTAGA
		AGCTAGCCACCATGGCTTGAGTAAGTCTGC
	TGFβRII floxed	GCAGGCATCAGGACCTCAGTTTGATCC
		AGAGTGAAGCCGTGGTAGGTGAGCTTG
	Smad4 Deletion	AAGAGCCACAGGTCAAGCAG (P8)
		GACCCAAACGTCACCTTCA (P10)

Assay	Marker	Primer Sequences
LOH		
	D18S46	FAM-GAATAGCAGGACCTATCAAAGAGC
		CAGATTAAGTGAAAACAGCATATGTG
	D18S474	FAM-TGGGGTGTTTACCAGCATC
		TGGCTTTCAATGTCAGAAGG
	D18S1110	FAM- TGACCTTGGCTACCTTGC
		TCGAAAGCCTTAAACTCTGA

Assay	Gene	Primer Sequences
Sequencing	Hras Exon 1	GCAGCCGCTGTAGAAGCTATGA
		GTAGGCAGAGCTCACCTCTATA
	Hras Exon 2	CATGACTGTGTCCAGGACATTC
		TAGGCTGGTTCTGTGGATTCTC
	Kras Exon 1	TACACACAAAGGTGAGTGTAAAAATATTGATAA
		AGAGCAGCGTTACCTCTATC
	Kras Exon 2	AAGATGCACTGTAATAATCCATAC
		ATTCAACTTAAACCCACCTATA

Assay	Gene	Primer Sequences
ChIP	Brca1 3031	GACTTTTCCAATGTCACAGGAAGG
		GCACATAATTGACTGGTTCGGC
	Rad51 1522	AACAAGCTACATGGGAGTCTGAGG
		CGTCTGGGGTTGCACAAAAAAAAG
	FancA 136	ATTAGCAATTCTGCGCCACT
		TAGGAGCATGCTTGACCACA
	Control	TTCTTGGCATAGAGTTAAGGAGCC
		GTTTCGAGACAGGGTTTCTCTGTG

Assay	Gene	siRNA Sequences
siRNA treatment	Smad1	CCUACUACUGUUUGCAAGAUCCCUA
	Smad2	UUCUCAAGCUCAUCUAACCGUCCUG
	Smad3	CCUGCUGGAUUGAGCUACACCUGAA
	Smad4	GGUGAUGUUUGGGUCAGGUGCCUUA
	Smad5	CCGUUGGAUAUUUGUGAAUUUCCUU

APPENDIX C

TAQMAN® PROBES

Probe Target	Species	Filter	Vendor	Catalog # or Sequence
Brca1	Mouse	FAM	Applied Biosystems	Mm00515386_m1
Brca1	Human	FAM	Applied Biosystems	Hs00173233_m1
FancA	Mouse	FAM	Applied Biosystems	Mm00516836_m1
FancA	Human	FAM	Applied Biosystems	Hs00164555_m1
FancD2	Mouse	FAM	Applied Biosystems	Mm01184622_m1
FancD2	Human	FAM	Applied Biosystems	Hs00945440_m1
GAPDH	Mouse	VIC	Applied Biosystems	4352339E
GAPDH	Human	VIC	Applied Biosystems	4326317E
K14	Mouse	FAM	Applied Biosystems	Mm00516876_m1
Rad51	Mouse	FAM	Applied Biosystems	Mm00485509_m1
Rad51	Human	FAM	Applied Biosystems	Hs00153418_m1
Smad4	Mouse	FAM	Applied Biosystems	Mm00484724_m1
Smad4	Human	FAM	Applied Biosystems	Hs00232068_m1